Seed-free short time synthesis of zincosilicate zeolite VPI-8 and its catalysis of methane dehydroaromatization reaction

by

Chaoran Huang

B.S., Kansas State University, 2015

A THESIS

submitted in partial fulfillment of the requirements for the degree

MASTER OF SCIENCE

Department of Chemical Engineering
College of Engineering

KANSAS STATE UNIVERSITY
Manhattan, Kansas

2018

Approved by:

Major Professor
Jennifer L. Anthony

Copyright

Abstract

Zeolite refers to a microporous material, which is also called a molecular sieve. There are three major industrial applications of zeolites: adsorbents, ion exchangers, and catalysts; and many other minor applications including: sensors, agriculture, medicine, veterinary, hydrogen storage, fuel cells, microreactors, membrane reactors, and racemic separations. Today, zeolite is not limited to aluminosilicate. Researchers are attempting to use other species (such as B, Ga, Ge, Ti, and Zn) to replace aluminum in zeolites framework to accomplish particular applications. In 1991, the first zincosilicate zeolite was synthesized by Annen et al.. Currently, only four zincosilicate zeolites have been synthesized. Theoretically, zincosilicate should balance divalent cations better than aluminosilicate zeolites to provide a stronger acid site especially for hydrogen cracking reactions. Large pore VET type VPI-8 ($Li_{1.914}Zn_{1.914}Si_{15.086}O_{34}$) is the most thermal stable of all the zincosilicate zeolites and has low chemicals cost, however, a high crystallinity VPI-8 required prohibitively long synthesis times or seeded synthesis procedures. In this work, a seed-free short time synthesis zincosilicate zeolite VPI-8 is presented.

Methane, also known as natural gas, had become the largest abundant carbon reserve today, more than the amount of the fossil fuel including conventional gas, oil, and coal. Unlike fossil fuel, methane can be recycled from landfill. Methane could be used to produce useful and/or expensive chemicals via syngas conversion to fuel, paraffin, methanol, alcohol, and dimethoxyethane. In addition to pathways via a syngas intermediate, methane could react directly to ethylene, formaldehyde, and aromatics. Because syngas preparation and compression usually expends 60-70% of the capital cost and consumes almost all the energy of operation, more and more researchers are exploring direct methane activation. However, the high stability of methane is one of the limitations, and coking is another limitation. In this work, methane dehydroaromatization

(MDA) over zincosilicate zeolite Li-VPI-8 and ion exchanged Ni/Li-VPI-8 are investigated, due to the stronger acid site in zincosilicate than aluminosilicate zeolites. This is the first time to study using zincosilicate as catalyst, capitalizing on the more efficient synthesis methods demonstrated in this work.

Table of Contents

List of Figures

List of Tables

Chapter 1 - Zeolites Introduction

Zeolites Background

History

"Zeolite" is derived from two Greek word meaning "to boil" and "a stone". The term "molecular sieve" was first used by McBain [1] to describe materials which could discriminate between small molecules on the basis of their size and/or shape, which is one of zeolites properties, but the expression "molecular sieve" has also been used to describe amorphous, porous materials such as certain carbons and polymers. In 1756, the first natural zeolite stilbite (STI) was discovered by the Swedish mineralogist Cronstedt when he heated an unidentified silicate mineral and observed that the mineral fused readily in a blowpipe flame with obvious intumescence [2]. Schafhaulte attempted to synthesize silicates under hydrothermal conditions in 1845 and reported the preparation of quartz by heating a silicate "gel" with water in an autoclave [3]. In 1862, the first hydrothermal synthesis of a zeolite "levynite" (LEV) was reported by St Claire Deville [4]. In 1882, de Schulten reported the synthesis of analcime (ANA) [5]. Other syntheses of several zeolites were reported in the succeeding years [6]. However, the early synthetic work was not very well established due to the lack of essential data for identification. In the early 1940, Barrer began his pioneering work in systematic synthesis of zeolites, initially investigating the conversion of known mineral phases in strong salt solution at fairly high temperature (170-270 °C). In 1948 by using this approach, Barrer synthesized the first zeolite with no natural counterpart, species P and Q [7-9] (KFI structure type as determined subsequently for zeolite ZK-5) [10, 11]. In the late 1940s,

Milton and co-workers successfully synthesized zeolites A(LTA), X(FAU), and P(GIS) by hydrothermal crystallization of reactive alkali metal aluminosilicate gels at low temperature ~100 °C and pressure (autogenous) under alkaline condition (pH typically higher than 12) [12, 13]. By 1953, they had synthesized 20 zeolites, of which 14 did not have natural counterparts [14]. The large-scale synthetic methodologies of Milton and co-works initiated zeolite technology.

In 1961, a creative use of quaternary ammonium cations was reported by Barrer and Denny [15]. An intermediate-silicate analog of zeolite A (LTA) was synthesized using tetramethylammonium cation (TMA^+). The framework Si/Al ratio could be increased by the addition of organic components in aluminosilicate gels. The use of organic components in zeolite synthesis played a pivotal role in initiating the significant advances of zeolite synthesis, particularly the tremendous growth of siliceous zeolites. Many high-silica zeolites were successfully crystallized using organic cations with aluminosilicate gels at 100-200 °C [16]. For example, the first high-silica zeolite β (BEA) with Si/Al ratio ranging from 5 to 100 was made by using the tetraethlylammonium cation [17]. High-silica zeolite ZSM-5 (MFI) was prepared by using the terapropylammonium cation [18].

In 1982, the synthesis of a new family of aluminophospate molecular sieves was reported by Wilson et al., designated $AlPO_4$ –n [19, 20]. The synthesis of $AlPO_4$ –n involves hydrothermal reaction of aluminophosphate gels with organic components at 100-200 °C under acidic or mildly basic conditions. The synthesis of $AlPO_4$ –n involves hydrothermal reaction of aluminophosphate gels with organic components at 100-200 °C under acidic or mildly basic conditions. In contrast to the aluminosilicate synthetic mixture, the discovery of the aluminophosphate family of molecular sieves has greatly expanded the structural diversity of zeolite materials.

Zeolites structure

Zeolites and zeolite-like materials comprise a large class of microporous crystalline oxide frameworks. They are composed of tetrahedral atoms (T-atoms) silicon, aluminum, boron, gallium, germanium, titanium and zinc. Framework density was defined as the number of T-atoms per cubic nanometer by Meier and Olson [21]. Most zeolite and zeolite-like materials have a framework density (FD) less than 21.

Zeolites have a T-atom/oxygen ratio of 1:2, and classified as aluminosilicate. The $SiO_{4/2}$ and $AlO_{4/2}^-$ tetrahedral have two charges 0 and -1, respectively. The -2 charge of each oxygen is shared between two tetrahedral, effectively contributing a -1 charge per oxygen to each tetrahedra. Since each silicon has a +4 charge and it is bonded to four oxygens, the silicate tetrahedron is neutral. Similarly, each aluminum has a +3 charge and hence, an $AlO_{4/2}^-$ tetrahedron has a net -1 charge. Loewenstein [22] observed that most known aluminosilicates have a Si/Al ratio $\geq$ 1.0. Based on this and other observations he proposed a rule requiring the avoidance of adjacent $AlO_{4/2}^-$ tetrahedra. The adjacent $AlO_{4/2}^-$ tetrahedra would involve neighboring negative charges which is unfavorable. The anionic charges of zeolite framework due to the Si/Al ratio $\geq$ 1.0 must be balanced by non-framework cations. These cations are not permanently fixed and can be replaced with other cations through ion-exchange with different corresponding salts. There is no ion-exchange capacity and acid site in aluminophosphate because the framework does not have any charge.

Zeolite compositions can be written in a general formula, which can be is divided into three terms: the non-framework cations, the framework portion, and the adsorbed phase.

$$[M^{m+}_{(1/m)}]\cdot[x\cdot SiO_2\cdot AlO_2]\cdot[nH_2O]$$

where M represents a non-framework cation of charge m^+, x represents the Si/Al ratio which is ≥ 1.0, and n represents the mole of water contains in zeolites.

Today, most of framework elements were limited to Al and Si atoms, and the upper limit of pore size exceeded the previous limit of 12 rings [23-25]. In zeolite system, pores are bounded by 8, 10, and 12 oxygen atoms or T-atoms are claimed as small, medium, and large pore materials. Based on this classification, the small, medium, and large pore diameters are approximately 4.0, 5.5, and 7.5 Å, respectively.

Applications

Zeolites have been widely used as adsorbents, ion exchangers, and catalysts [26]. In 2016, over two-third of total volume zeolites were consumed in home laundry detergent as builder. About 18% of the total volume zeolites are used as catalysts. An estimated 14% of world capacity is used as adsorbent or desiccant [27].

Zeolites can exchange Ca^{2+} and Mg^{2+} out from hard water. Usually, the resin in a water softening heater is made by zeolites. Zeolite 4A is commonly added in powder laundry detergent to soft the water as a builder, because detergents can only work in soft water. By 1990s, zeolites replaced the previous phosphate element builder which is not environment friendly. Also, by this ion exchange capability, heavy metals such as lead and mercury in water can be filleted out by zeolites. Additionally, zeolites can remove radioactive ions (such as caesium, strontium and thorium) from contaminated water. The ability had been demonstrated at nuclear accidents at Chernobyl and Three Mile Island [28, 29]. Today, zeolites are used in nuclear power plant to clean the huge amount contaminated water contains radioactive ions.

Moreover, when protons are balancing anionic framework charges, the zeolite is considered to be in the acid form and these protons can be used as acid sites for catalysis. Fluid

catalytic cracking (FCC) catalysts are the second largest volume of synthetic zeolites in use [27]. Most zeolite catalysis are related to petrol-chemicals. The most well-known zeolite catalyst is ZSM-5. Zeolite molecular sieve catalysts may have better selectivity than other catalysts. For example, ZSM-5 have a great selectivity of p-xylene in reaction, because the isomers o-xylene and m-xylene can not pass through the pore of molecular sieve. In the other hand, zeolites can be used to decrease the air pollution. The current leading technology is Selective Catalytic Reduction (SCR), which revert the harmed NO_x into harmless N_2 and H_2O by using a reducing agent such as ammonia.

For adsorption, in the natural gas market, drying agent zeolites are in demand to remove the water in the humidity natural gas. Since zeolites are molecular sieves, zeolites can trap volatile organic compounds (VOC) to prevent the release into environment. In the recovery of construction markets, insulated multi-glazed windows need zeolites as desiccants. Based on the water adsorption ability, zeolite can be used as a blood-clotting agent. For instants, FDA had approved QuikClot, which contains a dehydrated zeolite [30, 31]. In household, zeolites can be used as room odor control. Also, zeolites can be added in cat litter as pet odor control. It is interesting to notice that a zeolite with particular adsorption property is being used to remove the cork taint, which is 2,4,6-trichloroanisole (TCA), from wine without changing its taste. Besides the three major applications, zeolites also have other applications: sensor, membrane reactor, microreactor, agriculture, medicine, veterinary, hydrogen storage, fuel cells, and racemic separation.

Zeolites Synthesis

Zeolites crystal growth

Nucleation

The formation of a new crystalline entity from a solution starts through the nucleation process. Nucleation is defined as the series of atomic or molecular processes by which the atoms or molecules of a reactant phase arrange into a cluster of the product phase large enough as to have the ability to grow irreversibly to a macroscopically larger size. The cluster is defined as a nucleus or critical nuclei [32].

Nucleation can be homogeneous, in the absence of foreign particles or crystals in the solution, or heterogeneous, in the presence of foreign particles in the solution. Both types of nucleation are collectively known as primary nucleation. Secondary nucleation takes place when nucleation is induced by the presence of crystals of the same substance.

The driving force for the nucleation and growth of a crystal is referred to as supersaturation and is defined as the difference in chemical potential between a molecule in solution and that in the bulk of the crystal phase:

$$\Delta\mu = \mu_S - \mu_C \quad (1.1)$$

where μ_S is the chemical potential of a molecule in solution and μ_C is the chemical potential of the molecule in the bulk crystal. Following thermodynamics Eq. (1.1) can be expressed as:

$$\Delta\mu = kT \ln S \quad (1.2)$$

where k is the Boltzmann constant, T is the absolute temperature, and S is the supersaturation ratio. When $\Delta\mu > 0$ the solution is said to be supersaturated, meaning the

nucleation and/or growth is possible, whereas when $\Delta\mu < 0$ the solution will be undersaturated and dissolution will take place. The form of the supersaturation ratio will change depending on the system considered (i.e., gas/solid, solution/solid, melt/solid). For nucleation and growth from solutions it takes the following form:

$$S = \frac{\prod a_i^{n_i}}{\prod a_{i,e}^{n_i}} \qquad (1.3)$$

where n_i is the number of ith ions in the molecule of crystal, and a_i and $a_{i,e}$ the actual and equilibrium activities of the I molecule in the crystal.

Nucleation Rate

The rate of nucleation (the number of nuclei formed per unit time per unit volume) can be expressed by an Arrhenius-type equation [33]:

$$J = A \exp\left(\frac{-\Delta G^*}{kT}\right) \qquad (1.4)$$

where A also depends on supersaturation. The nucleation rate is a function of supersaturation (S).

The nucleation rate is virtually zero until a critical value of supersaturation is achieved, after which the rate increases exponentially. This critical supersaturation ($\Delta\mu$) defines a so-called metastable zone where crystal growth can proceed without concomitant nucleation taking place.

Induction Time

Induction time is defined as the amount of time elapsed between the achievement of a supersaturated solution and the observation of crystals. Its value will thus depend on the setting of

t = 0 and the technique used to detect the formation of crystals. The induction period can be influenced by factors such as supersaturation, agitation, presence of impurities, viscosity, and so on [33]. The induction time is defined as:

$$t_i = t_r + t_n + t_g \qquad (1.5)$$

The induction time is separated into three periods: t_r is the relaxation time, required for the system to achieve a quasi-steady-state distribution of molecular cluster; t_n is the time required for the formation of a nucleus; and t_g is the time required for the nucleus to grow to a detectable size.

Synthesis Mechanism

In 2005, Cundy and Cox summarized the principal proposals for zeolite synthesis mechanism from 1959 to 2004 in their review [34]. In 1959, zeolite synthesis mechanism was first considered by Barrer, Baynham, Bultitude and Meier [35]. The mechanism was understood as condensation polymerization of polygonal and polyhedral anions at the beginning. Later, in 1960, the zeolite crystal growth was thought to take place predominantly in the solid phase by morphological changes [36]. In 1966, Kerr reported the crystal growth from solution species which are formed fast from amorphous solid [37]. Later, Zhdanov reported an advance result that the relation between crystal growth rate and temperature. Also, a solubility equilibrium between solid and liquid are connected. Nucleation takes place in condensation, then crystal growth in solution [38]. In 1991, the mechanism was summarized as two steps. First, a clathrate-like water structures form around the template. Second, the clathrate-like hydrate converts to a clathrate-like silicate through isomorphous substitution of silicate for water in the embryonic units [39]. Today, the most believed mechanism was proposed by Burkett and Davis [40-42]. The pre-organized inorganic and

organic composites are aggregated around the SDA, where the nucleation takes place, then the crystal growth occurs layer-by-layer.

Synthesis approaches

Many new zeolite synthesizes routes have been developed after hydrothermal synthesis, such as solvothermal synthesis, ionothermal synthesis, F^- synthesis, microwave-assisted hydrothermal synthesis, microemulsion-based hydrothermal synthesis, dry gel conversion synthesis, and combinatorial synthesis. However, hydrothermal synthetic technique is still the most widely used for zeolites synthesis, since the pioneering work had been done by Barrer and Milton. Hydrothermal synthetic techniques have been applied not only in the preparation of zeolites and zeolite-related porous materials, but also in the preparation of most other important inorganic materials, such as superionic conductors, chemical sensors, electronically conducting solids, complex oxide ceramics and fluorides, magnetic materials, and luminescence phosphors.

Hydrothermal synthesis usually refers to reactions occurring under conditions of high temperature (>100 °C) and high pressure (>1 bar) in aqueous solutions in a close system. A hydrothermal apparatus requires a sealed vessel because of the safety concern that a high autogenous pressure is generated in the closed system at elevated temperature from the vapor pressure of the reactants. The most commonly used autoclaves for reactions in strongly acidic or alkaline media at elevated temperature and pressure are from Parr Instrument Company. For example, Figure 1-1 and Figure 1-2 show two types of Parr Teflon-lined stainless-steel bombs with capacities of 23 and 45 mL, respectively. Both bombs are lined with a thick wall of polytetrafluoroethylene (PTFE) cups with lids for a maximum temperature 240 °C and pressure 124 bar. A safety blow out protection is designed in the bomb cover with a rupture disc and a

corrosion disc. There are other types bombs used in laboratories, such as large capacity bombs of 125 mL and high pressure bombs up to 345 bar.

Figure 1-1: Parr Teflon-lined stainless-steel bomb with a capacity of 23 mL: acid digestion vessel (left), PTFE cup (right)

Figure 1-2: Parr Teflon-lined stainless-steel bomb with a capacity of 45 mL: acid digestion vessel (left), PTFE cup (right)

Hydrothermal Reactions

Zeolite crystallization is one of the most complex chemical problems in crystal nucleation and growth. According to reaction temperature, the hydrothermal synthesis can be classified into subcritical and supercritical synthetic reactions. In subcritical synthesis, the temperature is in the range of 100-240 °C. while in supercritical system, the temperature could reach up to 1000 °C and

pressure may increase to 3000 bar. Under hydrothermal conditions, the physical and chemical properties of reactants are also changed significantly. High temperature and pressure hydrothermal conditions accelerate the reaction rate among the complex ions, intensify the hydrolyzation reaction, and significantly change the redox potential of the reactants. Consequently, hydrothermal (high temperature and pressure) conditions can promote the reactivity of reactants have low solubility at ambient temperature. Many variables could affect the formation of a specific zeolite phase, such as bath composition, reactant sources, Si/Al ratio, alkalinity, water content, inorganic cations, organic cations, solvents, temperature, aging, stirring, seeding, and retreatment.

Bath composition

The bath composition of the reaction mixture plays a crucial role in determining the zeolite crystallization. In the early work, Breck used a phase diagram to clearly demonstrate the influence of batch composition on different zeolite phases. These ternary diagrams contain the concentration of Na_2O, Al_2O_3, and SiO_2 [43]. At the beginning, the silicon source in the mixture solution is sodium silicate with 90-98% water content. There are five zeolite phases, which are A (LTA), X (FAU), Y (FAU), B (ANA), and HS (SOD), were obtained in different regions. Phases may co-exist in the boundary region. When the water content decreases to 60-85% in the mixing gel, HS (SOD) was the only zeolite phase obtained while keeping other conditions and chemical components identical. When the silicon source sodium silicate was replaced by colloidal silica, the result of zeolite phases is: A (LTA), X (FAU), Y (FAU), R (CHA) and S (GME). If K_2O is added into the mixture solution, which water contents 95-98%, instead of Na_2O, only zeolite phases W and H were found.

Si/Al sources

The nature of chemical reactant has an important effect on zeolite crystal growth [44]. The silicon sources commonly used in the synthesis of zeolites are sodium waterglass, colloidal silica sol, fumed silica, tetramethylorthosilicate (TMOS), and tetraethylorthosilicate (TEOS). In the early work, Breck studied the influence of silicon sources [43]. The chemical nature of polysilicate species are different from one to another, so does their distributions. The silicon source plays important roles in both nucleation and crystallization of zeolites. It was found that different surface areas of the silicon source could affect the crystallization rate, crystal size, and particle size distribution as in the synthesis of zeolite A (LTA) [45]. Silica with high surface area is much easily dissolved in basic medium than low surface area silica. Also, high surface area silica can provide a higher supersaturation and a faster nucleation, which is favorable for small crystals formation. In contrast, the low surface area silicon source is low solubility and large crystal favorable. Later, many synthesis works have been reported which focus on controlling zeolite crystal size by proper choice of silicon source, because the silica sources can influence the zeolite size and morphology. Some studies showed that less reactive silicon sources may reduce both nucleation sites and favor for large crystal formation. For example, the conventional powder or solution silica source is replaced by a bulk silica source that could lead to synthesis giant zeolite crystal [46].

Most commonly aluminum sources used in zeolite synthesis are sodium aluminate, pseudo-boehmite, aluminum hydroxide, aluminum isopropoxide, aluminum nitrate, aluminum sulfate, and aluminum metal (Al powder or foil). In general, zeolites with low Si/Al ratio ≤ 5, are prepared from reaction mixtures with low Si/Al ratio and strong alkalinity, such as zeolites A (LTA), X (FAU), and HS (SOD). Whereas, high-silica zeolites Si/Al ratio > 5, are prepared from reaction mixtures with weak alkalinity or in neutral F^- medium, such as zeolite beta (BEA), ZSM-11 (MEL), and ZSM-5 (MFI). However, there is no quantitative correlation between the Si/Al ratio in the

initial reaction mixture and the final product. Thus, the Si/Al ratio in zeolite product cannot be simply adjusted by varying the Si/Al ratio in the initial reaction solution. It had been shown the proper SDA could be added into the initial solution to synthesis high-silica zeolites.

Alkalinity

There are several functions of alkalinity: increase the solubility of silicon sources, decrease the polymerization degree of the silicate anions, and accelerate the polymerization of the polysilicate and aluminate anions. Moreover, the increase of alkalinity will shorten the induction and nucleation periods and speed up the crystallization of zeolites [45]. Also, alkalinity can affect the zeolite morphology. For example, higher length/width ratio was found for MFI crystallized at lower alkalinity, which suggests the length/width increases at lower supersaturation [47].

Water content

In hydrothermal synthesis, water is the solvent in the reaction mixture. Reactant concentrations could be changed by the water content in the solution, then affects the zeolite crystallization. Water can act as a mineralizer or a catalyst under elevated pressure–temperature conditions. The thermodynamic and transport properties of supercritical water are remarkably different from those of ambient water. The solubility of nonpolar species increases whereas that of ionic and polar compounds decreases. A dilute mixture could cause lower supersaturation, which large crystals are favorable. Also, water may change the region of zeolite phases by affecting other variables.

For hydrothermal synthesis, both pressure and temperature of water is important. The dielectric constant of water will decrease while the temperature and pressure increase [48]. However, the effect of temperature is more than pressure. In general, electrolytes will be totally

dissociated in water. However, the dissociated ions will forward to recombine when temperature increases. This transition usually take place at 200 °C to 500 °C for most of the substances. In addition, the viscosity of water solution decreases while the temperature is increasing. Thus, the mobility of molecules or ions in water can be enhanced under hydrothermal conditions.

Inorganic cations

For the zeolite framework, inorganic cations function as the extra-framework cations to pair with the framework charges. Inorganic cations have important effects on the zeolite structure formation [15]. Low Si/Al ratio zeolites are prepared in basic medium by using alkali metal hydroxides as the alkali source. Sodium and potassium are the two most common cations used in zeolite synthesis. For example, sodium cation can be used for preparing: ANA, CAN, CHA, EMT, FAU (X), FAU(Y), FER, GIS, LTA, MAZ, MOR, MTT, MTW, MWW, and SOD. Potassium cation can be used for synthesized zeolites: EDI, KFI, LTL, MER, and TON. But some zeolites could not be synthesized in the absence of lithium, rubidium, or cesium. For some particular zeolites, co-cations are required. For instance, both sodium and potassium are used for preparing BEA, low-silica-type X (FAU), NAT, OFF, PAU, and PHI [49]. VPI-9 synthesis requires both potassium and rubidium [50]. Flanigen proposed there are two rules of alkali-metal cations in zeolite synthesis: a.) the source of hydroxide ions needed to solubilize silicate and aluminate species, due to the cation is added as a base form; and b.) a limited structure-directing role [51]. There is an interaction between sodium and water molecules. Sodium cations attract water molecules forward to it due to the polarization of water molecules. Then, these organized water molecules surrounding sodium cations can be replaced by silicon or aluminum tetrahedra partially and lead to the cage-like structure formation. The dissolution and polymerization-

depolymerization reaction of silicates and aluminosilicates can be affected by the hydroxide ion. It is suggested that the structure-directing role of the alkali-metal cations can be involved in the ordering of water molecules around the cations with subsequent displacement by silicate and aluminate species to form region of micro-organization that lead to nucleation centers [52, 53].

Organic cations

The organic cation tetramethylammonium (TMA^+) was first introduced by Barrer and Denny which high Si/Al ratio zeolite was synthesized in 1961 [15]. The presence of TMA^+ was clarified as the structure-directing agent. After that, other quaternary ammonium cations were used in the extension of zeolite framework composition to high Si/Al ratio $\geq$ 20 and the synthesis of new zeolites. In 1982, it had been shown that a family of aluminophosphate molecular sieves is synthesized by using organic amines and quaternary ammonium ions as the templates or SDAs [19, 20]. Today, the organic molecule can be summarized as structure-directing agent, pore-filling agent, and template.

In the early review, templating was defined as the phenomenon occurring during either the gelation or the nucleation process whereby the organic species organic oxide tetrahedra into a particular geometric topology around themselves and thus provide initial building blocks for a particular structure [54]. It is suggested that both gel chemistry and template are important in a specific molecule sieve structure formation. And templates work only in proper solution condition. Organic molecule as “templates” became a common function in zeolite synthesis after 1982. The word “templating” could be only used when a zeolite structure adopts the geometric and electronic configurations which are unique to the templating molecule, and upon removal the organic species retains the shape of the guest molecules. However, there is no true “templating” in zeolite synthesis.

The true "templating" may only occur in ZSM-18 synthesis, which is triply-charged tris-quaternary ammonium cation 2,3,4,5,6,7,8,9-octahydro-2,2,5,5,8,8-hexamethyl-1H-benzo[1,2-c:3,4-c':5,6-c"]tripyrrolium [55]. Davis and Lobo claimed the action of organic molecules as structure-directing agent rather than strict template [56].

In general, SDAs can affect the zeolite formation significantly by the following [52, 57]. During synthesis, the precursor species for further nucleation and crystal growth are provided by a particular geometry which is organized from the TO_4 units around themselves. Both gelation and nucleation could be effected by SDAs. The chemical potential of lattice formation would be lowered upon SDAs or "templates" in synthesis process. New interactions, such as H-bonds, electrostatic, and London dispersion interactions, could be impacted by SDAs (or templates). Furthermore, the crystal structure geometry including both form and size can be controlled by SDAs. The extra-large pore materials could be synthesized via appropriately size organic SDAs. UTD-1, CIT-5, and SSZ-53 had been successful synthesized via large organic SDAs [58]. More works were studied on understanding the SDAs properties and product crystalline structure [59-62]. Usually, higher Si/Al ratio zeolites are obtained by adding SDAs. The SDA can provide both larger cations and more hydrophobic than alkali cations. Organic cations require less framework charge to balance their positive charge; and the larger Si/Al ratio, the more hydrophobic is the pore space. The influence of the hydrophobic character of structure-directing agents for the synthesis of pure-silica zeolites was studied on pure-silica MFI type zeolite [63]. Comparing three organic structure-directing agents tetrapropylammonium, ethanoltripropylammonium and diethanoldipropylammonium cations, for the synthesis of pure-silica zeolites, it is necessary to control the hydrophobicity of the organic structure-directing agent in pure-silica zeolites synthesis. Today, unfortunately zeolite still cannot be "designed" by choosing the "right" SDA.

Organic SDAs are not necessary for some zeolites synthesis. The advantages of not using of organic SDAs are the elimination of the expansive SDA cost and the removal the organic chemicals after synthesizing. In common, as-made zeolite has to be calcined before using. The exhaust gases could contain toxic oxides of carbon and nitrogen, and other not environmental or health friendly gases. In addition, the organic-free synthesis is preferred for scale up and commercialization. In 2008, the first zeolite beta created in the absence of an organic SDA was synthesized [64]. However, zeolite beta structure exists in nature as mineral tschernichite [65]. Later, the Si/Al of organic-free beta can be prepared as low as 5 [66]. Commercial organic-free zeolites are still hard to prepare today. Another choice to prepare organic-free zeolite is using seed, which will be discuss in the "seeding" section.

Later, pore-filling agent (PFA) appeared as a more economic chemical in zeolite synthesis. Zones presented a series of structures (SSZ-13, SSZ-35, SSZ-33, SSZ-42) could be synthesized by combining less expensive and expensive organic cations. This methodology has been use in commercial manufacture. The less expensive organic molecule fills pore space during the synthesis of a zeolite can be classified as pore-filling agent [67].

Besides the three major functions of SDAs, choosing the appropriate SDA is also important. Liebau summarized the most appropriate organic cation conditions in synthesizing clathrasil [68]. Later, these conditions could be considered as the zeolite synthesis requirements of SDAs:

1. The molecule must have sufficient room within the particular cage or pore of the desired zeolite framework.
2. The molecule must be stable under the synthesis conditions. For example, SDA must be stable in the presence of water in hydrothermal synthesis.

3. The molecule should fit the inner surface of the cage with as many van der Waals contacts as possible, but with the least deformation.
4. The tendency of the guest molecule to form complexes with the solvent should be weak.
5. If other parameters are equally favorable, a higher stiffness molecule could be easier to form a clathrasil.
6. The tendency to form a clathrasil will increase with the basicity or polarizability of the guest molecule.

In current methods, almost all the zeolite synthesis requires SDAs. Before the zeolites can be used, a high temperature calcination step is necessary to remove the SDAs from the framework, which could destroy the SDAs. Also in calcination, the water production can course the inorganic structure damage. The "recycle SDA" concept was reported to synthesis ZSM-5 in 2003 by Davis's group [69]. The idea is assembling an SDA from at least two components by using covalent bonds or non-covalent interactions which would be stable in synthesis condition such as high pH. After synthesizing, the assembled SDA is cleaved into fragments without destroying the framework. At the end, the fragments are removed to reassemble the SDA again.

Solvents

The properties of solvents are important in zeolite synthesis upon their interactions with reaction species. Zeolite is synthesized in aqueous medium, especially for hydrothermal approach. Non-aqueous medium, which is alcohols, had been proved by Biddy and Dale [70]. There are four categories based on the strength of hydrogen bonds: high, high-medium, low-medium, non-hydrogen bonding [71]. This strong interaction with solvent would resist the framework species which forming the interactions with SDAs. Consequently, high hydrogen bonding solvents is not

preferred in synthesizing zeolites, nucleation will be prevented interactions from shielded framework species and SDAs with each other. The interactions between framework species and SDAs can be achieved in high-medium and low-medium hydrogen bonding solvents.

The size and morphology of zeolites could be affected by the viscosity of the solvent. Solvents with higher viscosity than water could reduce convection currents, especially in gel solutions. Both secondary nucleation and crystallization from sedimentation can be reduced by diffusion in mass transfer. Moreover, the rate of reaction species diffusion is reduced by increasing viscosity of solvents. It is suggested that the solvents of both intermediate viscosity and hydrogen bonding should be favorable for zeolite synthesis, especially for large size crystals [71].

Temperature

Temperature plays a significate role in synthesis of zeolite. The expected zeolite can only be synthesized in a specific temperature range. The nucleation and crystal growth can be affected by the crystallization temperature significantly [72, 73]. The silica solubility can be affected extremely [74]. Both the nucleation rate and crystal growth rate can be increased by increasing temperature. Thus, the higher crystal growth rate is achieved, the larger crystal can be formed. The relation between growth rate and temperature was studied on NaX synthesis in four different temperatures. The growth rates at 100 °C, 90 °C, 80 °C, and 70 °C are approximately 5.00 μm/day, 2.86 μm/day, 1.82 μm/day, and 0.91μm/day, respectively [75]. Temperature can not only influence the crystal size, but also the morphology of crystals. For example, the length/width ratio of silicalite-1 (MFI) can be increased at higher temperature. The crystal growth kinetic was studied based on different activation energies [76, 77].

Time

Crystallization time is another parameter could be affect by temperature. Generally, the crystallinity could be increased with a longer synthesis time. Zeolites are thermodynamically metastable phases. The successive reactions could take place in zeolite synthesis. In Ostwald's law, a metastable phase appears first, then more stable phases replace it [78]. For example, the intermediate CIT-6 is a prior phase of final product VPI-8 [79].

Aging

Aging refers to the period from homogeneous mixture to the onset of heating to the crystallization temperature. Also, the reagents phase change happens in aging from heterogeneous to homogeneous with stirring. Studies were done on the aging affect in both zeolite nucleation and crystal growth in zeolite synthesis [75, 80, 81]. It is suggested that the germ nuclei are formed during the aging period, which effectively lie dormant until the reaction temperature is elevated [82]. Even though the aging process period is not well understood yet, there are several parameters that may affect the nucleation and crystal growth kinetics, such as increasing the nucleation rate, reducing the induction period and duration of crystallization, reducing the crystal size, and increasing the crystal population.

Stirring

Usually, zeolites are synthesized under static conditions. However, several studies showed that stirring can affect the crystallization kinetics, especially the crystal size [82]. Smaller crystal could be achieved due to the supersaturation from accelerated mass transfer. It had been found

zeolite phase selectivity could be change by stirring. Zeolite A (LTA) was preferred to form zeolite X (FAU) in stirring synthesis, and MFI is favored to replace zeolite TON in a not stirring system [83].

Seeding

Like other crystal growth, zeolite crystal could growth on seed. A seed crystal can be seen as a small crystal from which a larger crystal of the same substance is grown on. There are two major effects about seeding: reducing the synthesis time and directing the synthesis to a desired phase with consequent reduction in impurities. It is possible to control the size of the final crystals [84-86]. In addition, seeding can improve the crystallization [87]. Seed synthesis could reduce the synthesis time since skipping the nucleation time and result in a high crystallinity zeolite. However, the yield in with-seed synthesis is low.

Zincosilicate

Most of the known smallest T-atom unit in molecular sieve structures contains more than four. These two are lovdarite [88] and ZSM-18 [89] which contain rings of 3 T-atoms (3MR) and larger. And cloverite has the lowest framework density which is 11.1 [90]. A relation between minimum framework density (FD) and the minimum ring size in the structure (MINR) had been proved [91]. If the smallest ring in a structure is 4, the framework density decreases, when the average number of 4-rings per T-atom increases. Based on this relation, it is postulated that materials containing a 3-member ring could achieve a lower framework density than currently

attainable framework with 4-member ring. It had been shown that the density in frameworks can change the topology in crystal. Meanwhile, in the same work, a theory was developed to describe the relationship between FD and MINR (FD decreases, then MINR decreases) [92]. In another work, Monte Carlo simulations shown that the number of fractions of 3-member ring increases as the density decreases [93]. Theoretically, there are three potential gel reaction mixtures that could be used to prepare 3-member ring containing molecular sieves by considering bond angles and bond lengths [94-97]. Only two molecular sieves contain 3-member ring, which are aluminosilicate ZSM-18 and beryllosilicate lovdarite. ZSM-18 sythesis is required an unusual organic SDA (or template) triply-charged tris-quaternary ammonium cation 2,3,4,5,6,7,8,9-octahydro-2,2,5,5,8,8-hexamethyl-1H-benzo[1,2-c:3,4-c':5,6-c"]tripyrrolium [55]. It is not a general synthetic route to 3-member ring framework aluminosilicate because the organic specie function more as a template then SDA, which is the general organic chemical function in zeolite synthesis. Beryllosilicate is limited by that most beryllium sources are highly toxic. Thus, zincosilicate reaction mixture seems to be the most potential solution to synthesis 3-member ring contains materials.

The first zincosilicate zeolite VPI-7 (VSV) was synthesized by Annen at 1991 contains three-member rings with a framework density 17.1 [98]. Other zincosilicates were successfully synthesized following VPI-7 named VPI-8 (VET), VPI-9 (VNI) [50], and RUB-17 (RSN) [99]. Zincosilicate analogues of aluminosilicate zeolites are also reported for analcime [100], sodalite [101], beta [79, 102, 103], mordenite [104], and ZSM-5 [105-109]. Table 1-1 shows the minimum and maximum member ring units, and pore size of each zincosilicate zeolites.

Table 1-1: The minimum and maximum member ring unit of zincosilicate zeolites with ring levels

Name	Min. MR	Max. MR	Pore Size
VPI-7 (VSV)	3	9	Middle
VPI-8 (VET)	5	12	Large
VPI-9 (VNI)	3	8	Middle
RUB-17 (RSN)	3	9	Middle

The signification advantage of zincosilicates and zincosilicate analogues zeolites over aluminosilicates is the divalent cations balancing the anionic charges of the framework instead of monovalent cations. Unlike aluminosilicates, the $ZnO_{4/2}^{2-}$ tetrahedra has charge -2. In zincosilicates, the -2 charge of each oxygen is shared by one $ZnO_{4/2}^{2-}$ tetrahedra that one divalent cation requires only one $ZnO_{4/2}^{2-}$ tetrahedra. But for aluminosilicates, the contribution of two -1 charge of each oxygen, which is shared between two neighbor $AlO_{4/2}^{-}$ tetrahedrals, is required to pair the divalent cation, Figure 1-3. Theoretically, this divalent cation from zincosilicate framework can provide a stronger acid site than aluminosilicate.

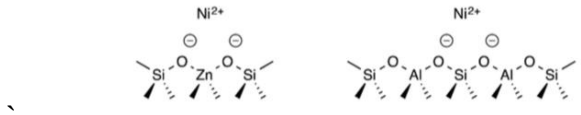

Figure 1-3: Divalent cation comparison between zincosilicate and aluminosilicate

Until recently, there were only a few people in the world investigating the zincosilicate synthesizes, properties, characterizations, and applications. The first zincosilicate zeolite characterization study was the Raman spectroscopy of VPI-7 in 1992 which was investing the stability of three-ring containing zeolitic silica polymorphs [110]. Other zincosilicate zeolites Raman spectroscopies were reported later [111, 112]. Solid state ^{29}Si MAS NMR of

tectozincolicates was studied including zincosilicate zeolite VPI-7 and VPI-9 [113]. In this work, the local structures of zincosilicate zeolites were signed successfully. The diffuse reflectance Ultra-Violet (UV) spectra of VPI-8 was reported due to the zinc oxide is a semiconducting material which has electronic absorptions in the UV region. In the same work, the superficial Si/Zn ratio was measured by X-ray photoelectron spectroscopy (XPS) [114]. The IR spectroscopy of CIT-6, was invested in all the near-, mid-, and far- regions [115]. Also, the near-, mid-, and far- region IR of both VPI-7 and VPI-9 were studied [116]. A Japanese group reported studies on the three-member ring in VPI-7 and *cas* unit in VPI-8 synthesis mechanism by High Energy X-Ray Diffraction (HEXRD,) which measured by a synchrotron [111, 112]. The ionic conductivity was invested by impedance spectroscopy [117]. A generally catalysis by framework zinc in silica-based molecular sieves was reported by FTIR [118].

The only extra-large pore zeolite is phosphate-based molecular sieve VPI-5 which contains an 18-member ring [119]. The industrial application of VPI-5 has not been found yet, due to the low thermal stability. The large pore zincosilicate material VPI-8 (12-member ring) was the first studied on synthesis mechanism, even though it was clarified as high-silica (Si/Zn > 2000) molecular sieve [120]. This is because VPI-8 has a unique “pinwheel” building unit (Figure 1-4) which could lead to extra-large pore molecular sieves synthesis. In the same work, based on the novel “pinwheel” building unit, the hypothetical structures of theoretical extra-large pore analogues of VPI-8 was reported including 14-, 16-, 18-, and 20-member rings with simulated XRD patterns.

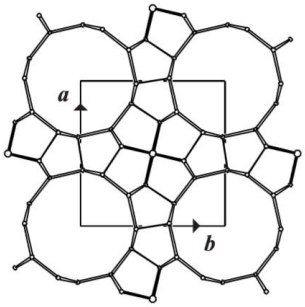

Figure 1-4: The novel "pin-wheel" unit in VET type framework from IZA (http://www.iza-structure.org/databases/ModelBuilding/VET.pdf)

In 1997, the synthesis of VPI-8 studies were separated into two parts at 150 °C: the effects of reaction components and mechanism of crystallization. The influence of zinc cations, inorganic cations, and organic cations were investigated. The zinc cation is necessary in the synthesis reaction mixture. Without the zinc cation, MTW will be formed either with or without seed. Also, the choice of silica source was mentioned in this work. Small amount (overall yield is about 6%) of BEA was found in with-seed synthesis in the absence of zinc cation. This could be caused by the impurity Al in silica source, which is Ludox colloidal silica. The beta phase could be eliminated by using fumed silica (Cab-O-Sil, M-5), which only contains 2-4 ppm Al. Three common inorganic cations were compared, which are Li^+, Na^+, and K^+. All these three cations can function countering balance charge created by the framework. VPI-8 could be synthesis by adding either Li^+ or Na^+, but the K^+ is the inhibitor in VPI-8 synthesis. The reaction is sensitive to Li^+ concentration. Either low or high Li^+ concentration could course a slower crystallization rate. TEA^+ is VPI-8 preferred organic cations [121]. The mechanism of crystallization study was focused on synthesis time: 48, 52.5, 72 and 96 hours. Because it is hard to observe the changes in XRD patterns, the local environment was studied by solid state ^{29}Si MAS NMR. Two resonances at -65 and -95 ppm are the major differences. The resonances around -65 and -95 ppm are assigned to so-called Si(4Zn) of "phase B" and Si(1Zn) of "phase A", respectively. The peak around -65 ppm is increased slowly

from 48 to 96 hours. The peak around -95 ppm increases rapidly first from 48 to 52.5 hours, then decreases to disappear from 52.5 to 96 hours. However, the resonance around -95 ppm of as-made VPI-8 at 150 °C for 52.5 hours could be eliminated by HCl wash. For contrast, the solid state ^{29}Si MAS NMR of synthesis at 135 °C at 3, 6, 7, and 8 days are reported. The resonance around -95 ppm changes slowly from 3 to 7 days, but increases rapidly at 8 days. It is not clear why this happened, so the resonance around -95 ppm is called "phase B". Meanwhile, the Si/Zn ratio of between superficial and bulk are different [114].

Davis' group attempted to synthesis extra-large pore zincosilicate zeolite based on the novel unique "pinwheel" building structure in VPI-8. Two years later, a large pore zincosilicate analogue CIT-6, which has a *BEA topology, was found in attempting to synthesis extra-large pore zincosilicate molecular sieve from the base line VPI-8 [102, 103]. CIT-6 could be synthesized by using the same chemicals in VPI-8 synthesis, but the components and conditions are different. For CIT-6 synthesis, both Zn^+ and Li^+ concentrations have a critical range. Comparing with VPI-8 synthesis, CIT-6 is formed prior to VPI-8 at a lower temperature and higher TEA^+ concentration. The aging procedure was important for CIT-6 crystallization. Silica source could be a variation in aging due to different Al^{3+} or Na^+ contains. A low Al (2-4 ppm) containing silica source could be used. The aging mixture color is cloudy by using low Al containing fumed silica at room temperature, but the color can be changed to clear at 80 °C for 3 hours. A clear solution is required to prepare CIT-6, and a cloudy solution is a VPI-8 preferred [102]. In 2002, the mechanism of CIT-6 and VPI-8 crystallization was reported [122]. CIT-6 could be understood as an intermedium phase in VPI-8 synthesis. At 140 °C, 12% crystallinity CIT-6 with amorphous was observed for 92 hours, and 100% crystallinity CIT-6 was observed at 164 hours. For longer time at 140 °C, such as 189 hours, 25% crystallinity VPI-8 were found with 75% crystallinity CIT-6. For 137 hours

synthesis, a well-defined pseudo-cubic morphology is observed with the crystal size about 1 μm. For 189 hours synthesis, the needle-shaped crystals were found with pseudo-cubic morphology. This needle-shaped crystal was assigned to VPI-8. Also, the CIT-6 and VPI-8 phases change could be observed in XRD patterns.

In 2014, a Japanese group reported a seed-directed OSDA-free synthesis of VPI-8, and attempted to broaden the applicable scope of zincosilicate zeolites [112]. High crystallinity VPI-8 could be synthesized by adding co-cations (Li^+ and Na^+) in the absence of OSDA TEAOH. This with-seed synthesis time could be decreased to 80 hours with 38% yield, which Si/Zn ratio is 13.5. In this work, a zincoaluminosilicate type VPI-8 zeolite could be prepared by adding commercial high-silica FAU type zeolites (Si/Al > 800). This zincoaluminosilicate yield is also low (31.4%) with Si/Zn ratio is 14.2 and Si/Al ratio is 295. A unseeded synthesis was tried and resulted in dense phase material - either magadiite or kenyaite. The solid state ^{29}Si MAS NMR spectra shows a much more reasonable result than previous studies on with-seed synthesis [114, 121]. The "phase B" resonance around -95 ppm was not found. However, this seed-direct OSDA-free synthesis is not truly "OSDA-free". Because the OSDA TEAOH is required to prepared the seed crystal VPI-8. The OSDA is not avoid completely in this synthesis.

Due to the thermal stability, only a few zeolites of the whole zeolite family can be used in high temperature (>200 °C) applications. Zincosilicate VPI-7 and RUB-17 have the same disadvantage – thermal stability. The structure of as-made VPI-7 and RUB-17 will collapse at 250 °C and 220 °C, respectively. It is interesting to notice that both VPI-8 and VPI-9 are thermally stable up to 650 °C [123]. Also, zincosilicate analogue CIT-6 is thermally stable up to 650 °C. Thus, VPI-8, VPI-9 and CIT-6 show the potential for high temperature applications in the future.

It should be mentioned that VPI-9 synthesis required a rubidium cation which is an expensive element. The chemicals cost of synthesizing as-made VPI-9 is at least $90/g.

To date, for applications, both ion exchange and gas adsorption have been reported by using zincosilicate VPI-7 and VPI-9 [124]. Zincosilicate analogues CIT-6 (*BEA) had been proved for catalyzing two reactions. One is dehydrogenation of propane over Pt-CIT-6 [125]. The other one is oligomerization of propylene on Ni-CIT-6 [126]. No other investigations for catalysis of either zincosilicate or zincosilicate analogue materials have been done. The bulk of what has been reported on zincosilicates can be found in only 19 publications about zincosilicate materials that covers synthesis, properties, characterization, and applications [50, 98-100, 102, 103, 111-115, 118, 120-122, 124, 127-129].

CIT-6 is the most studied zincosilicate material, even though zincosilicate molecular sieves are not well studied yet. CIT-6 (*BEA) has the same topology with industrial aluminosilicate zeolite beta (BEA), which has a large-pore (10-member rings) with a 3-D diffusion property. Or the original zincosilicate, VPI-8 shows the most potential for high temperature applications due to the thermal stability and low chemical material cost. Currently, the challenge of VPI-8 synthesis is how to prepare pure phase uniform VPI-8 in a short time with low Si/Zn ratio conveniently.

Hypothesis

Zincosilicates offer unique properties, such as divalent cationic acid sites, that have potential to make them excellent catalysts. VPI-8 is the most thermally stable of the reported zincosilicates, but it requires prohibitively long synthesis times or seeded synthesis procedures. There is a potential to improve VPI-8 synthesis through variables such as synthesis temperature,

synthesis time and SDA concentration as well as minor variables such as different types of inorganic species. As a result, the seed-free short time synthesis of pure phase zincosilicate zeolite VPI-8 should be achieved.

Chapter 2 - Zeolites Characterizations

X-Ray Diffraction (XRD)

XRD is a technique used to analyze material crystalline structure. Each crystal has its own XRD pattern, like "fingerprint". The principle behind XRD is the Bragg's law:

$$2 \cdot d \cdot \sin(\theta) = n \cdot \lambda \qquad (2.1)$$

Where d is the crystal lattice spacing, θ is the angle of incidence, n is the number of wavelengths (integer), and λ is the wavelength of the X-ray, Figure 2-1.

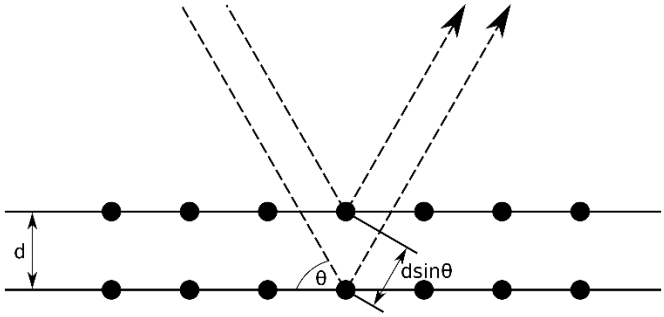

Figure 2-1: Scheme of Bragg's law

As-made samples were dried overnight at 50 °C, then grinded to very fine powder by mortar and pestle to reduce the preferred orientation. Then samples were pressed into 1 mm deep magnetically rotational sample holder was filled full of sample powder. Then, a spatula was used to make sure the height of sample powder is even with the sample holder. After the sample was prepared, sample holder was set on the magnetically rotational carousel (automatic 6 position

sample changer with spinner). For calcined sample preparation, samples were calcined at 550 °C overnight after drying but before grinding. To reduce the experimental error, the sample powder was measured with rotation and repeat start over three times which starting with grinding. XRD analysis was completed by using Rigaku Miniflex II desktop X-ray diffractometer with Cu Kα radiation. Data were measured in rotation under the condition 30 kV and 15 mA with a 2°/min scanning rate.

Scanning Electron Microscopy (SEM)

The morphology of a material could be studied by SEM. First, a piece of electrically conductive tape was stuck on a sample holder. Then, calcined sample powder was placed on the electrically conductive tape. The compressed nitrogen gas was blown to remove the unstuck sample powder. Next, the prepared sample holder was transferred to the SEM chamber. After the SEM chamber pressure reached a ultravacuum, the measurement condition set to 15 kV and 9.0 mm. SEM was performed on Hitachi S-3500, Figure 2-2. The SEM figures were collected by the electron microscopy facility Ravindra Thakkar at Nanotechnology Innovation Center of Kansas State (NICKS).

Figure 2-2: Hitachi S-3500 SEM apparatus

Nuclear Magnetic Resonance (NMR)

Solid state NMR is the technique to study the local environment in a structure. TMS was used for ^{29}Si calibration. The ZrO_2 rotor was dipped in 3 M HCl for overnight, then was rinsed by DI water. Before the grinded calcined sample powder filling into the rotor, the rotor was washed by acetone then ethanol. Because the Si atoms are hard to relax, the measurement was maintained for 7 days each sample. Deconvolutions of the spectra were performed by using the Lorentzian-gaussian fitting from TopSpin software. Both ^{1}H and ^{29}Si ss-NMR was performed on Bruker Avance III spectrometer, Figure 2-3. The resonance result was collected by the director of the NMR core laboratory Justin T. Douglas at University of Kansas.

Figure 2-3: NMR apparatus

X-Ray Photoelectron Spectroscopy (XPS)

XPS is a surface technique. In this experiment, the super surface chemical composition was studied by XPS. Calcined sample powder was pressed on the electrically conductive tape, then taped on a sample holder. Next, the sample was vacuumed overnight in the transfer chamber before moving into the main chamber. The instrument was calibrated by testing binding energies of standard sample (half gold and half copper foil), which are Cu 2p3/2 (932.7 eV) and Au 4f7/2 (84.0 eV). This calibration was completed before measuring other samples. Sample was measured at Ultra-High Vacuum (UHV) condition, which is about 2.1×10^{-8} torr. The electrical gun operation condition is 300 W (15 kV and 20 mA). The elements were measured below: C (1s), Li (1s), O (1s), Zn (2p3), and Si (2s). XPS was performed on PerkinElmer PHI 5400 by achromatic Al Kα radiation source (1486.6 eV), Figure 2-4.

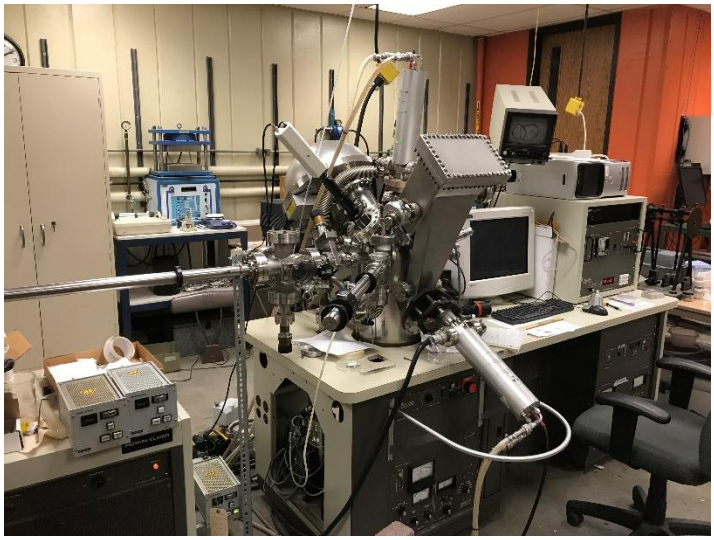

Figure 2-4: PerkinElmer PHI 5400 XPS apparatus

Chemical Analysis

Both short and long VPI-8 were sent to Galbraith Laboratories, Inc. for bulk elemental analysis. GLI procedure ME-70 was applied in Inductively Coupled Plasma Optical Emission Spectroscopy (ICP-OES). The reported error was below 100 ppm.

Chapter 3 - Experiments and Results Discussion

Introduction

In this work, a short time seed-free high crystallinity high yield synthesis of VPI-8 will be presented. Two major variations of temperature and SDA concentration will be compared. Some minor variations also will be studied such as type of zinc source, type of silica source, and water concentration.

Overview of Experiments

Chemicals

The materials used for large seed-free VPI-8 include zinc acetate (Fisher), zinc oxide, (Fisher), lithium hydroxide (Fisher), Tetraethylammonium hydroxide (Sigma-Aldrich), colloidal silica (Ludox, HS-40, Sigma-Aldrich) and powder silicate (Syloid FP-63, Grace). For seed-synthesis, NaOH (Fisher) is also used.

Experiment setup

The zincosilicate gel was prepared as follows. After the LiOH was dissolved in water, $Zn(CH_3COO)_2 \cdot 2H_2O$ was added and stirred. Then, TEAOH was added in and stirred until all the solid was disappeared. Next, SiO_2 was added and the reaction mixture was stirring at least 2.5 hours for aging. After the homogeneous phased of the mixture was obtained, the gel was

transferred to a 23 ml or 45 ml Teflon-lined stainless autoclave (Parr, Inc.). The mixture was heated at 150-200 °C. After the hydrothermal treatment, the as-made VPI-8 was recovered by filtration with water and dried at 50 °C for at least 24 hours. The VPI-8 product was calcined at 550 °C and maintained at least 6 hours. Table 3-1 shows the experiment phase results. Exp. 6 and exp. 18 are the baseline, which are from previous work [120]. Each experiment was repeated as least three times to test the reproducibility. Only with-seed synthesis was not reproducible, as will be further discussed in the following sections.

Table 3-1: Reaction composition for VPI-8 synthesis with mole ratio: a LiOH : b $Zn(CH_3COO)_2 \cdot 2H_2O$: c TEAOH : SiO_2 : d H_2O

Exp.	A	b	c	d	T (°C)	Time (hr)	Phase
1	0.2	0.1	0.4	30	200	6	VPI-8
2	0.2	0.1	0.4	30	200	48	VPI-8
3	0.2	0.1	0.4	30	200	240	VPI-8
4	0.2	0.1	0.4	30	175	12	amorphous
5	0.2	0.1	0.4	30	175	240	VPI-8
6	0.2	0.1	0.4	30	150	240	VPI-8
7	0.2	0.1	1.18	30	200	17.5	VPI-8 + amorphous
8	0.3	0.1	0.4	30	200	24	VPI-8
9	0.2	0.1	0.78	30	200	36	VPI-8
10	0.2	0.01	0.4	30	200	55	Unknown
11	0.2	0.01	0.4	30	175	55	Impurity VPI-8
12	0.2	0.01	0.4	30	150	55	VPI-8
13	0.2	0.1	0.78	30	200	24	VPI-8
14	0.2	0.1	0.78	30	200	48	VPI-8
15*	0.26	0.036	0.78	21	150	36	amorphous
16*	0.26	0.036	0.78	21	150	60.5	amorphous + VPI-8
17*	0.26	0.036	0.78	21	150	120	VPI-8
18*	0.26	0.036	0.78	21	150	260	VPI-8
19*	0.26	0.036	0.78	21	200	36	Disorder phase
20*	0.26	0.036	0.78	21	200	120	VPI-8
21*	0.26	0.036	0.78	21	200	260	Disorder phase

*with 0.4 wt.% seed synthesis, NaOH is used instead of LiOH

Comparison to published work

VPI-8 was originally reported as high-silicate zeolite with a Si/Zn ratio > 2000 [120]. Later, a mechanistic study on VPI-8 was investigated by Davis's group [114, 121]. In this work, zinc cations, inorganic cations, organic and organometallic cations were studied. The Si/Zn ratio of seed product is near 12. The Si/Zn ratio of with-seed synthesis VPI-8 is 19, and the size is approximately 4 μm. VPI-8 synthesis time is around 52.5 hours, which was proposed as the shortest time for seed product synthesis. The with-seed VPI-8 synthesis required 10 days. The yield of seed-product and large VPI-8 are 91% and 99%, respectively.

In 2014, a Japanese group reported an SDA-free synthesis mechanism [112]. The idea of this work is using a VPI-8 seed crystal to direct the crystal growth instead of using SDA. However, the synthesis of the seed crystal still required SDA. The Si/Zn ratio of this SDA-free synthesis is about 13.6. The highest yield was reported as 38%. The synthesis time was 144 and 80 hours for seed-product and SDA-free VPI-8, respectively. For both synthesis mechanisms, the seed-product has to be prepared by filtration then calcination before synthesizing large and well crystallized VPI-8. This process usually need 24 hours to complete. Therefore, the minimum time requires to synthesis VPI-8 is 10 days. In addition, high crystallinity VPI-8 synthesis requires a two-step synthesis process – one step to synthesize the seed crystals and one step to synthesize the final crystal.

The previous work synthesis temperature was either 135 °C, 140 °C or 150 °C [112, 114, 120-122, 130, 131]. Due to the low temperature synthesis, the crystal growth rate was slow. For low temperature synthesis, 135 °C is an awkward phasing zincosilicate analogous CIT-6 preferred condition; and VPI-8 could be synthesized at 150 °C for a longer time, since the short time could cause a CIT-6 or CIT-6 and VPI-8 mixing phases [122, 131].

XRD results of VPI-8 samples

Figure 3-1 shows the XRD pattern of as-made short-time synthesized VPI-8, and Figure 3-2 shows the calcined pattern. All the peaks of calcined sample are sharper than as-made sample. Also, the calcined VPI-8 has one more peak at $2\theta = 15.06°$, and a clearer peak than as-made VPI-8 at $2\theta = 19.04°$. XRD pattern of long VPI-8 is shown in Figure 3-3. And the calcined long VPI-8 appears the same change as short VPI-8 that has sharper peaks, has one more peak as 15.06°, and a clearer peak at $2\theta = 19.04°$. These XRD pattern variations may be caused by the water and TEA^+ contain in samples. Table 3-2 shows the formulas to synthesize both short and long VPI-8. No amorphous phase was found. Also, intermediate phase, such as CIT-6, and other impurity phases, such as kenyaite and magadiite, were not found in XRD results.

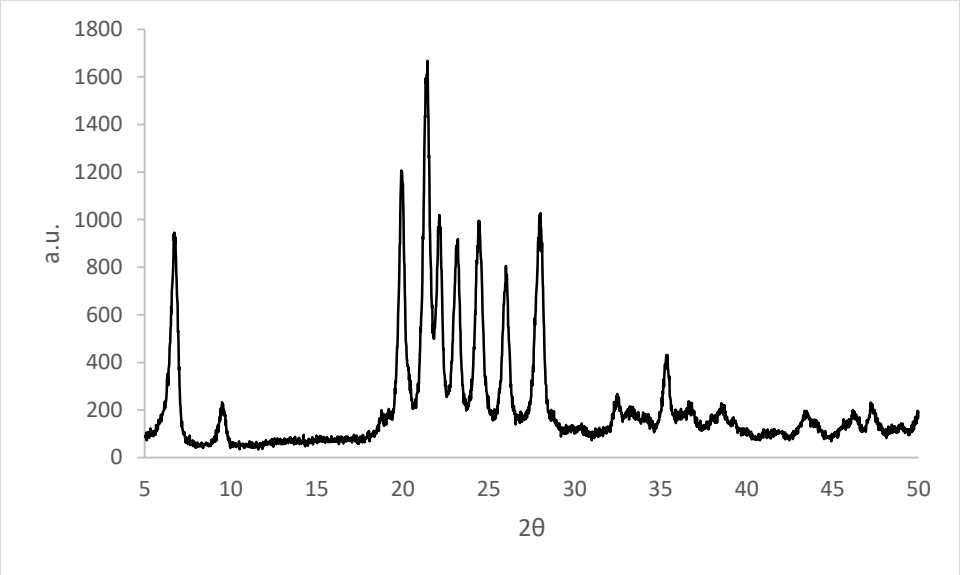

Figure 3-1: XRD pattern of as-made VPI-8 at 200 °C for 6 hours, reaction composition: 0.2 LiOH : 0.1 $Zn(CH_3COO)_2 \cdot 2H_2O$: 0.4 TEAOH : SiO_2 : 30 H_2O (exp. 1)

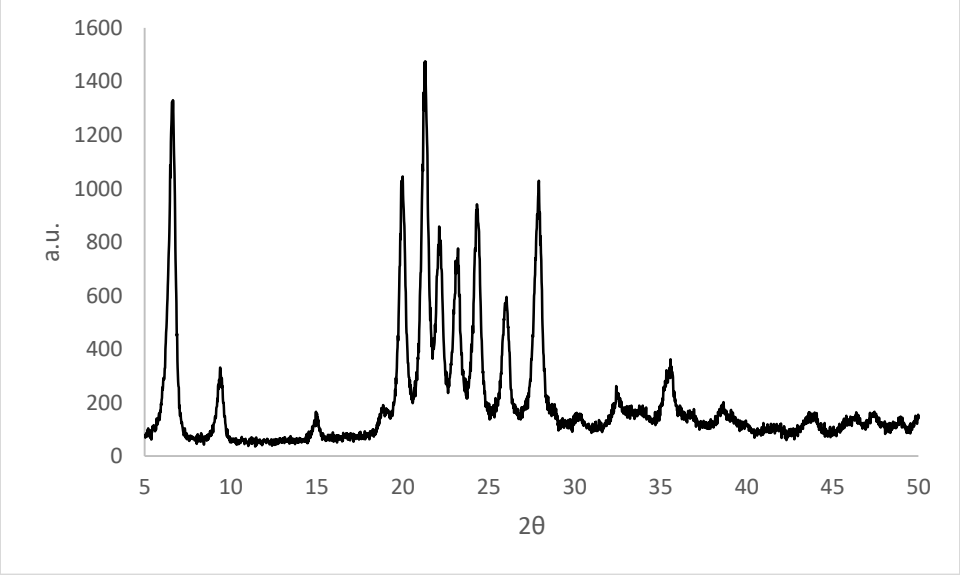

Figure 3-2: XRD pattern of calcined VPI-8 at 200 °C for 6 hours, reaction composition: 0.2 LiOH : 0.1 $Zn(CH_3COO)_2 \cdot 2H_2O$: 0.4 TEAOH : SiO_2 : 30 H_2O (exp. 1)

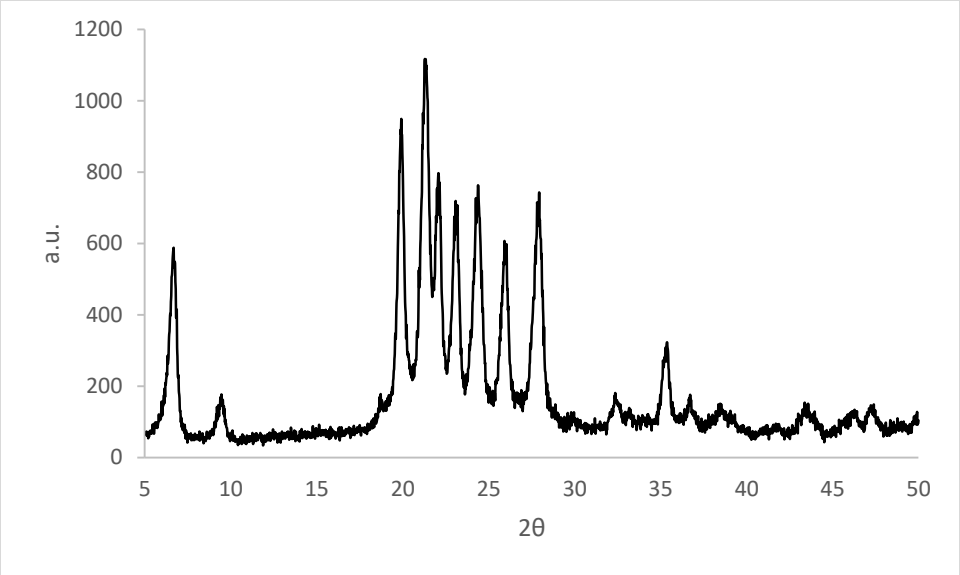

Figure 3-3: XRD pattern of as-made VPI-8 at 200 °C for 24 hours, reaction composition: 0.2 LiOH : 0.1 $Zn(CH_3COO)_2 \cdot 2H_2O$: 0.78 TEAOH : SiO_2 : 30 H_2O (exp. 14)

Table 3-2: Reaction composition and temperature for both short and long VPI-8 synthesis with mole ratio: a LiOH : b $Zn(CH_3COO)_2 \cdot 2H_2O$: c TEAOH : SiO_2 : 30 H_2O

Exp.	a	b	c	T (°C)	Time (hr)	Phase
1	0.2	0.1	0.4	200	6	VPI-8
10	0.2	0.1	0.78	200	36	VPI-8

XRD results for non-VPI-8 samples

VPI-8 was claimed as a high-silica molecular sieve zeolite, where the Si/Zn ratio is higher than 2000 [120]. High-silica zeolites have their particular advantages than either aluminosilicate or zincosilicate zeolites, such as purification catalysts for high temperature exhaust gases. Thus, the synthesis of high-silica VPI-8 for a short time at high temperature becomes to be an attractive study. In order to increase the Si/Zn ratio, the concentration of Si:Zn was increased in the initial solution mixtures. Table 3-3 shows the three temperatures are studied in this work.

With a reaction temperature at 200 °C, the final product phase is completely changed, when the Zn/Si mole ratio of the initial solution was decreased to 0.01. An unknown product was observed via XRD pattern, Figure 3-4. This unknown product has peaks which have extreme high intensity at 2θ = 26.66° and high intensity at 2θ = 20.90°, 25.02°, and 25.10°. Hence, VPI-8 can not be synthesized at high temperature with a Zn source shortage. It is noticed that this unknown product is thermal stable until at least at 550 °C. When the synthesis temperature is decreased to 175 °C, an impurity VPI-8 XRD pattern was observed, Figure 3-5. Three peaks at 2θ = 11.84°, 12.76°, and 29.9° do not belong to VET phase. Besides, the relative intensities (I/I_0, I is the peak intensity, and I_0 is the highest peak intensity overall) is too high at 2θ = 9.51° and 36.26°, which are 0.30 and 0.15, respectively. The relative intensities for as-made VPI-8 at 2θ = 9.51° and 36.26° are 0.12 and 0.10, respectively. It implies that other phases are formed during the synthesis which cause the XRD pattern overlap each other to generate the higher relative intensities. For comparison, at 150 °C synthesis with this low Zn/Si mole ratio, a VPI-8 XRD pattern was observed, Figure 3-6.

Table 3-3: Reaction composition for non-VPI-8 synthesis with mole ratio: a LiOH : b $Zn(CH_3COO)_2 \cdot 2H_2O$: c TEAOH : SiO_2 : 30 H_2O

Exp.	a	b	c	T (°C)	Time (hr)	Phase
11	0.2	0.01	0.4	200	55	Unknown
12	0.2	0.01	0.4	175	55	Impurity VPI-8
13	0.2	0.01	0.4	150	55	VPI-8

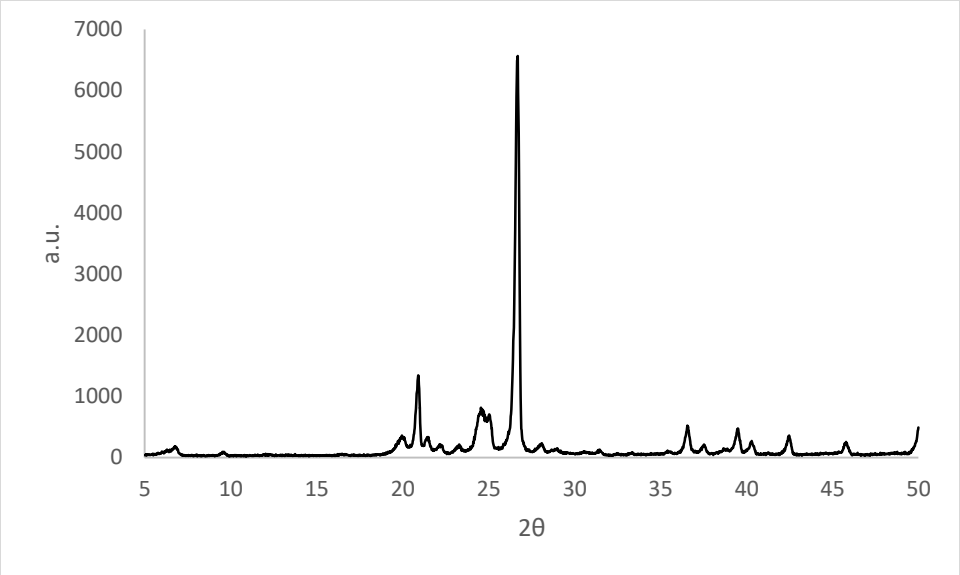

Figure 3-4: XRD pattern of the unknown phase synthesis at 200 °C for 55 hours, reaction composition: 0.2 LiOH : 0.01 $Zn(CH_3COO)_2 \cdot 2H_2O$: 0.4 TEAOH : SiO_2 : 30 H_2O (exp. 11)

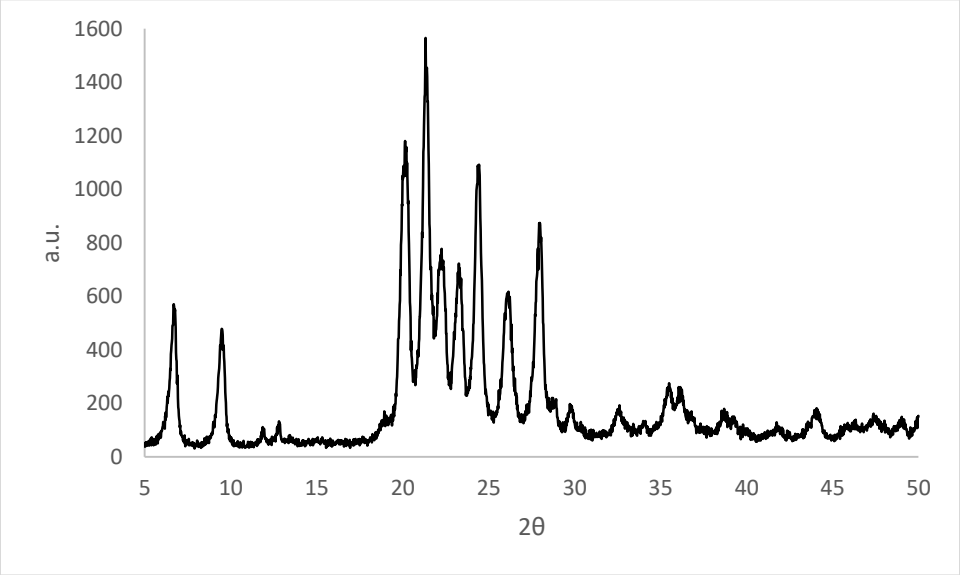

Figure 3-5: XRD pattern of as-made impurity VPI-8 synthesis at 175 °C for 55 hours, reaction composition: 0.2 LiOH : 0.01 $Zn(CH_3COO)_2 \cdot 2H_2O$: 0.4 TEAOH : SiO_2 : 30 H_2O (exp. 12)

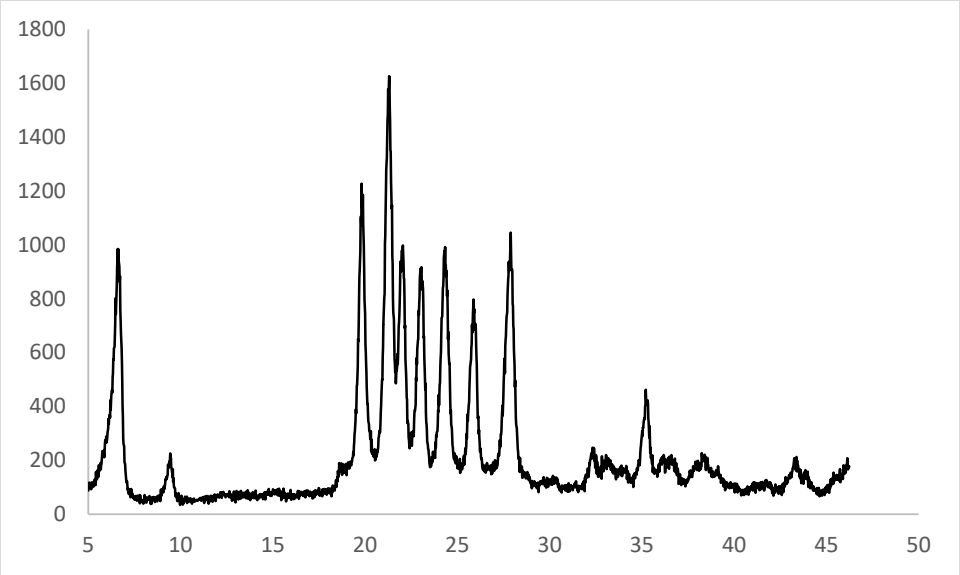

Figure 3-6: XRD pattern of as-made VPI-8 synthesis at 150 °C for 55 hours, reaction composition: 0.2 LiOH : 0.01 $Zn(CH_3COO)_2 \cdot 2H_2O$: 0.4 TEAOH : SiO_2 : 30 H_2O (exp. 13)

Influence of temperature effects

Table 3-4 and Table 3-5 show comparisons with different synthesis times at high temperature. At 150 °C (exp. 6), VPI-8 requires long time synthesis like 240 hours. When reaction temperature increases to 175 °C, VPI-8 still can not be synthesized at 12 hours (exp. 4). In Figure 3-7, two broad peaks at $2\theta = 33.58°$ and 35.38° was observed in the amorphous phase. These two peaks imply the crystal structure is forming at 12 hours. VPI-8 could be successful synthesized at 175 °C for 24 hours the same as low temperature synthesis (150 °C). For a higher temperature at 200 °C, VPI-8 could be synthesized for 240 hours similarly, Figure 3-8. A 48 hours synthesis at 200 °C was attempted and resulted VPI-8. Next, the synthesis time could be decreased to 6 hours (exp. 1). For the synthesis time below 6 hours at 200 °C, only amorphous and partial VPI-8 phases were observed. It indicates that VPI-8 is directly made from amorphous phase without an

intermediate phase. There was not a significant improvement for longer time synthesis (240 hours) comparing with short time (6 hours) at high temperature by contradistinguishing XRD patterns, exp. 3 (Figure 3-8) and exp.1 (Figure 3-1), respectively. The XRD pattern of 240 hours synthesis was only slightly sharper than 6 hours synthesis at 200 °C. For additional comparison, VPI-8 was synthesized at 150 °C for 10 days (exp. 6). The XRD patterns of both synthesis at 2 °C for 240 hours (Figure 3-9) and 200 °C for 6 hours (Figure 3-1) are similar.

Table 3-4: Synthesis temperature study on short VPI-8 with reaction composition mole ratio: a LiOH : b $Zn(CH_3COO)_2 \cdot 2H_2O$: c TEAOH : SiO_2 : 30 H_2O

Exp.	a	b	c	T (°C)	Time (hr)	Phase
1	0.2	0.1	0.4	200	6	VPI-8
2	0.2	0.1	0.4	200	48	VPI-8
3	0.2	0.1	0.4	200	240	VPI-8
4	0.2	0.1	0.4	175	12	amorphous
5	0.2	0.1	0.4	175	240	VPI-8
6	0.2	0.1	0.4	150	240	VPI-8
8	0.3	0.1	0.4	200	24	VPI-8

Table 3-5: Synthesis temperature study on long VPI-8 with reaction mole ratio: a LiOH : b $Zn(CH_3COO)_2 \cdot 2H_2O$: c TEAOH : SiO_2 : 30 H_2O

Exp.	a	b	c	T (°C)	Time (hr)	Phase
7	0.2	0.1	1.18	200	17.5	VPI-8 + amorphous
10	0.2	0.1	0.78	200	36	VPI-8
14	0.2	0.1	0.78	200	24	VPI-8
15	0.2	0.1	0.78	200	48	VPI-8

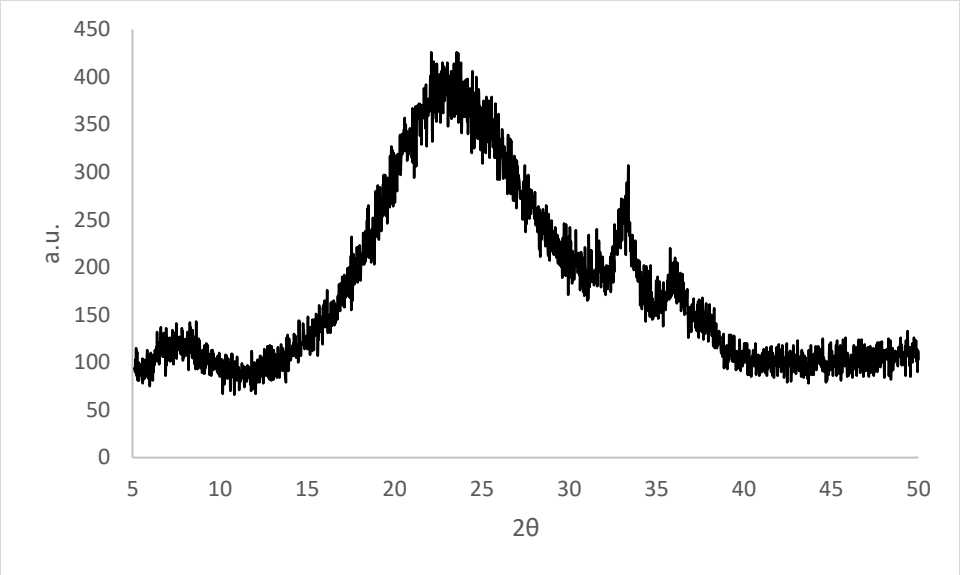

Figure 3-7: XRD pattern of as-made VPI-8 at 175 °C for 12 hours, reaction composition: 0.2 LiOH : 0.1 $Zn(CH_3COO)_2 \cdot 2H_2O$: 0.4 TEAOH : SiO_2 : 30 H_2O (exp. 4)

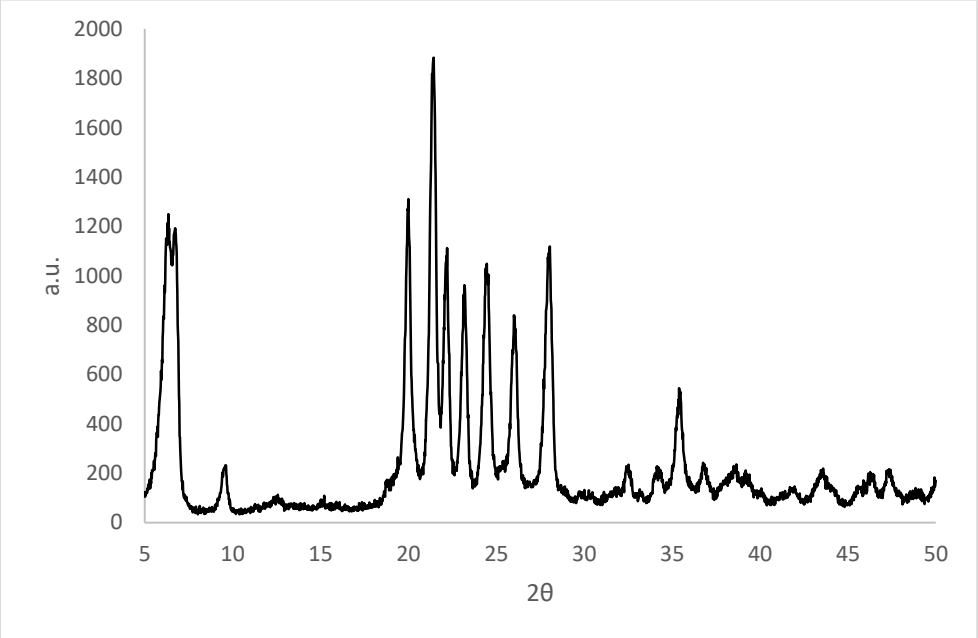

Figure 3-8: XRD pattern of as-made VPI-8 at 200 °C for 240 hours, reaction composition: 0.2 LiOH : 0.1 $Zn(CH_3COO)_2 \cdot 2H_2O$: 0.4 TEAOH : SiO_2 : 30 H_2O (exp.3)

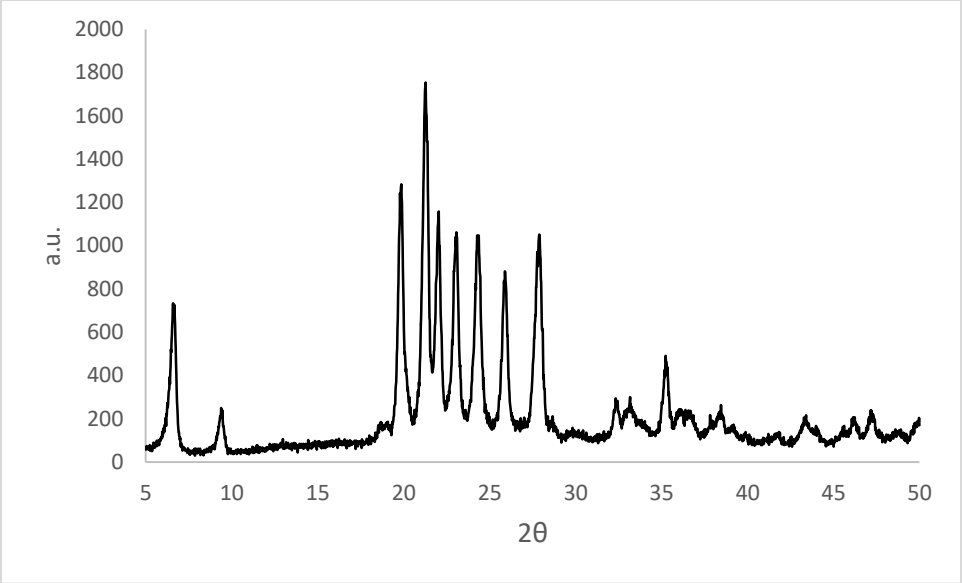

Figure 3-9: XRD pattern of as-made VPI-8 at 150 °C for 240 hours, reaction composition: 0.2 LiOH : 0.1 $Zn(CH_3COO)_2 \cdot 2H_2O$: 0.4 TEAOH : SiO_2 : 30 H_2O (exp.6)

A high concentration TEAOH in the reaction mixture is able to synthesize long VPI-8, exp. 14. Due to the increased length of VPI-8 crystal, it required a longer synthesis time. The long VPI-8 can be synthesized at 200 °C for 24 hours (exp. 14). XRD patterns of short and long VPI-8 are similarly, Figure 3-1 and Figure 3-3, respectively. More details will be discussed in the morphology section.

Temperature plays a significate role in synthesis of zeolite. The expected zeolite can only be synthesized in a specific temperature range. With low Zn concentration, phase changes take place at high temperature, Table 3-3, which is discussed in section above. Previous publications were focused on lower synthesis temperature at 135 °C, 140 °C or 150 °C [112, 114, 120-122, 130, 131]. Temperature appears to play a remarkable role in VPI-8 synthesis as a small temperature reduction (e.g. 10 °C to 15 °C) can preferentially form the product phase CIT-6 (*BEA) phase [122, 131]. CIT-6 is known as an intermediate phase of the final product VPI-8. Therefore, in this work, high reaction temperatures are investigated at both 175 °C and 200 °C to avoid the intermediate phases occurring during synthesis. Also, impurity phases are another difficulty to

overcome. There are two impurity phases reported before, kenyaite and magadiite [112]. Even with 10 wt.% seed synthesis, a kenyaite peak 2θ below 5° was observed for 120 hours with the identical hydrothermal condition in Table 3-7. At high temperature condition (200 °C and 175 °C), neither the intermediate phase or nor the impurity phases, such as CIT-6, kenyaite, and magadiite, were observed.

In addition to the impact on the phase changes, the nucleation and crystal growth is also affected by the crystallization temperature significantly [72, 73]. The higher temperature decreases the zeolite crystallization time by increasing both crystal nucleation rate and crystal growth rate. Silica solubility is notably affected by temperature as well [74]. The shorter nucleation and crystallization time can be achieved by the easier silica dissolving in the mixture at higher heating temperature. Moreover, as the higher crystal growth rate is achieved, larger crystals can be formed. For example, the relation between growth rate and temperature was studied on NaX synthesis in four different temperatures. The growth rates at 100 °C, 90 °C, 80 °C, and 70 °C are approximately 5.00 μm/day, 2.86 μm/day, 1.82 μm/day, and 0.91μm/day, respectively [75].

Temperature can not only influence the crystal size, but also the morphology of crystals. For instance, the length/width ratio of silicalite-1 (MFI) can be increased at higher temperature, which the crystal growth kinetic was studied based on different activation energies [76, 77]. Accordingly, it may be another reason that both short and long VPI-8 are longer than the previous studies. Also, long VPI-8 is needle shape form instead of the bulk shape. Consequently, VPI-8 can be synthesized at high temperature for a short time.

Influence of Zn and Si source

Different zinc and silica sources were used during the synthesis. Differences were observed depending on both the zinc and silica source as well as the aging procedure used. There were two different aging orders tried in this experiment:

Procedure 1:
$H_2O \rightarrow LiOH \rightarrow Zn(CH_3COO)_2 \cdot 2H_2O \rightarrow TEAOH \rightarrow SiO_2$

Procedure 2:
$H_2O \rightarrow LiOH \rightarrow TEAOH \rightarrow Zn(CH_3COO)_2 \cdot 2H_2O \rightarrow SiO_2$

The molar ratio of chemical components was identical in both procedure 1 and 2. At the beginning, water was added in liner to dissolve LiOH powders. In both procedures, all LiOH powders were completely dissolve, and solution color was clear. The order of adding zinc acetate and TEAOH was different between procedure 1 and 2. In procedure 1, zinc acetate was added before TEAOH. The solution color changed to light milk color after adding zinc acetate. However, the solution color became colorless again after adding TEAOH, then returned to milk color in about half hour, which was whiter than before. While, the more TEAOH was added in the solution, the longer time was needed to return back to milk color. The mixture was stirred about 1 hours, then SiO_2 was added in, with no color changing. This solution was well mixed in 2 hours. Unlike procedure 1, TEAOH was added in liner before zinc acetate, and the solution color retained as colorless. Few small “rectangle” or “needle” shape shine crystals could be observed floating on the top of the solution after about 4 hours. After SiO_2 was added, the solution turned to “colorless ointment” color, not as white as procedure 1. In procedure 2, the stirring speed had to be fast, and stirring bar had to be the same size of liner. Because undissolved SiO_2 gel could be found at bottom

if the stirring speed was slow, and between outside of stirring region and the corner of liner if the stirring bar was too short. Aging could not be finished in 12 hours. Otherwise, undissolved SiO_2 could be observed. It does not matter how long the aging was (12 hours to 36 hours), undissolved white powder, which did not appear before, could be found at the bottom near stirring bar. Most powder could not be dissolved in water when the liner was washed, Figure 3-10. Figure 3-11 shows the XRD pattern of the unknown crystal. There is a broad high peak at $2\theta = 17.78°$.

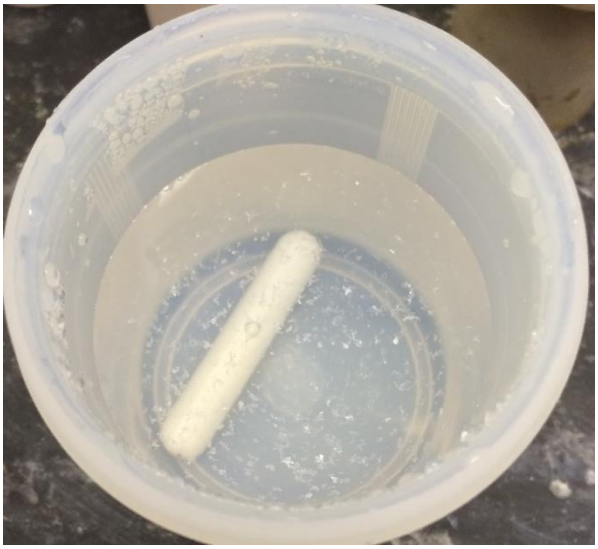

Figure 3-10: Undissolved floating aging powder in water

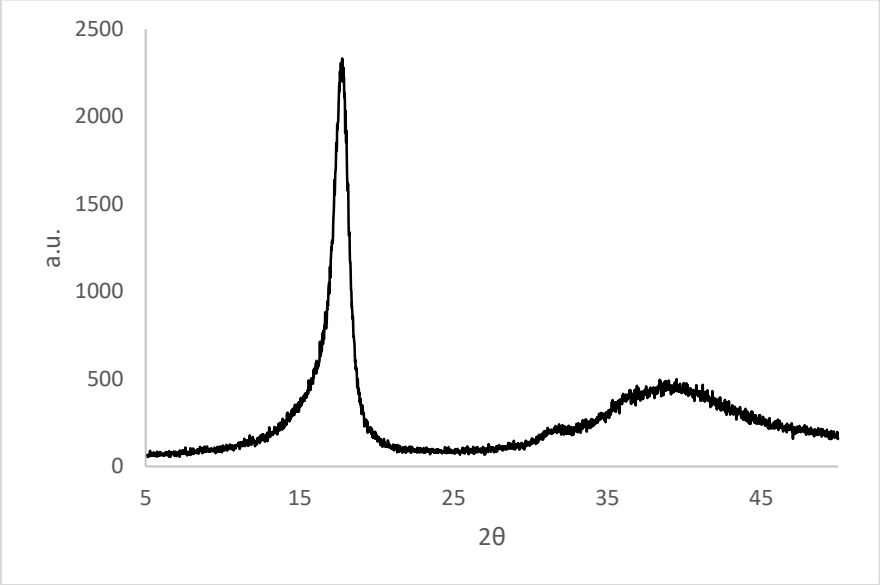

Figure 3-11: XRD pattern of the undissolved aging powder in water

Since the aging mixture could be influenced by the Na^{+} or Al^{3+} in the silica source [102, 121, 122], the colloidal silica Ludox HS-40 was replaced by a pharmaceutical amorphous silica Syloid 63-FP as the new silica source, which has been added as the silicon source for synthesizing zincosilicate zeolite VPI-9 and other zeolites. Syloid FP-63 can provide a very large amorphous silica surface area. Further, ZnO powder was used as the new zinc source instead of zinc acetate. Neither new silica source nor zinc source could overcome the unknown crystal in procedure 2. However, either procedure 1 or procedure 2 could form VPI-8 eventually. The only difference is the XRD pattern $2\theta = 6.66°$ of ZnO synthesis is broader then Syloid FP-63 synthesis, Figure 3-12 and Figure 3-13, respectively. Different zinc source or silica source could still make VPI-8. Both procedure 1 and procedure 2 could result VPI-8 products with XRD patterns that are very similar with short VPI-8. It is not clear why these crystals appear during aging, but the XRD patterns show the product after hydrothermal reaction is still VPI-8.

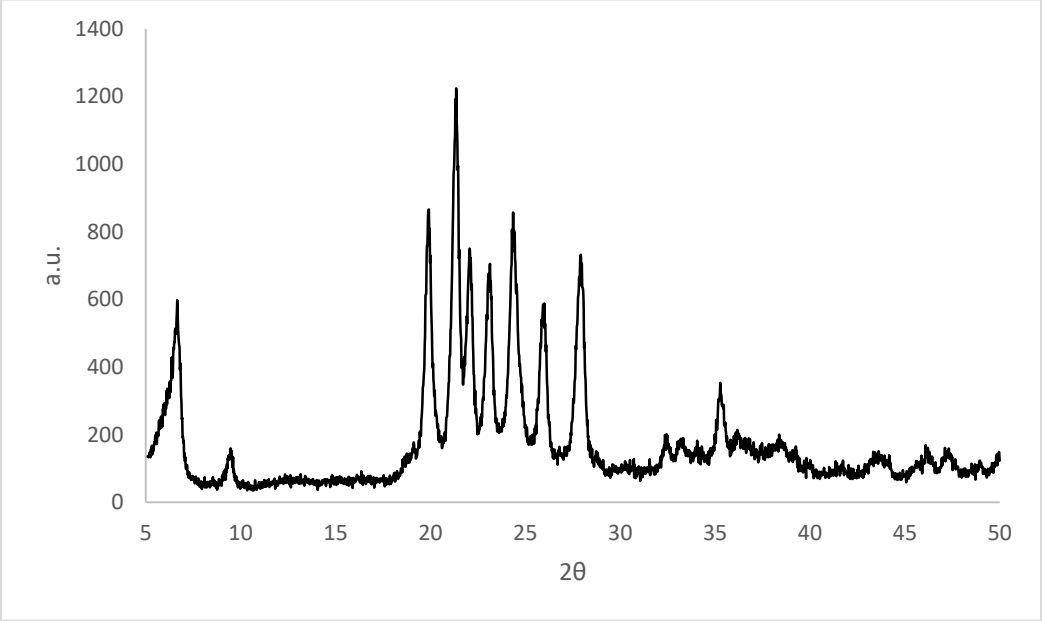

Figure 3-12: XRD pattern of ZnO as zinc source synthesis at 200 °C for 6 hours, reaction composition: 0.2 LiOH : 0.1 $Zn(CH_3COO)_2 \cdot 2H_2O$: 0.4 TEAOH : SiO_2 : 30 H_2O

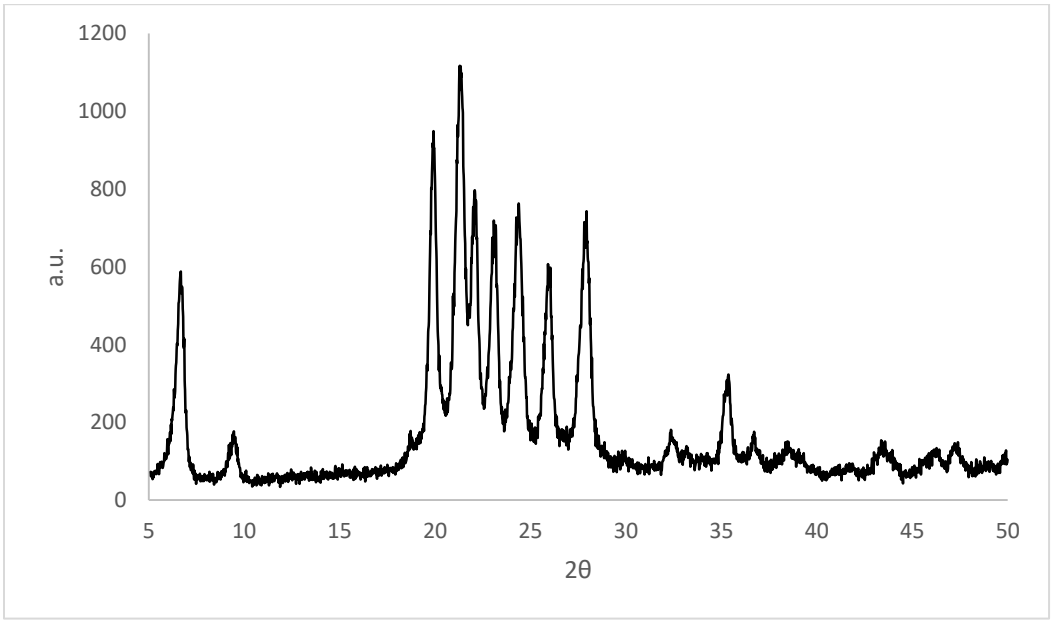

Figure 3-13: XRD pattern of Syloid FP-63 as silica source synthesis at 200 °C for 6 hours, reaction composition: 0.2 LiOH : 0.1 $Zn(CH_3COO)_2 \cdot 2H_2O$: 0.4 TEAOH : SiO_2 : 30 H_2O

Seeded vs seed-free synthesis

Table 3-6 shows a summary of with-seed synthesis and comparison with seed-free synthesis formulas. Short and long seed-free synthesis are represented by exp. 1 and exp. 13, respectively. Exp. 6 is treated as the VPI-8 seed, and exp. 18 is the with-seed synthesis by using previous procedure [120]. Two temperatures are studied at 150 °C and 200 °C, which are the heating temperatures used before and focused on this work.

Table 3-6: Summary of with-seed VPI-8 synthesis and comparison with seed-free synthesis, reaction mixture mole ratio: a LiOH : b $Zn(CH_3COO)_2 \cdot 2H_2O$: c TEAOH : SiO_2 : d H_2O

Exp.	A	b	c	d	T (°C)	Time (hr)	Phase
1	0.2	0.1	0.4	30	200	6	VPI-8
6	0.2	0.1	0.4	30	150	240	VPI-8
13	0.2	0.1	0.78	30	200	24	VPI-8
15*	0.26	0.036	0.78	21	150	36	amorphous
16*	0.26	0.036	0.78	21	150	60.5	amorphous + VPI-8
17*	0.26	0.036	0.78	21	150	120	VPI-8
18*	0.26	0.036	0.78	21	150	260	VPI-8
19*	0.26	0.036	0.78	21	200	36	Disordered
20*	0.26	0.036	0.78	21	200	120	VPI-8
21*	0.26	0.036	0.78	21	200	260	Disordered

*with 0.4 wt.% seed synthesis, NaOH is used instead of LiOH

Comparing the XRD patterns between seed-free (Figure 3-1) and with-seed (Figure 3-14) synthesizes, with-seed synthesis shows a better result on both shape of peaks and the signal/noise ratio. The reason could be that with-seed synthesized VPI-8 is thicker (pseudo-cubic shape) and synthesis time is longer than seed-free VPI-8. However, it is clear that using seed crystals is not required to synthesis VPI-8 at high reaction temperature. VPI-8 were not synthesized with seed at 150 °C for 36 hours. At 60.5 hours synthesis, crystal peaks start to appear in XRD pattern, Figure 3-15. Comparing synthesis time at 260 hours (Figure 3-13) to synthesis time at 120 hours (Figure

3.15), the longer time has a lower intensity of 2θ = 13.92°. VPI-8 can be successfully synthesized at 200 °C with seed, Figure 3-18. Unfortunately, in this work the seed-synthesis is not reproducible at this high heating temperature. Figure 3-17 and Figure 3-19 show the examples of failed synthesis XRD patterns. It implies that product is a mixture phase which VPI-8 and other impurity phases overlap each other in XRD pattern. More failures are found during heating time between 36 and 260 hours (60.5, 120, 144, 169.5, 192, and 216 hours). With low synthesis temperature at 150 °C, the reproducibility is higher. However, it is still not guaranteed to reproduce with-seed synthesis VPI-8 at 150 °C reaction temperature.

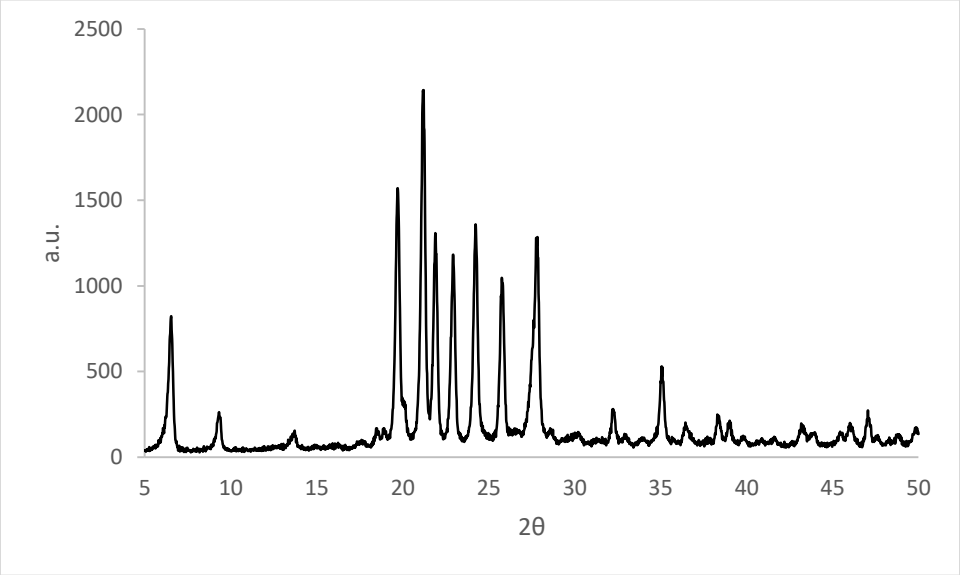

Figure 3-14: XRD pattern of as-made with 0.4 wt.% seed synthesis VPI-8 at 150 °C for 260 hours, reaction composition: 0.26 NaOH : 0.036 $Zn(CH_3COO)_2 \cdot 2H_2O$: 0.78 TEAOH : SiO_2 : 21 H_2O (exp. 18)

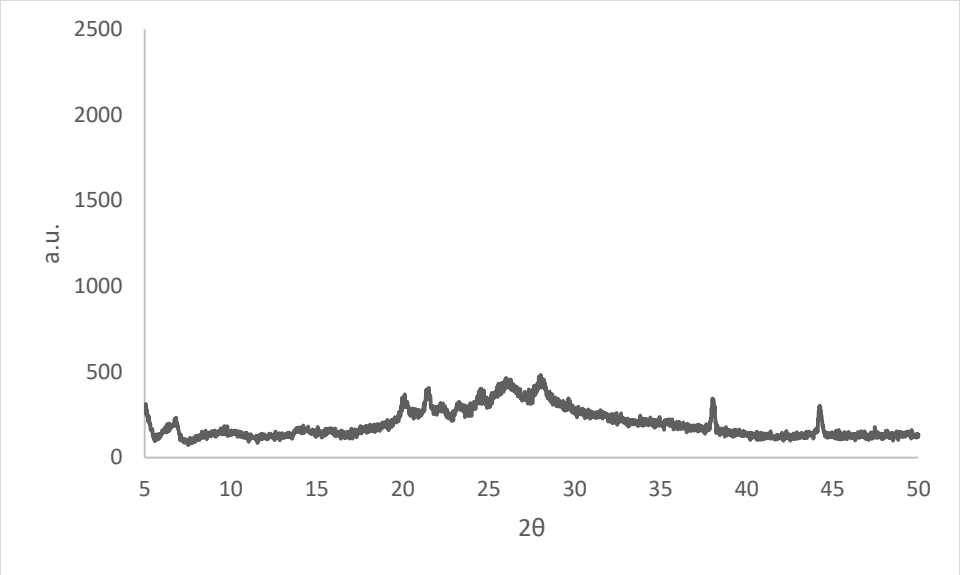

Figure 3-15: XRD pattern of as-made with 0.4 wt.% seed synthesis VPI-8 at 150 °C for 60.5 hours, reaction composition: 0.26 NaOH : 0.036 $Zn(CH_3COO)_2 \cdot 2H_2O$: 0.78 TEAOH : SiO_2 : 21 H_2O (exp. 16)

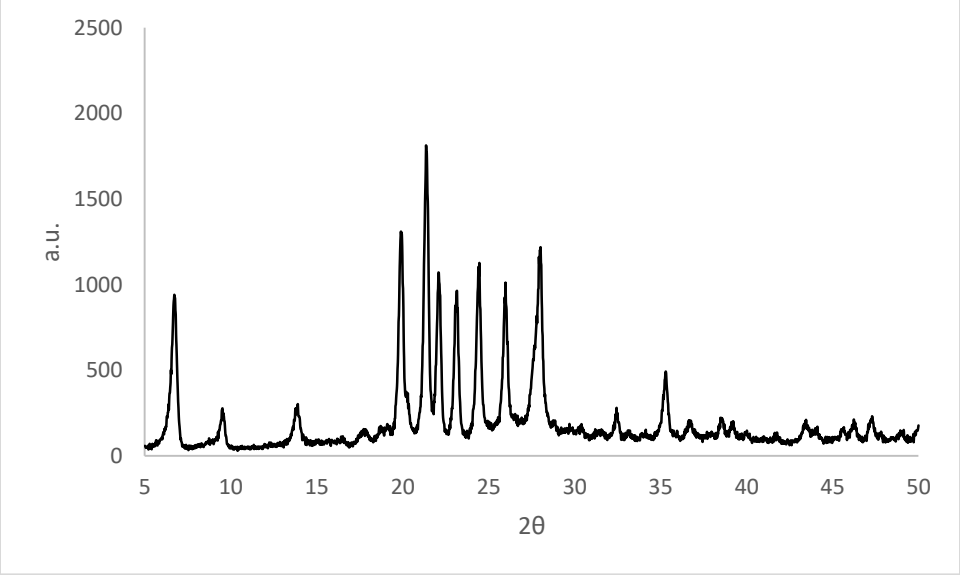

Figure 3-16: XRD pattern of as-made with 0.4 wt.% seed synthesis VPI-8 at 150 °C for 120 hours, reaction composition: 0.26 NaOH : 0.036 $Zn(CH_3COO)_2 \cdot 2H_2O$: 0.78 TEAOH : SiO_2 : 21 H_2O (exp. 17)

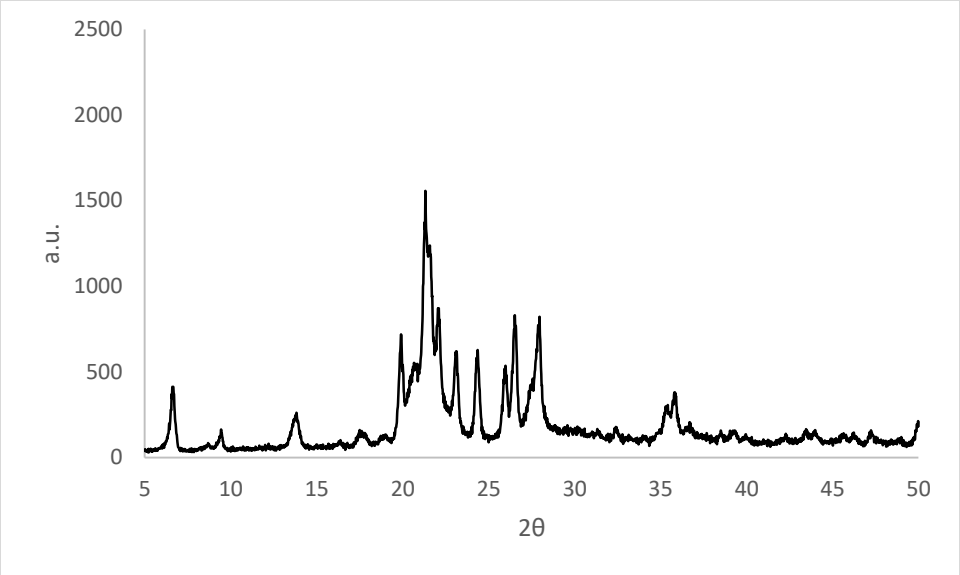

Figure 3-17: XRD pattern of as-made with 0.4 wt.% seed synthesis VPI-8 at 200 °C for 36 hours, reaction composition: 0.26 NaOH : 0.036 $Zn(CH_3COO)_2 \cdot 2H_2O$: 0.78 TEAOH : SiO_2 : 21 H_2O (exp. 19)

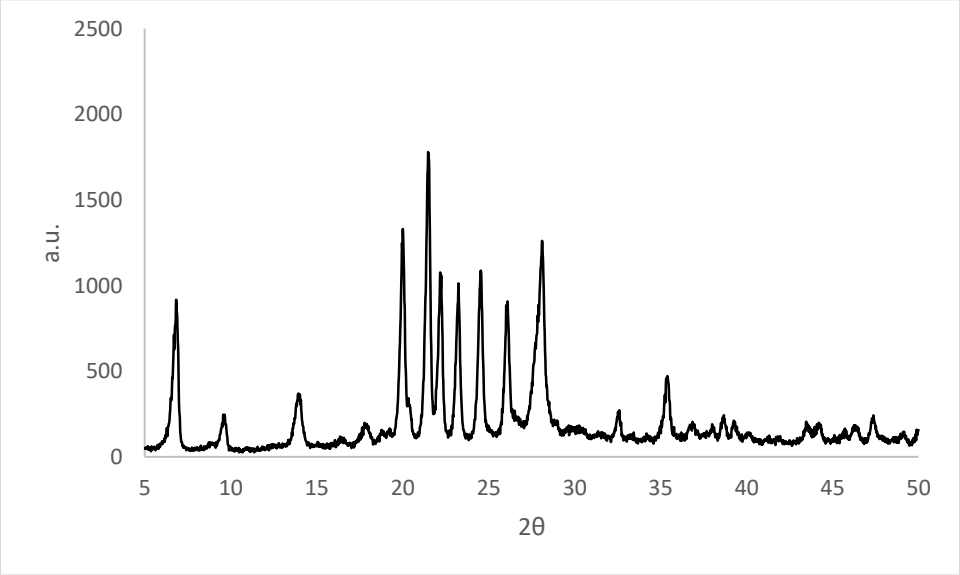

Figure 3-18: XRD pattern of as-made with 0.4 wt.% seed synthesis VPI-8 at 200 °C for 120 hours, reaction composition: 0.26 NaOH : 0.036 $Zn(CH_3COO)_2 \cdot 2H_2O$: 0.78 TEAOH : SiO_2 : 21 H_2O (exp. 20)

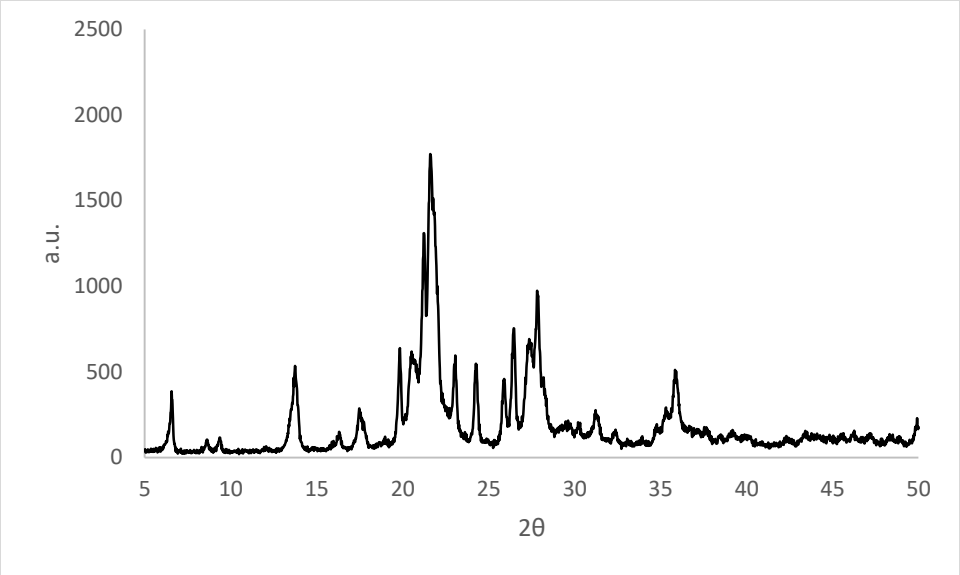

Figure 3-19: XRD pattern of as-made with 0.4 wt.% seed synthesis VPI-8 at 200 °C for 260 hours, reaction composition: 0.26 NaOH : 0.036 $Zn(CH_3COO)_2 \cdot 2H_2O$: 0.78 TEAOH : SiO_2 : 21 H_2O (exp. 21)

It was necessary to use seed to synthesis high crystallinity product. The previous publications could not synthesiz highly crystallized VPI-8 in the absence of a seed. Thus, the final VPI-8 has to be prepared using a two long-time syntheses and two post-treatments (filtration, dry, and calcine). Also, a seed may use to direct the crystal to growth the desired product. Table 3-7 shows the relation between reaction time and product phase without seed studied before [112]. First, a amorphous material was maintained at 12 hours reaction time. Second, a Magadiite phase was observed at 80 hours and 96 hours. Third, a magadiite and kenyaite mixture phase appeared at 144 hours. At the end 168 hours, kenyaite was the only phase found. The same group also reported a “OSDA-free” synthesis, which used seed to replace OSDA TEAOH in the reaction mixture. For the seed synthesis, reaction composition of exp. 6 was chosen for heating 144 hours at 150 °C. Then, a high crystallinity of VPI-8 was synthesized by adding seed without OSDA.

Table 3-7: Hydrothermal reaction composition mole ratio: 0.01 LiOH : 0.015 NaOH: 0.02 $Zn(CH_3COO)_2 \cdot 2H_2O$: SiO_2 : 20 H_2O at 150 °C [112]

Time (hr)	Phase
12	Amorphous
80	Magadiite
96	Magadiite
144	Magadiite + Kenyaite
168	Kenyaite

It is not clear why the product formation is different between with-seed synthesis and seed-free synthesis, Figure 3-20 and Figure 3-21, respectively. For the with-seed synthesis, a white disk product was deposited at the bottom of the reactor with very basic aqueous solution (pH>>14), like other common hydrothermal zeolite synthesis product format. Instead, the seed-free synthesis formed a "mashed potatoes" type product that fills over half of the reactor for both short and long VPI-8 product. The short VPI-8 product shows a neutral condition (pH ≈ 7). In contrast, the long VPI-8 product's pH is >14 due to more TEAOH is added in the reaction gel than short VPI-8. Even though the product formats between with-seed and seed-free synthesis are different, the product weights are similar. Both with-seed synthesis and seed-free synthesis can produce about 1.1g as-made VPI-8 in 23 mL reactor and 2.2 g in 45 mL. The calcined product will be 0.1g lower than as-made VPI-8. The solid yield of this work is at least 85 wt.%, some solid sticks at bottom and on the wall of linear which can not be recovered. Incorporated silica is found at the bottom in linear of both short and long products synthesis. To overcome the unreacted silica, more Li/Si (0.4), Zn/Si (0.2), and TEAOH/Si (0.78) are added into mixture gel. This mixture gel could provide a higher OH^- concentration to dissolve silica, and more other reactants to react with silica. But the incorporated silica still can be observed after hydrothermal reaction.

In the previous work, the yield of seed and the with-seed VPI-8 was 91 wt.% and 99 wt.%, respectively [121]. However, the synthesis time was extremely long, over 20 days. The "OSDA-

free" synthesis seems like a more economic procedure, but the maximum yield of was only 38 wt.% plus long time (over 10 days) to synthesis [112]. However, the "OSDA-free" synthesis was not "truly" OSDA free, because TEAOH was added into initial reaction gel for producing seed. The zincosilicate applications were limited by the previous long period of preparations.

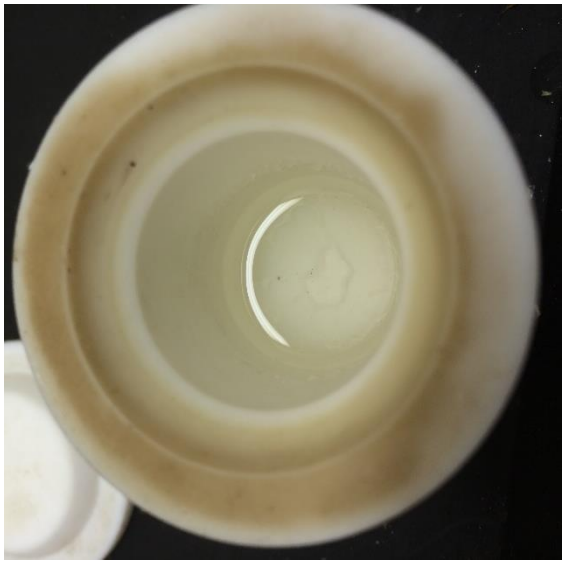

Figure 3-20: Product picture of with-seed synthesis, a hard disk format lay at the bottom of the reactor (exp. 18)

Figure 3-21: Product picture of seed-free synthesis, a "mashed potatoes" format (exp.1)

Morphology of VPI-8

In this work, a high crystallinity VPI-8 could be formed at a higher temperature condition (200 °C). Figure 3-22 and Figure 3-23 show the morphologies of VPI-8 crystals. Pseudo-cubic intermediate CIT-6 crystals are not observed. Both short and long VPI-8 are well crystallized in a needle shape. Thus, it is not necessary to synthesis VPI-8 with seeds to carry out high crystallinity VPI-8. The length of short VPI-8 crystal is approximate 1.5 μm; and the length of long VPI-8 crystal is up to 6.5 μm. The width of both short and long VPI-8 crystal is about 0.2 μm with a thin thickness. Since VPI-8 is a 2-D channeled zeolite, the crystal width and thickness are not as important as the crystal length.

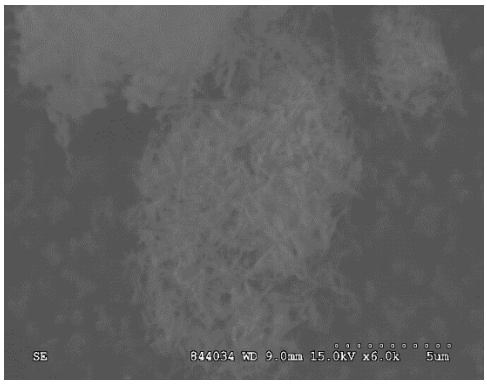

Figure 3-22: SEM of short calcined VPI-8 synthesis synthesis at 200 °C for 6 hours, reaction composition: 0.2 LiOH : 0.1 $Zn(CH_3COO)_2 \cdot 2H_2O$: 0.4 TEAOH : SiO_2 : 30 H_2O (exp.1)

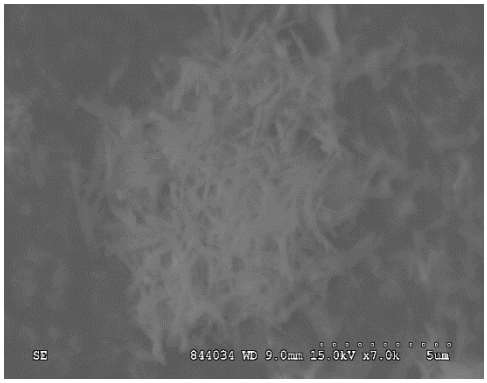

Figure 3-23: SEM of long calcined VPI-8 synthesis at 200 °C for 24 hours, reaction composition: 0.2 LiOH : 0.1 $Zn(CH_3COO)_2 \cdot 2H_2O$: 0.78 TEAOH : SiO_2 : 30 H_2O (exp.14)

In contrast, seeded synthesis was required to produce highly crystallinity larger crystals of VPI-8 in the previous works [112, 114, 120-122, 130, 131]. A Japanese group reported a SEM figure for synthesis over 6 days at 150 °C. The seed-free synthesis could only form center-bundled smaller needles like VPI-8 with decreased crystallinity [112]. Davis' group reported the seed product is needle-like crystal with length approximate 1.3 μm, while the with-seed synthesis product is more like a bulk crystal up to 4 μm, which was called the large VPI-8 [114, 120, 121].

In this work, the length of VPI-8 crystal could be controlled by the TEAOH concentration. The final product crystal length could be increased by adding more TEA^+ into the reaction mixture. When the TEA^+/Si was increased from 0.4 to 0.78, the crystal length could be increased from 1.5 μm to 6.5 μm. There are three major functions of organic cation in zeolites synthesis: Structure-Directing Agent (SDA), Pore-Filling Agent (PFA), and template. Therefore, TEA^+ not only acts as the SDA, but also PFA in this synthesis. The usage of TEA^+ can be understood as SDA for the crystal nucleation, then stays in the pore as PFA during crystal growth to help maintaining the channel shape. Hence, VPI-8 could grow longer at higher TEA^+ concentration condition.

Contrarily, very short crystal or not well crystallized pieces should be formed instead of long high crystallinity VPI-8.

Another advantage of higher TEA^+ concentration is that the organic compound TEA^+ is provided by TEAOH, which can increase the OH^- concentration of the solution gel. And more silica can be dissolved at stronger alkalinity environment [74]. The reactions are given below:

$$(SiO_2)_x + 2H_2O \rightarrow Si(OH)_4 + (SiO_2)_{x-1} \qquad (3.1)$$

$$Si(OH)_4 + OH^- \rightarrow Si(OH)_5^- \qquad (3.2)$$

Si to Zn ratio

Figure 3-24 shows the ^{29}Si NMR spectra of calcined short seed-free VPI-8. The resonance at -66.68 ppm is signed to Q^4 (4Zn) Si atom which is suggested to be the zinc rich zincosilicate species [114]. The peak at -99.77 ppm is the signal of Q^4 (3Si, 1Zn). The peak at -106.03 ppm is the signal of Q^3 (3Si), which could be the layer at the edge of each crystal. The peak at -112.51 ppm is a particular Q^4 (4Si) Si atom. Due to the chemical shift in ^{29}Si NMR spectra is strongly dependent on the tetrahedra atom - oxygen atom - tetrahedra atom (T-O-T) angle which the Zn–O-Si angle is smaller than Al-O-Si in zeolites. Plus, the charge differences between Zn^{2+} and Al^{3+}, the Si (nZn) resonances are expected to appear at lower field than Si (nAl) resonances. For example, the 2Si 2T chemical shifts of zincosilicate and aluminosilicate range for are -75 ppm < Si (2Si, 2Zn) < -85 ppm and -90 ppm < (2Si, 2Al) < -100 ppm, respectively [113, 132]. The resonances of long-time synthesized VPI-8 (Figure 3-25) have similar results with short-time synthesized VPI-8, which are -67.07 ppm, -100.01 ppm, -105.54 ppm, and -112.48 ppm. Instead, there are only two

peaks observed at -103.52 ppm and -112.24 ppm for with-seed product, which is synthesized by using the previous recipe (exp. 17), Figure 3-26. Moreover, in this work, there is a resonance around 3.4 ppm observed in ^{1}H MAS NMR spectrum of calcined short VPI-8, which is a particular water peak caused by the humidity of room after calcining, Figure 3-27. Furthermore, neither H-Si band nor silanol protons is observed. It should be noticed that the so-called "phase B" (~95 ppm) in the previous work is not observed in this work at all [114]. Also, the undesired ^{29}Si NMR spectra change of unseeded synthesis is not found [112].

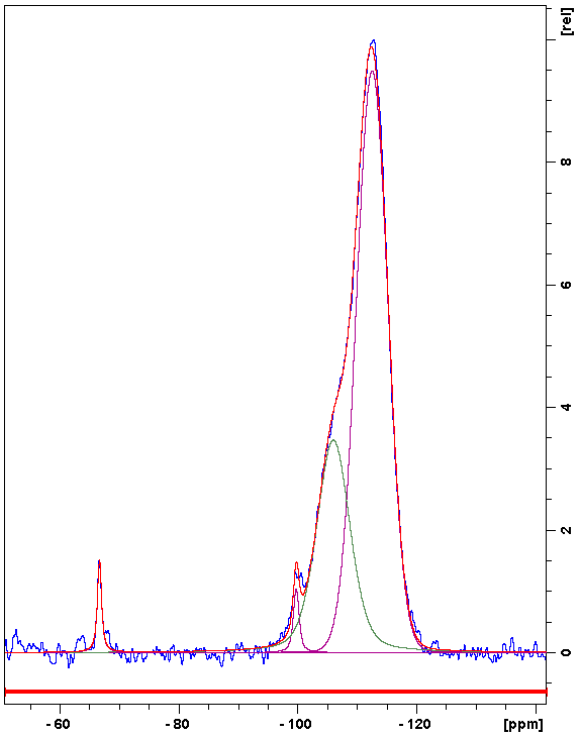

Figure 3-24: ^{29}Si solid state NMR spectra of calcined short VPI-8 synthesis at 200 °C for 6 hours, reaction composition: 0.2 LiOH : 0.1 $Zn(CH_3COO)_2 \cdot 2H_2O$: 0.4 TEAOH : SiO_2 : 30 H_2O (exp.1)

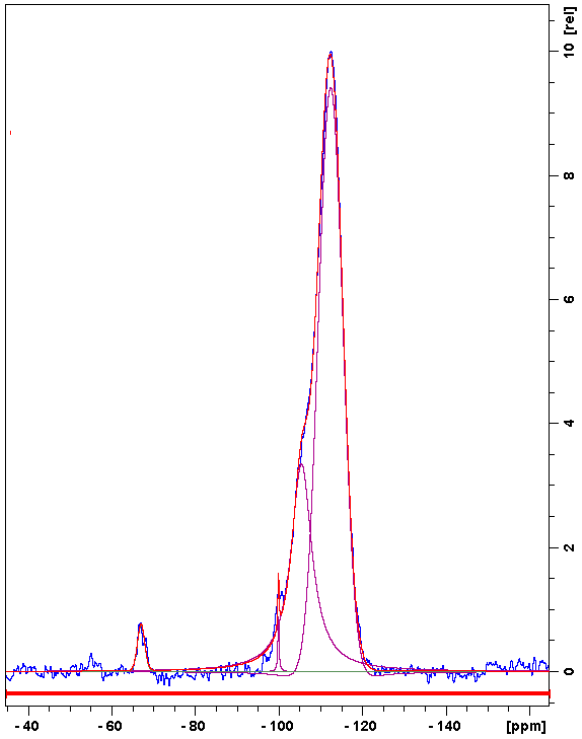

Figure 3-25: ^{29}Si solid state NMR spectra of calcined long VPI-8 synthesis at 200 °C for 24 hours, reaction composition: 0.2 LiOH : 0.1 $Zn(CH_3COO)_2 \cdot 2H_2O$: 0.78 TEAOH : SiO_2 : 30 H_2O (exp.14)

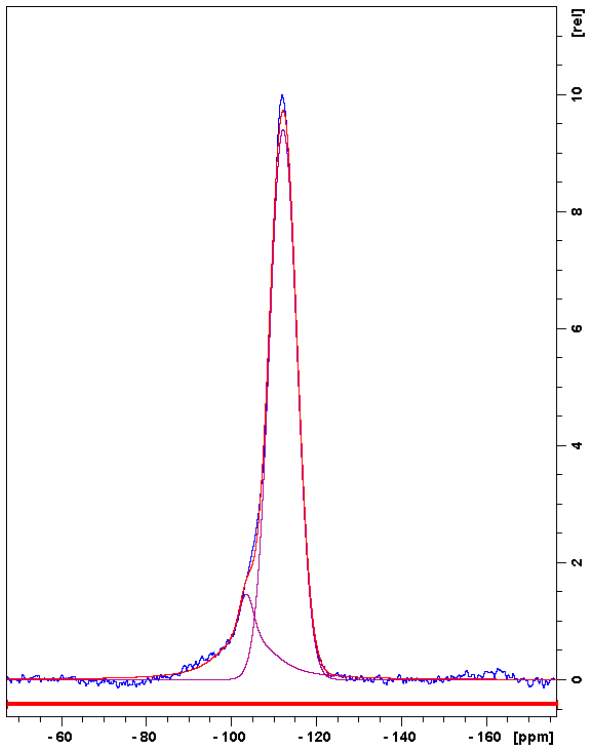

Figure 3-26: ^{29}Si NMR spectra of calcined with-seed VPI-8 (exp. 9)

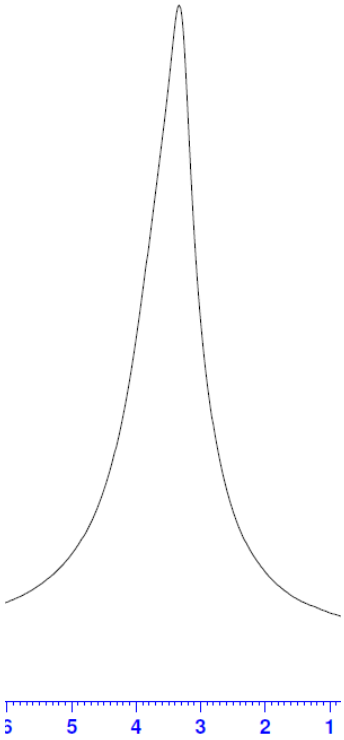

Figure 3-27: ^{1}H MAS NMR spectra of calcined short VPI-8 synthesis at 200 °C for 6 hours, reaction composition: 0.2 LiOH : 0.1 $Zn(CH_3COO)_2 \cdot 2H_2O$: 0.4 TEAOH : SiO_2 : 30 H_2O (exp.1)

Davis' group investigated the ^{29}Si NMR spectra at low-temperature (150 °C) synthesized VPI-8 via different reaction times (48, 52.5, 72, 96, and 144 hours) [114]. The very broad resonance was noted at a reaction time of 48 hours. At times longer than 52.5 hours, there were two resonances around -105 ppm and -113 ppm remained the same. The intensity of resonance at -65 ppm was increased when the heating time increased. It should be noticed that with the increasing reaction time, the resonance at -95 ppm was increased first, then decreased, at the end disappeared. A Japanese group later studied the ^{29}Si NMR spectra of both with-seed and without-seed synthesis [112]. For 12 hours heating at 150 °C, resonances at about -65 ppm, -85 ppm to -120 ppm, and -112 ppm were observed. At a longer heating time, the broad resonance from -85 ppm to -120 ppm started to separate, then achieved three resonances at around -93 ppm, -103 ppm, and -106 ppm. Instead, the without-seed synthesis could not result into a well crystallized VPI-8

even for a longer time at 80 hours. Consequently, a pure zincosilicate VPI-8 phase should contain at least three resonances at approximate -95 ppm, -103 ppm, and -112 ppm. The existence of resonance at around -65 ppm can be caused by the solid-state phase transfer [3]. In conclusion of the ^{29}Si NMR spectra, VPI-8 are synthesized by exp. 1 and exp. 14 should be seen as pure phases of VPI-8.

A "extended Lowenstein rule" was introduced to calculate Si/Zn ratio in zincosilicate zeolites framework via the ^{29}Si NMR spectra [113]. By the analogy of Lowenstein rule, which the Al-O-Al pairing is avoided in aluminosilicate zeolites, the Zn-O-Zn pairing is not considered in zincosilicate zeolites. Also, the more unfavorable than aluminosilicate zeolites bond order of O and charge repulsion are assumed to be eliminated. The ^{29}Si NMR Si/Zn ratio calculation: Si/Zn atomic ratio of the tetrahedral aluminosilicate framework was calculated by the equation [133]:

$$Si/M = \frac{\sum_{m=0}^{4} I_{Si(nM)}}{\sum_{n=0}^{4} (n/4) I_{Si(nM)}} \qquad (3.1)$$

where M is metal atom, and n is the number of metal atoms O-bridged to a given Si atom. This equation was used to calculate Si/Al ratio in aluminosilicate zeolite originally. In this work and other zincosilicate publications, the "extended Lowenstein rule" is used, which shares the same equation formula. In this work, both short and long VPI-8 could be synthesized in a pure phase at short time, which the Si/Zn ratio is low to 6.84.

The previous work showed the superficial and bulk Si/Zn ratio are different, approximate 10 and 16, respectively [114]. Zincosilicate zeolite applications could be limited by quality of this non-uniform product. While, in this study, short VPI-8 Si/Zn ratio from chemical analysis, NMR, and XPS were 7.88, 6.84, and 7.34, respectively. XPS spectra can be found in Appendix A. These results show the agreement about surface and bulk Si/Zn ratios. This is the first time that a uniform surface and bulk Si/Zn ratio of VPI-8 has been reported to be less than 10. The Zn/Li ratio is 1:1

in elemental analysis result. In the conclusion, the general chemical composition formula for zincosilicate VPI-8 can be written as $Li_{1.914}Zn_{1.914}Si_{15.086}O_{34}$.

A higher concentration LiOH (exp. 8) was added into the reaction mixture. The concentration of LiOH affects crystallization rates [121]. Also, more LiOH provides more OH^- in solution. The absence of Li^+ cation has been shown to only form low crystallinity product, then turned to an unknown phase after prolonged synthesis [112]. Therefore, a higher concentration of Li^+ in mixture solution is investigated in this work. The hypothesis is that more extra-framework cation Li^+ could balance more anionic sites created by Si-O-Zn-O-Si instead that Zn atoms to form pin-wheel unit in framework. In Figure 3-28, there are two peaks in the region between $2\theta = 30°$ and 35°, which are 32.54° and 33.16°. The peak intensity around $2\theta = 33.16°$ should be very low or barely to be observed in a VPI-8 XRD pattern. Nevertheless, the relative intensity (I/I_o) is high up to 0.15 when the Li^+/Si ratio was increased from 0.2 to 0.3. Unfortunately, higher LiOH contrition in solution synthesis is not highly reproduceable. Figure 3-29 shows a repeat experiment with 0.3 Li/Zn mole ratio. Beside above, the intensities of two peaks at $2\theta = 30.86°$ and 44.26° are much higher. It reveals that impurity phases could be form during high LiOH concentration VPI-8 synthesis.

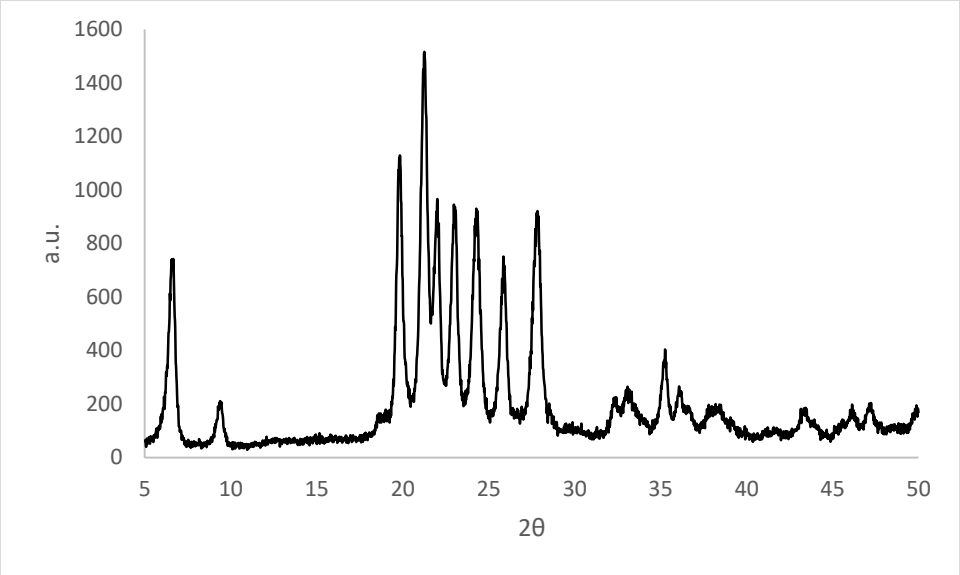

Figure 3-28: XRD pattern of as-made VPI-8 at 200 °C for 24 hours, reaction composition: 0.3 LiOH : 0.1 $Zn(CH_3COO)_2 \cdot 2H_2O$: 0.4 TEAOH : SiO_2 : 30 H_2O (exp.8)

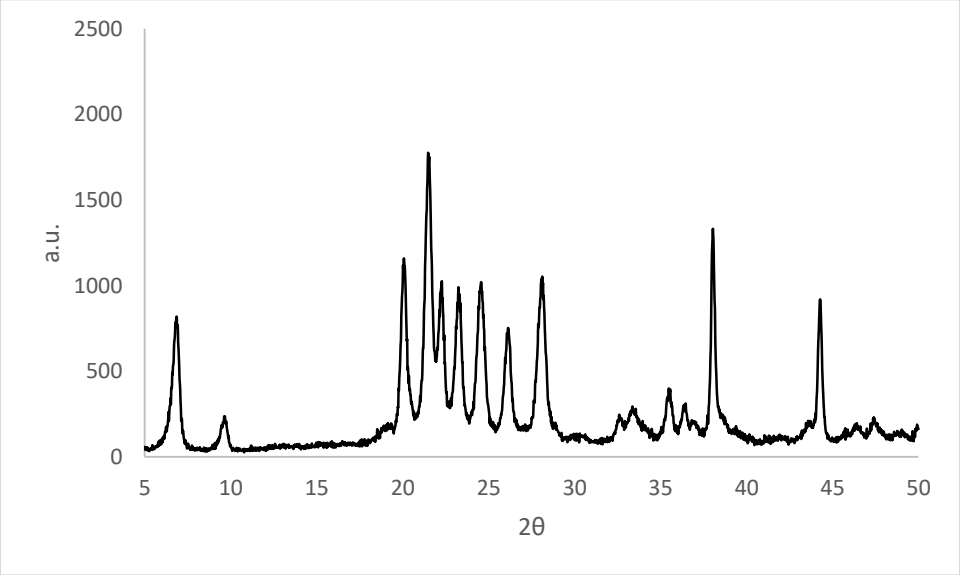

Figure 3-29: Repeat exp.8 XRD pattern of as-made VPI-8 at 200 °C for 24 hours, reaction composition: 0.3 LiOH : 0.1 $Zn(CH_3COO)_2 \cdot 2H_2O$: 0.4 TEAOH : SiO_2 : 30 H_2O

Summary

A reproducible, short-time seed-free synthesis of VPI-8 with high crystallinity is reported. At high reaction temperature (200 °C), the synthesis time of VPI-8 can be reduced to a day. Both short and long VPI-8 only requires 6 and 24 hours to form, respectively. Also, well crystallized VPI-8 does not demand seeds, therefore one-step synthesis is achieved instead of two. No undesired intermediate or impurity phases were found. The functions of TEAOH are suggested as both OSDA and PFA to increase crystal nucleation and growth, respectively. An unknown phase was found in the low zinc concentration synthesis. There were undissolved floating powders observed in the aging procedure. Using different Si and Zn sources were not available to overcome these powders. However, these powders do not affect the synthesis results. Because VPI-8 is a 2-D channeled material, it is not necessary to synthesis big or small crystal size in bulk shape. In this work, the morphologies of both short and long products are needle shape. A uniform Si/Zn ratio between super surface and bulk is achieved below 10. Whereas, not all the Zn atoms provide $(\text{-O-Zn-O-})^{2-}$ to balance divalent cations to form active sites due to the Si/Zn ratio is suggested as 1/4 of the novel "pin-wheel" unit in the framework. Overall, the general chemical formula of VPI-8 is expected as $Li_{1.914}Zn_{1.914}Si_{15.086}O_{34}$. In the future, there are more chances for high temperature applications of zincosilicate zeolites, such as reaction and adsorption.

Chapter 4 - Computational Calculation

Introduction

Theoretical calculations were performed to be compared with the experimental findings. The computational calculations use the Density Functional Theory (DFT) method which uses the Gaussian type orbitals (GTO) as the basis set. However, Slater type orbitals (STO) or numerical basis set is used in ADF [134] and $Dmol^3$ [135]. STO basis set could perform a faster convergence than GTO, because the reliability of calculations increases with the size of basis sets increasing. The advantage of GTO is carrying out the calculations with larger basis sets easier than medium STO basis sets. These calculations were performed to study the fundamental T-atom Zn locations to find the most stable configurations via comparing with experimental characterization results.

Experiments

Extra framework cation location on VPI-8 was studied by computational simulation. The DFT calculation was performed by BAND (a periodic DFT calculation) in Amsterdam Density Functional (ADF) program from Software for Chemistry & materials (SCM) company [136]. The exchange-and-correlation (XC) functional, also called density functional, was chosen as GGA:PBE [137]. Bulk periodicity was used. Basis set is double zeta, and single point calculation was chosen to reduce the calculation times. All the DFT calculations were performed on the supercomputer (Beocat) with one node (4-cores) from the computer science department at Kansas State University.

Results and discussion

According to Löwenstein's rule, there are no Al-O-Al pairings in the aluminosilicate zeolite framework [22]. By the analogy of Löwenstein's rule, Zn-O-Zn pairing cannot occur in zincosilicate zeolite, since both the charged repulsion and bond order of the O will make this environment even more unfavorable than the Al-O-Al pairing in aluminosilicate zeolite [113]. Based on the ^{29}Si NMR spectra in this work, there are only two types of local positions associated with Zn in the framework, which are Q^4 Si (4Zn) and Q^4 Si (1Zn, 3Si). Elemental analysis result shows Zn/Li ratio is about 1. To satisfy the experimental characterization results above, there are only four types of structures considered: pure silica, four Zn atom on the pin-wheel, one Zn in the framework, and two Zn in the framework.

For contrast, a pure-silica VET type was calculated as a baseline, scheme A in Figure 4-1. Next, in scheme B, the Q^4 Si (4Zn) is set to be the center in the pin-wheel unit. The energies of formation of both scheme A and B are -323.4240 kcal/mol and -266.7469 kcal/mol, respectively. Table 4-1 summaries the energies of formation for all the hypotheses schemes. Scheme A is more favorable than scheme B due to a lower energy of formation. This may explain that Q^4 Si (4Zn) could not be observed in the final product in previous work which the synthesis temperature is too low (150 °C) that Q^4 Si (4Si) required less energy to form. It may also the reason that the bulk Si/Zn ratio decreases with longer synthesis time due to the solid-state transfer from a higher energy state to a more stable lower energy state.

Achieving a Zn/Li ratio to 1, it is required to balance the Zn rich phase with a lower Zn/Li ratio. One Zn in framework on active site (Zn/Li ratio is 1/2) was needed. Then, three Zn T-atom

locations were studied for one Zn in the framework as close (scheme C), middle far-away (scheme D), and far-away (scheme E) from the center of pin-wheel unit that the energies of formation are -316.2060 kcal/mol, -317.2343 kcal/mol, and -316.8036, respectively. The energies of formation of different scheme C, D, and E are not significantly different. Anyway, scheme E is considered as the most stable structure for one Zn in the framework because it has the lowest energy in scheme C, D, and E. Moreover, there may be two Zn atoms appeared in the same framework (Zn/Li ratio is 1), like scheme F and G, Figure 4-3, one on active site, the other one on non-active site which could be located at the pin-wheel. For scheme F and G, the energy of formation is -303.0805 kcal/mol and -303.3878 kcal/mol, respectively. Scheme G is considered as the most stable configuration, even though the energies of formation are closed.

In conclusion, VPI-8 is not preferred to form the Q^4 Si (4Zn). Because the only possibility of Q^4 Si (4Zn) can be formed is the four Zn surrounding one Si for the pin-wheel unit, which the energies of formation are slightly higher than other configurations. Higher temperature synthesis could provide higher energies to form Q^4 Si (4Zn). For the Zn locations in this work, it could be scheme G, and a combination between scheme B and E. The new coordination of structures could be found in Appendix A.

Figure 4-1: Scheme A (left): pure-silica VET as baseline; and scheme B (right): 4 Zn atoms surrounded the pin-wheel center Si atom (left bottom), Si (yellow), O (red), Zn (white), and Li (grey)

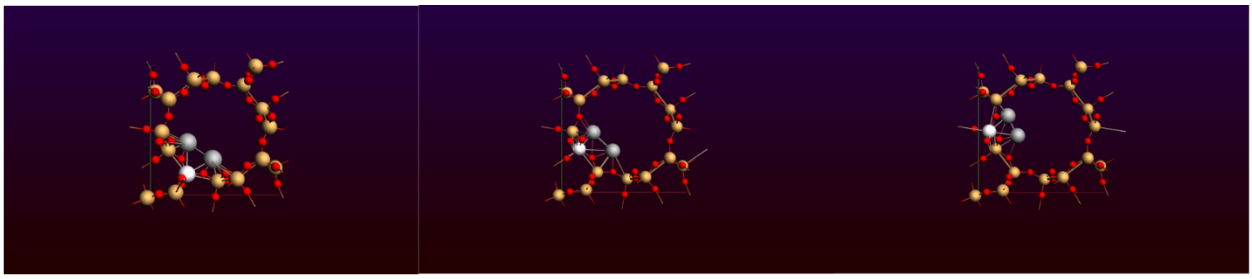

Figure 4-2: Scheme C (left): Zn T-atom locates close to the center of pin-wheel unit (left bottom Si atom); scheme D (middle): Zn T-atom locates middle far-away to pin-wheel unit; scheme E (right): Zn T-atom locates far-away to pin-wheel unit, Si (yellow), O (red), Zn (white), and Li (grey)

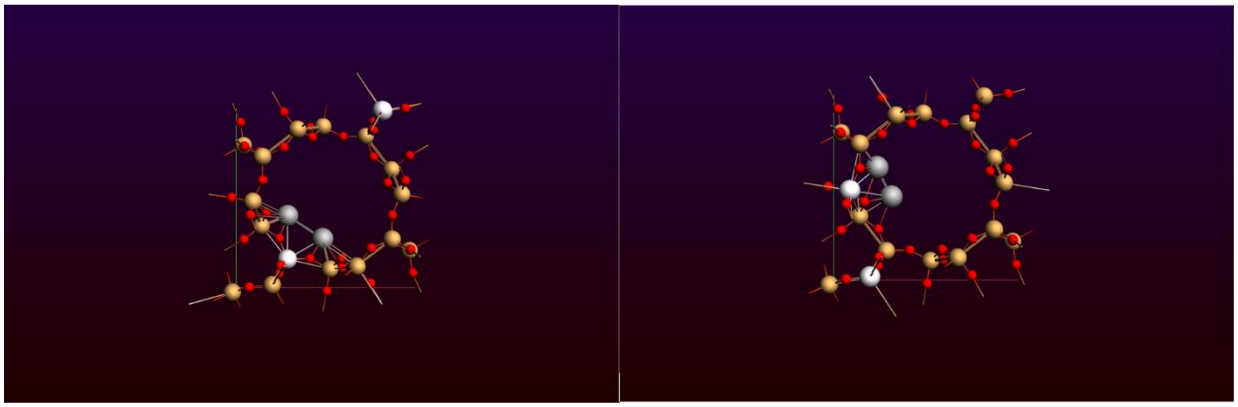

Figure 4-3: Scheme F (left): one Zn close to pin-wheel on active site, and the other Zn on non-active site, Scheme G (right): one Zn far away from pin-wheel on active site, and the other Zn on non-active site, Si (yellow), O (red), Zn (white), and Li (grey)

Table 4-1: Summary of formation energies calculated by DFT simulation

Scheme	Energy of Formation (kcal/mol)
A	-323.4240
B	-266.7469
C	-316.2060
D	-317.2343
E	-316.8036
F	-303.0805

G	-303.3878

Chapter 5 - Methane Dehydroaromatization over Zincosilicate Zeolite Catalyst VPI-8

Introduction

The shale methane production in 2015 increased to 15213 billion ft^3 from 1293 billion ft^3 at 2007 [138]. More and more methane hydrate were found under the sediment of the ocean floors [139]. In 2012, the U.S. Department of Energy reported the successful field trial of methane hydrate production [140]. Methane becomes to the largest abundant carbon reserve today which is much more than the amount of all the fossil fuel including conventional gas, oil, and coal. Unlike fossil fuel, methane may be produced from landfills. The applications of methane have become a hot topic for researchers. There are two uses of methane: indirect conversion and direct conversion. For indirect conversion, methane could produce fuel, paraffin, alkenes, methanol, Dimethoxyethane (DME), and alcohol via syngas. For direct conversion, methane could react to ethylene, aromatics, and formaldehyde. Methane conversion is limited by its thermodynamic properties. For example, methane's direct conversion to benzene could be represent as:

$$6\,CH_4 \rightarrow C_6H_6 + 9\,H_2 \qquad \Delta H°_{298\,k} = +532\ kJ \qquad (4.1)$$

Due to the extremely strong C-H bond (~439 kJ/mol) in methane, all the indirect methane conversion schemes require synthesis gas, such as O_2, H_2, CO, and CO_2. The well-known methane reaction was Oxidative Coupling of Methane (OCM) to ethylene which appeared in the early 1980s [141]. Today, the indirect conversion of methane to more valuable chemicals had been

commercialized. Several industrial facilities in the world have operating methane conversion indirectly including: Sasol (Johannesburg, South Afica), PetroSA (Mossel Bay, South Africa), Shell (Bintulu, Malaysia), Oryx (Ras laffan industrial City, Qatar), and Chevron (Escravos region, Nigeria). It should be noticed that the syngas preparation and compression usually makes up 60-70% of the capital cost and consumes almost all the energy of operation [142].

The first direct conversion of methane to aromatics over Mo supported ZSM-5 was reported in 1993 [143]. Later, a summary of different metal cations were studied including [142]: Zn [144, 145], W [146-152], Re [153-157], Cu [158], Mn [159], Ga [160, 161], Ni, Cr, Fe and V [162]. The advantage of using a zeolite catalyst is the good product selectivity, and the disadvantage is that the framework collapse temperature is not as high as metal or metal-oxide catalyst. There are about 20 articles published each year related to MDA reactions after 2000 [163]. However, the Mo supported by impregnation method and Ni ion-exchanged zeolite H-ZSM-5 or H-MCM-22 are still the two best catalysts for MDA reaction. The disadvantage of the catalysts above is short lifetime caused by coking. Mo based zeolites deactivate usually in 150 minutes. Zn is only cation showing a longer lifetime than other cations. But, the methane conversion on Zn-exchanged zeolite is too low (<3%). Unfortunately, to the date, there is no significantly progress on MDA reaction yet, due to the low methane conversion. Thus, people are attempting to improve both methane conversion and aromatics selectivity by other methods. For example, a membrane reactor was used to increase the reaction equilibrium [164] . Products are removed from the reactor, then the more methane can be converted.

Hypothesis

This work is the first study on the zincosilicate zeolite in catalyzing a reaction. The signification advantage of zincosilicate and zincosilicate analogues zeolites over aluminosilicates is the divalent cations balancing the anionic charges of the framework instead of monovalent cations. Unlike aluminosilicates, the $ZnO_{4/2}^{2-}$ tetrahedra has charge -2. In zincosilicate, the -2 charge of each oxygen is shared by one $ZnO_{4/2}^{2-}$ tetrahedra that one divalent cation requires only one $ZnO_{4/2}^{2-}$ tetrahedra. For aluminosilicates, the contribution of two -1 charge of each oxygen, which is shared between two neighbors $AlO_{4/2}^{-}$ tetrahedrals, is required to pair the divalent cations. The active sites provided from zincosilicate zeolites may be more efficienct than aluminosilicate zeolites because only one Zn is required to balance the divalent cations instead of two Al. Theoretically, this divalent cation from zincosilicate framework can provide a stronger acid site than aluminosilicate, due to a smaller bond angle and bond length between extra-framework cation and framework can be achieve in zincosilicate zeolites. Since methane activation is the most difficult in alkanes, zincosilicate zeolites have potential ability to active more methane than aluminosilicate zeolites. VPI-8 has a 12-member ring which is classified as large pore zeolite. ZSM-5 only has a 10-member ring which is a middle pore zeolite. So, aromatics such as benzene, toluene, and xylene (BTX) could pass through the pore in VPI-8 easier than middle pore materials. The most thermal stable zincosilicate VPI-8 is investigated on methane dehydroaromatization (MDA) reaction in this work. The Li-VPI-8 will be studied as the baseline. Furthermore, Ni-exchanged VPI-8 will be studied which is a commonly catalyst for MDA and other reactions.

Experiments

The reaction system is setup as Figure 5-1. There are two types of reactors used in these experiments. A 1/4 inches diameter of stainless-steel 316 tube is used for temperature below 600 °C at pressure up to 10 bar; while a quartz tube is used for temperatures above 650 °C at atmospheric pressure. The reactor is passed through the center of the heater, Figure 5-2. Figure 5-3 shows the configuration inside the reactor which is packed-bed reactor (PBR). The thermal couple was used as the catalysts supporter.

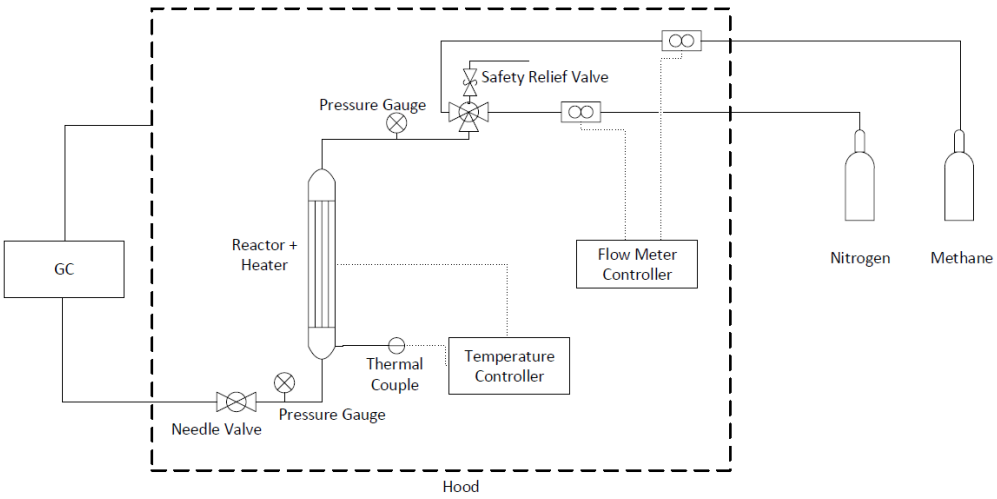

Figure 5-1: Scheme of reaction system

Figure 5-2: The stainless-steel 316 tube reactor and furnace setup in the hood

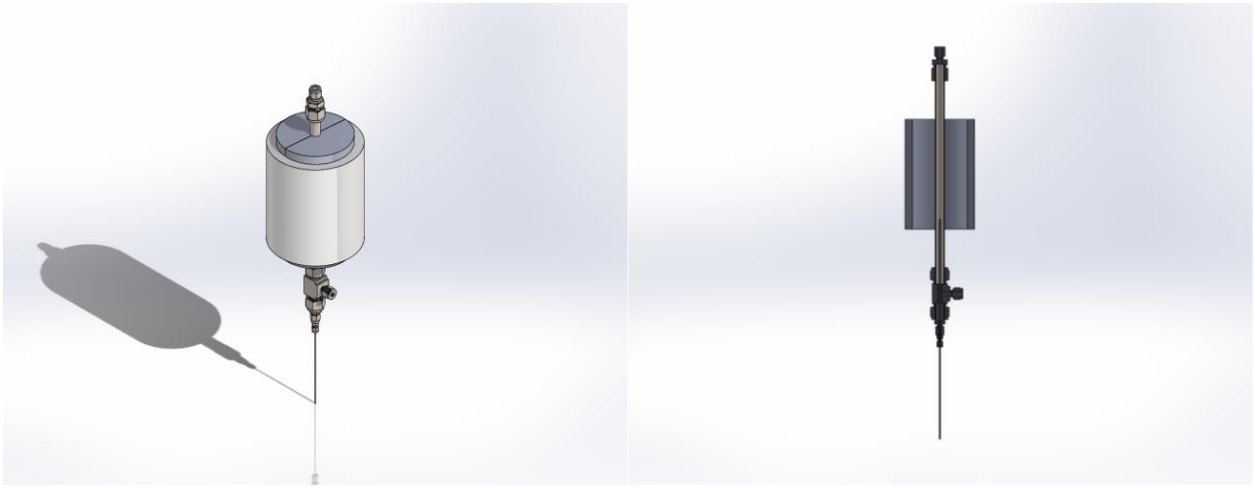

Figure 5-3: The scheme of the full view of the reactor and heater (left), and the cross-section view of the reactor and heater (right)

Ni/Li-VPI-8 catalysts was prepared by ion-exchange. 1 g calcined Li-VPI-8 was ion-exchanged by 100 mL 1 M $NiCl_2$ solution at 80 °C for 8 hours. Then, ion-exchanged VPI-8 catalysts were dried at 250 °C for overnight. 2 g catalyst were loaded on cotton wools which is supported by thermal couple. Nitrogen gas was set to 1600 mL $N_2/(g_{cat} \cdot h)$ at 550 °C for 3 hours as the pretreatment of reaction to remove the water molecule in the framework. During the reaction,

the flow rate was 900 mL $CH_4/(g_{cat}\cdot h)$ and 1600 mL $N_2/(g_{cat}\cdot h)$ to keep a CH_4/N_2 flow rate ratio 9/16. Chemical concentrations were measured by on Gas Chromatography (SRI Instruments).

Temperature Programed Desorption of ammonia (NH_3-TPD) was performed by AMI-200. 150 mg VPI-8 sample was treated under 40 mL/min helium gas for 30 minutes. Next, the temperature was increased to 550 °C with a heating rate 10 °C/min, then hold for 30 minutes. After the pretreatment, 30 mL/min 1% ammonia in helium was flowed through sample at 100 °C for 240 minutes. After the catalyst sample reach ammonia saturated, 30 mL/min helium was used to blow the physical adsorption ammonia on catalyst sample out at 100 °C for 200 minutes. Then, the temperature was ramping up to 900 °C with a 5 °C/min step under 30 mL/min helium gas. The amount of adsorptive ammonia was measured by Temperature Conductivity Detector (TCD). The area under the TCD signal curve was converted to mmol acid sites per gram sample by the average of pulse calibration results.

Results discussion

The XRD pattern of Li-VPI-8 catalyst is shown in chapter 3. The XRD pattern of Ni^{2+} ion-exchanged VPI-8 (Figure 5-4) shows the same result with calcined Li-VPI-8 (Figure 3-2). The previous work reported VPI-8 structure started to collapse at 600 °C then became to amorphous phase at 650 °C [123], but this phenomena was not found in this current work. Li-VPI-8 could keep the structure at 600 °C reaction for 6 hours, Figure 5-5. The Ni/Li-VPI-8 could keep the crystallinity at 600 °C and 5 bar, Figure 5-6. However, most peaks in XRD of post-reaction are

broader than before the reaction. However, two 2θ peaks at both 42.7° and 49.8° are sharper with a high relative intensity than before the reaction. It may be caused by the coking on catalyst surface.

Because the VPI-8 made by using the recipe in chapter 3 is much more thermal stable than previous work, the thermal stability was studied again. The calcination at 700 °C overnight was attempted first. All the 2θ peaks are boarder than before, and the relative intensity of peak at 26.66° is higher than before, Figure 5-7. So VPI-8 structure can survive at least at 700 °C. Next, Figure 5-8 shows the XRD pattern of 750 °C calcination. All the peaks blow 20° were disappeared, except the barely viewed at 15.02°. Peaks at 2θ = 23.22°, 27.92°, 30.36°, 38.58°, and 43.8° were not found in this result. On the other hand, there are extra peaks observed at 2θ = 21.3°, 28.95°, 36.51°, 39.45°, 40.33°, 42.33°, and 45.79°. In Figure 5-9, comparing with Figure 3-2, there are three peaks disappeared at 2θ = 6.58°, 9.40°, and 15.02°; and two extra peaks were observed at 23.80° and 24.88°. The intensity of two peaks at 2θ = 21.96° and 26.60° become much higher and shape become much sharper than previous.

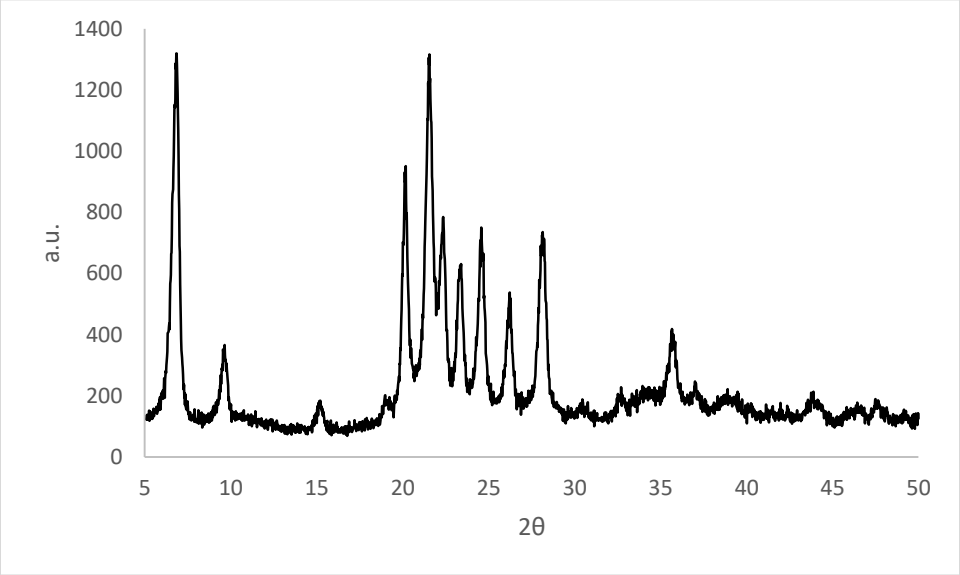

Figure 5-4: XRD pattern of Ni/Li-VPI-8 after drying overnight at 250 °C

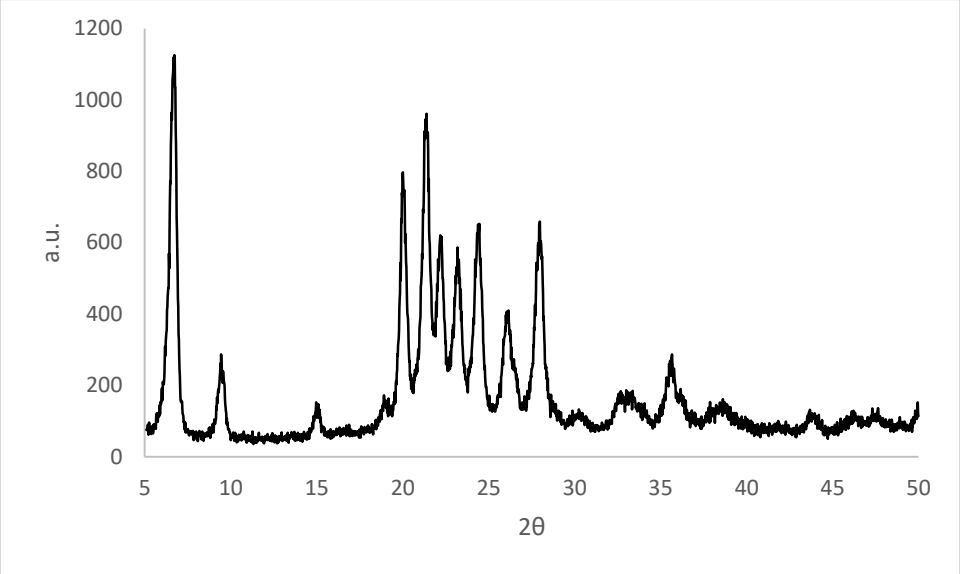

Figure 5-5: XRD pattern of Li-VPI-8 after reaction at 600 °C for 6 hours

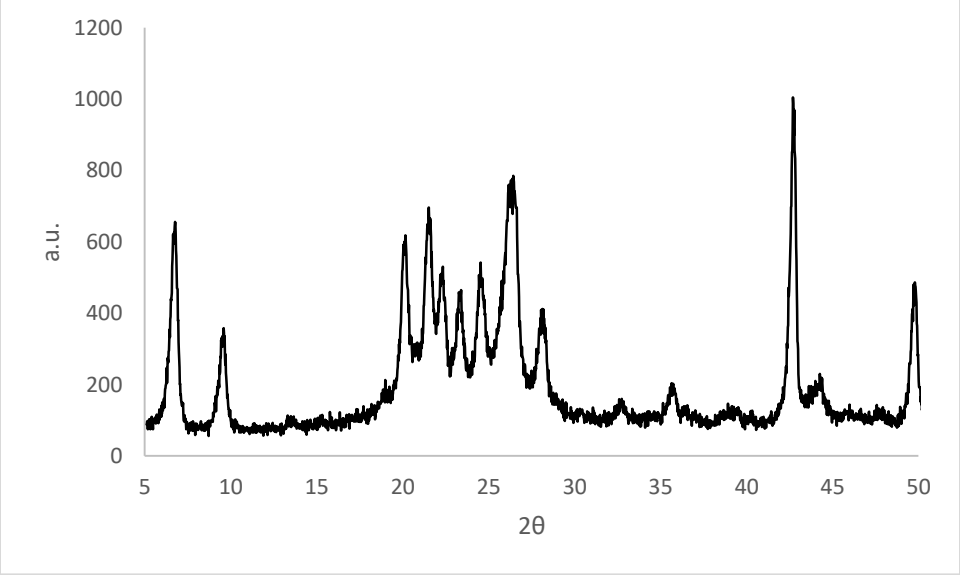

Figure 5-6: XRD pattern of Ni/Li-VPI-8 after 389 minutes reaction at 600 °C and 5 bar

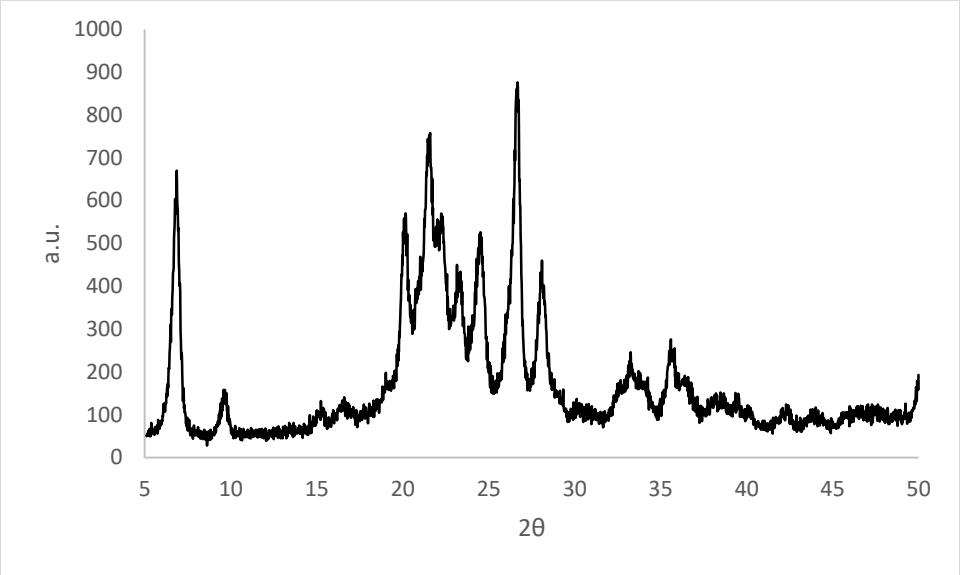

Figure 5-7: XRD pattern of Li-VPI-8 calcined at 700 °C overnight

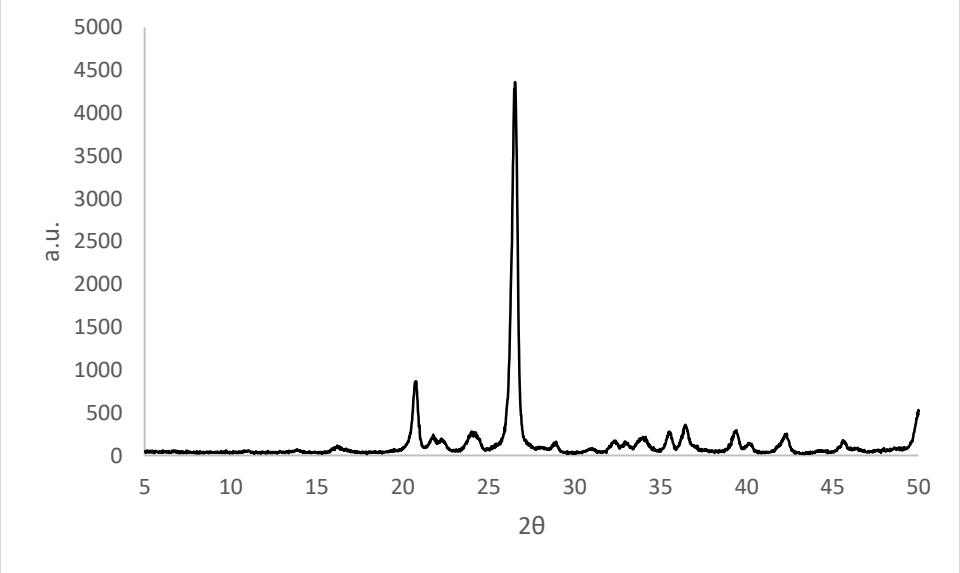

Figure 5-8: XRD pattern of Li-VPI-8 calcined at 750 °C overnight

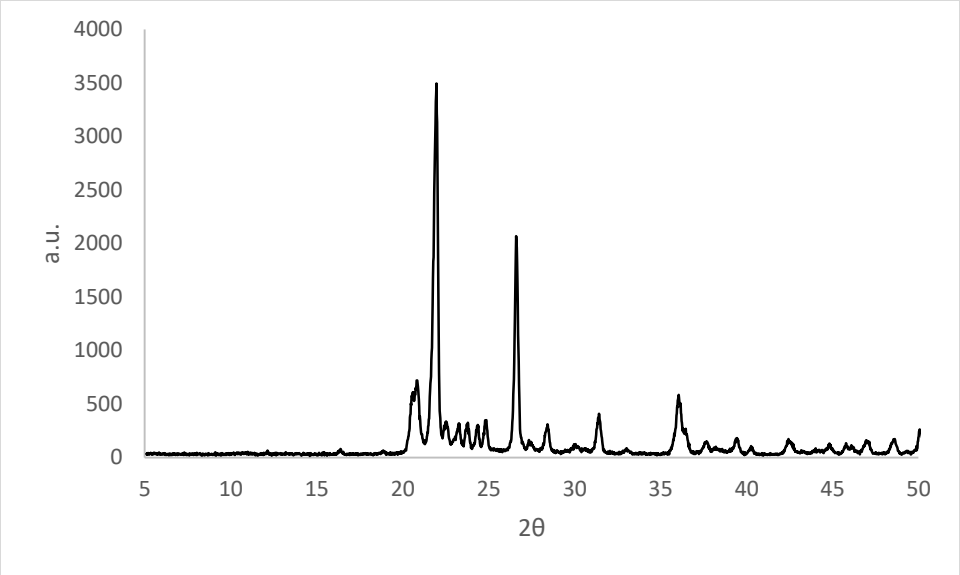

Figure 5-9: XRD pattern of Li-VPI-8 after 1046 minutes reaction at 750 °C

There was only one NH_3-TPD of VPI-8 investigated before. In 2014, the acid sites of H-formed VPI-8 seed and final product were reported as 0.1 mmol/g and 0.14 mmol/g, respectively [112]. Figure 5-10 shows the NH_3-TPD result of Li-VPI-8 in this work. The weak and strong acid peak is assigned to 150 °C and 375 °C, respectively. The active sites of VPI-8 is 0.16 mmol/g which is higher than previous with-seed synthesis. Figure 5-11 shows NH_3-TPD result of Ni/Li-VPI-8 with weak acid peak at 212 °C and strong acid peak at 700 °C. The acidity of Ni/Li-VPI-8 is much stronger than Li-VPI-8. Also, the Ni/Li-VPI-8 acid sites are 0.20 mmol/g which are more than Li-VPI-8.

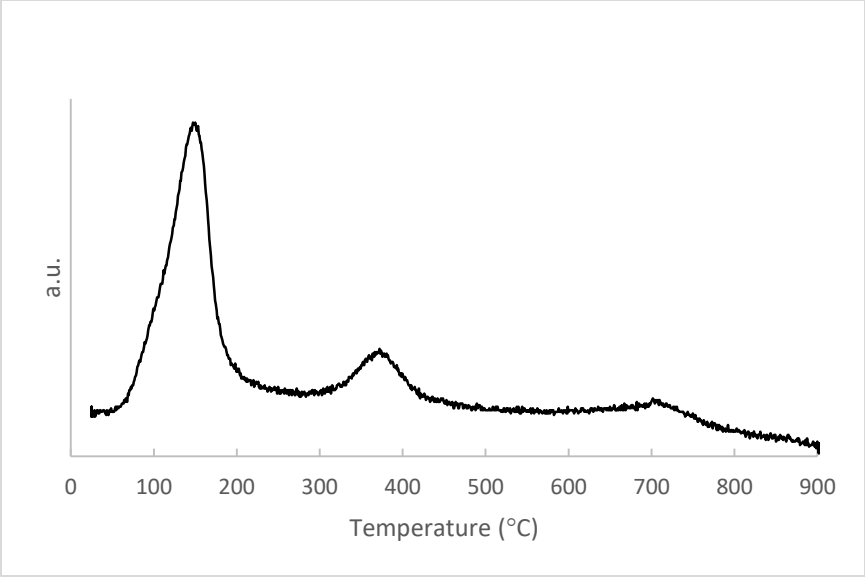

Figure 5-10: NH_3-TPD result of Li-VPI-8

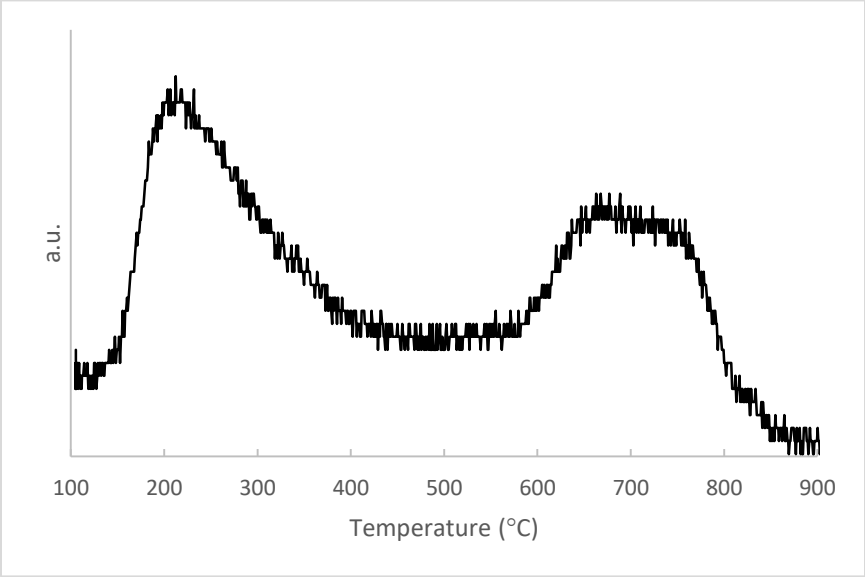

Figure 5-11: NH_3-TPD result of Ni/Li-VPI-8

In the previous report, VPI-8 is stable at 550 °C, but will lose its structure starting at 600 °C forward to an amorphous phase [123]. So, the first reaction condition was set to 550 °C at atmospheric pressure. In this case, no conversion of methane was noted. Then the reaction temperature was increased to 600 °C. Methane still did not convert at a 50 °C higher temperature.

Thus, a 5 bar pressure was applied on the reaction at 600 °C. Figure 5-12 shows methane conversion under reaction condition at 600 °C and 5 bar. At the beginning, the methane conversion on Li-VPI-8 catalyst is 100%. Then, the conversion decreases to 20% at 84 minutes. The conversion decreases slowly from 84 min to 212 min, which is about 9%. At the end, the methane conversion maintains about 11%. For Ni/Li-VPI-8, the tendency is similar with Li-VPI-8. However, the final stable conversion is about 15% which is about 4% higher than Li-VPI-8. When the pressure increases from 5 bar to 10 bar and keep the temperature at 600 °C, the methane conversion could reach about 20% instead of 11% on Li-VPI-8 catalyst.

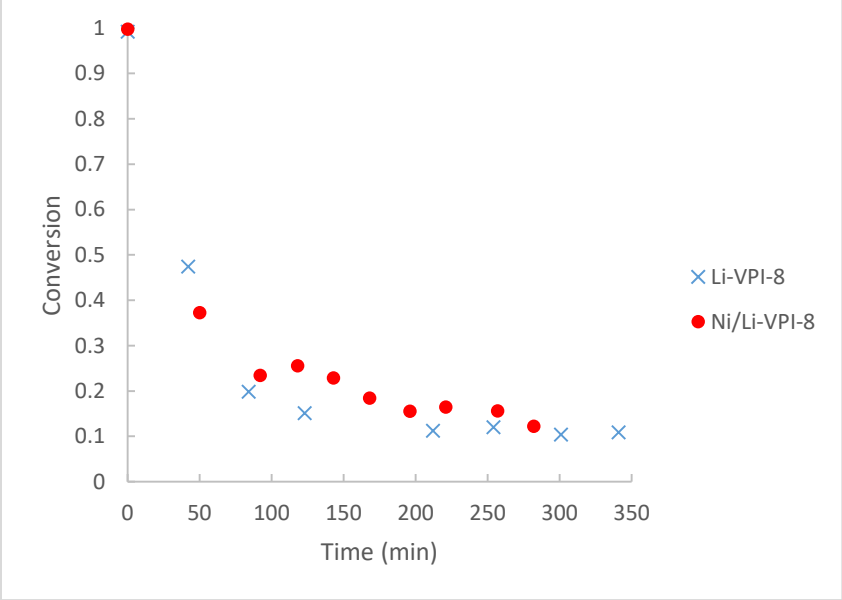

Figure 5-12: Methane conversion vs time under reaction condition at 600 °C and 5 bar

No aromatics were found at either 550 °C or 600 °C with and without pressure. The only products were hydrogen and carbon. It may be that the temperature is too low to form aromatics because of the thermal dynamics property [165]. Hence, a higher temperature was applied which is higher than 650 °C. Due to the maximum operating temperature for stainless-steel 316 tube is

648 °C, a quartz tube is employed instead of previous stainless-steel 316 tube. At 700 °C, the previous flow rate, 900 mL $CH_4/(g_{cat}\cdot h)$ and 1600 mL $N_2/(g_{cat}\cdot h)$, was tested as a base line, Table 5-1. For comparison, both the N_2 and CH_4 flow rate were doubled, there was still no aromatics found at 700 °C. But aromatics were appeared when N_2 flow was turned off with 1800 mL $CH_4/(g_{cat}\cdot h)$ at 700 °C. When the CH_4 flow rate was decreased back to 900 mL/$(g_{cat}\cdot h)$ without N_2, there was no aromatics observed. Without carrying gas, 1800 mL $CH_4/(g_{cat}\cdot h)$ was tested at both 725 °C and 750 °C, resulting in aromatics. This may be becaused the methane partial pressure was higher. However, at 725 °C, the aromatics is negligible. At 750 °C, more aromatics could be formed with 900 mL $CH_4/(g_{cat}\cdot h)$ and no N_2 flowing. Table 5-2 shows the stability of MDA reaction yield on Li-VPI-8 at 750 °C for a long time. And the H_2 yield was about 1.5%.

Table 5-1: Result for reaction on Li-VPI-8 catalsty at temperature above 700 °C and atmospheric pressure with varying reactant flow rate

Temperature, °C	CH_4 Flow Rate, mL/$(g_{cat}\cdot h)$	N_2 Flow Rate, mL/$(g_{cat}\cdot h)$	Results
700	900	1600	No Aromatics
700	900	3200	No Aromatics
700	1800	1600	No Aromatics
700	1800	0	Aromatics
700	900	0	No Aromatics
725	1800	0	Aromatics
750	1800	0	Aromatics
750	900	0	Aromatics

Table 5-2: Hydrocarbon yield in MDA reaction result on Li-VPI-8 catalyst at atmospheric pressure at 750 °C with 900 mL $CH_4/(g_{cat}\cdot h)$, C_2-C_5 represents chain hydrocarbons

Name	Reaction Time (minutes)					
	858	883	906	931	1002	1046
C_2	8.56%	8.79%	9.25%	4.45%	7.32%	9.20%
C_3	0.48%	0.49%	0.51%	0.58%	0.50%	0.46%
C_4	0.09%	0.11%	0.12%	0.15%	0.14%	0.11%

C_5	0.00%	0.00%	0.00%	0.13%	0.12%	0.09%
Benzene	6.10%	6.05%	6.28%	7.06%	6.42%	5.45%
Toluene	0.45%	0.41%	0.41%	0.46%	0.41%	0.30%
Xylene	0.94%	0.09%	1.05%	1.15%	1.56%	1.32%

Unfortunately, there was an issue found during the experiments. Li-VPI-8 was shrinking during the reaction, Figure 5-13. Li-VPI-8 powders were packed between two quartz wools before the reaction. After the 1046 minutes reaction, the catalysts only presented about 1/4 of the original volume. The reactant gas would bypass the catalyst to affect both methane conversion and aromatics selectivity which is lower than actually result. Coking is a general problem to limit the MDA reaction for long time. However, coking is not a problem in these experiments. Figure 5-13 shows the color changed on Li-VPI-8 after 472 minutes MDA reaction. Most of the catalysts are still white and starting to turn to grey, but not black yet. The actual product yield may be higher, because reactant gas by-pass may happen.

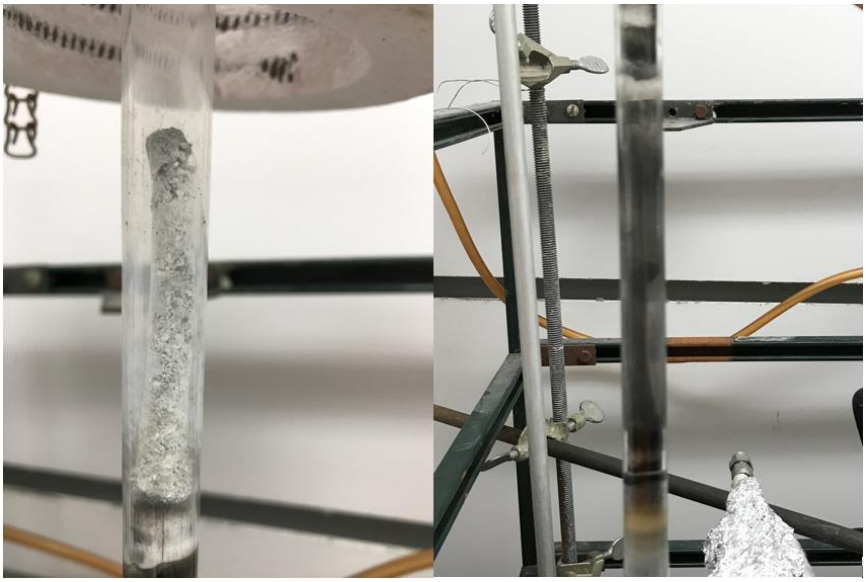

Figure 5-13: Li-VPI-8 catalyst shrinked after 750 °C reaciton 472 minutes (left) and 1046 minutes (right)

Chapter 6 - Conclusions and Recommendations

Conclusions

The successful synthesis of seed-free zincosilicate zeolite VPI-8 is reported in this work. Impurities or intermediate phases were not found during the synthesis. The final VPI-8 product is formatted directly from amorphous phase without solid state transfer. The synthesis method in this work results in VPI-8 with a uniform Zn dispersion, a higher thermal stability, and an increased number of acid sites than has been previously reported. Synthesis temperature and SDA concentration are the two major variables affecting VPI-8 synthesis. The synthesis time is decreased to 6 hours by increasing the synthesis temperature. For longer VPI-8, the synthesis time is decreased to 24 hours. The morphology of VPI-8 can be controlled by the TEA^+ concentration. The more TEA^+ add into the reaction mixture the longer the crystal is. Some other variables were also studied. VPI-8 can be synthesized by using different silica and zinc sources, and different order of preparing aging solution. The Zn T-atom does not have a favorite location, because the energies of formation are similar.

Methane conversion starts at 600 °C and increases while pressure increasing. Li-VPI-8 and Ni/Li-VPI-8 can keep the methane conversion about 11 % and 15 %, respectively. Coking is not the significant limitation for methane dehydroaromatization reaction over Li-VPI-8 due to the methane conversion could maintain above 10 % stable for at least 1000 minutes under 750 °C reaction temperature. However, the crystallization of VPI-8 is changed at 750 °C.

Recommendations

In the future, a stirring reactor may be used to reduce the non-dissolved silicate so that the filtration could be completed much faster. A high zinc concentration in the mixture solution may decrease Si/Zn ratio to achieve more active sites. The cost of SDA can be decreased by finding a proper PFA. There is an unknown phase appearing during the experiments which need to be characterized.

To continue the MDA reaction, the molybdenum-based VPI-8 may be studied due to Mo-based ZSM-5 is best catalyst for MDA reaction. But the configuration of Mo species on VPI-8 is not clear. Because the oxygen bridge of zincosilicate is different with aluminosilicate zeolites. In zincosilicate (O-Zn-O), the center of active site is the Zn atom with two charged oxygen atoms to balance the cation. In contrast, the center of active site in an aluminosilicate (O-Al-O-Si-O-Al-O) is Si atom and the charges of oxygen atoms is provided by further Al atom. The shrinking problem of VPI-8 during the high temperature reaction need to be fixed to avoid the reaction gas bypass around catalyst. The catalyst may need to be packed during the reaction. The ion-exchanged nickel weight on Li-VPI-8 and dispersion need to be measured. Because one of the catalyzing limitations on MDA reaction is that catalyst can not be regenerated to its original condition, due to the carbon nano-tube growths on the active metal. It is necessary to study the regeneration of VPI-8 after reaction. For high temperature pressured attempting, a suitable material reactor is required. For example, the operation temperature of stainless steel 347 is up to 900 °C, which also can carry pressure. For a better understanding the MDA reaction over zincosilicate, DFT simulations are necessary to compare with experimental results.

Due to the thermal stability of VPI-8, most the reactions over aluminosilicate zeolites can be catalyzed by VPI-8 hypothetically. Different metals, such as Cu, Fe, Re, Ga, Zn,

V, Co, Cr, W, and Mn, should be attempted to load on VPI-8 either by ion-exchanged or impregnated method, then need to be characterized. Since VPI-8 is a large pore material, it also can be used to select large size product. The selective catalytic reduction may be improved by using zincosilicate zeolite due to the stronger acid site.

References

1. Mcbain, J. W. ,1932.

2. Leonard B. Sand; Frederick Albert Mumpton ,1978, 85-98.

3. Cejka, J.; van Bekkum, H.; Corma, A.; Schueth, F. ,2007, 168.

4. de St Claire Deville ,Comptes Rendus Acad. Sci.,1862, 54, 324.

5. Anonymous,Bull. Soc. Min.,1882, 5, 7-9.

6. Breck, D. W. ,1984.

7. Barrer, R. M. ,Journal of the Chemical Society (Resumed),1948, 0, 127-132.

8. Barrett, P. A.; Curd, F. H. S.; Hepworth, W. ,Journal of the Chemical Society (Resumed),1953, 0, 50-58.

9. Barrer, R. M.; Marcilly, C. ,Journal of the Chemical Society A: Inorganic, Physical, Theoretical,1970, 0, 2735-2745.

10. Kerr, G. T. ,Inorganic Chemistry,1966, 5, 1537-1539.

11. Kerr, G. T. ,Science,1963, 140, 1412.

12. Robert M Milton ,1959.

13. Robert M Milton ,1959.

14. Milton, R. M. ,Molecular Sieves,1989, 398, 1-10.

15. Barrer, R. M.; Denny, P. J. ,Journal of the Chemical Society (Resumed),1961, 0, 971-982.

16. Jacobs, P. A.; Martens, J. A. ,1987.

17. Robert L Wadlinger, George T Kerr, Edward J Rosinski ,1967.

18. Robert J Argauer, George R Landolt ,1972.

19. Wilson, S. T.; Lok, B. M.; Messina, C. A.; Cannan, T. R.; Flanigen, E. M. ,Journal of the American Chemical Society,1982, 104, 1146-1147.

20. Stephen T. Wilson, Brent M. Lok, Edith M. Flanigen ,1982.

21. Meier, W. ,1987.

22. Walter Loewenstein ,American Mineralogist,1954, 39, 92.

23. Flanigen, E. M.; Lok, B. M.; Patton, R. L.; Wilson, S. T. ,Pure and Applied Chemistry,1986, 58, 1351-1358.

24. Davis, M.; Saldarriaga, C.; Montes, C.; Garces, J.; Crowder, C. ,Nature,1988, 331, 698.

25. Yu, J.; Xu, R. ,Chemical Society Reviews,2006, 35, 593-604.

26. Davis, M. E. ,Nature,2002, 417, 813-821.

27. Anonymous,2016.

28. Nikolai Tsarik ,Journal (American Water Works Association),1993, 85, 42-45.

29. King, L. J.; Campbell, D. O.; Collins, E. D.; Knauer, J. B.; Wallace, R. M. ,1983.

30. Lt, N. C. 2.; Lt, R.; C.COL, C.; S, V. ,Military Medicine,2004, 169, 716-720.

31. Wright, J. K.; Kalns, J.; Wolf, E. A.; Traweek, F.; Schwarz, S.; Loeffler, C. K.; Snyder, W.; Yantis, L. D.; Eggers, J. ,The Journal of Trauma,2004, 57, 224-230.

32. Kashchiev, D. ,2000.

33. Mullin, J. W. ,2001.

34. Cundy, C. S.; Cox, P. A. ,Microporous and Mesoporous Materials,2005, 82, 1-78.

35. Barrer, R. M.; Baynham, J. W.; Bultitude, F. W.; Meier, W. M. ,Journal of the Chemical Society (Resumed),1959, 0, 195-208.

36. Breck, D. W. ,Journal of Chemical Education,1964, 41, 678.

37. Kerr, G. T. ,The Journal of Physical Chemistry,1966, 70, 1047-1050.

38. ZHDANOV, S. P. ,1974, 101, 20-43.

39. Chang, C. D.; Bell, A. T. ,Catalysis Letters,1991, 8, 305-316.

40. Burkett, S. L.; Davis, M. E. ,The Journal of Physical Chemistry,1994, 98, 4647-4653.

41. Burkett, S. L.; Davis, M. E. ,Chemistry of Materials,1995, 7, 1453-1463.

42. Burkett, S. L.; Davis, M. E. ,Chemistry of Materials,1995, 7, 920-928.

43. Breck, D. W. ,1973.

44. Kühl, G. ,Microporous and Mesoporous Materials,1998, 22, 515-516.

45. MEISE, W.; SCHWOCHOW, F. E. ,1973, 121, 169-178.

46. Shimizu, S.; Hamada, H. ,Angewandte Chemie International Edition,1999, 38, 2725-2727.

47. Fegan, S. G.; Lowe, B. M. ,Journal of the Chemical Society, Faraday Transactions 1: Physical Chemistry in Condensed Phases,1986, 82, 785-799.

48. Seward, T. M. ,Physics and Chemistry of the Earth,1981, 13, 113-132.

49. Robson, H. ,2001.

50. McCusker, L. B.; Grosse-Kunstleve, R. W.; Baerlocher, C.; Yoshikawa, M.; Davis, M. E. ,Microporous Materials,1996, 6, 295-309.

51. FLANIGEN, E. M. ,1973, 121, 119-139.

52. Hölderich, W.; Karge, H. G.; Weitkamp, J.; Pfeifer, H.; Pfeifer, H.; Holderich, W. ,1994.

53. Derouane, E.; Ribeiro, F.; Lemos, F.; Naccache, C. ,1992.

54. Lok, B. M.; Cannan, T. R.; Messina, C. A. ,Zeolites,1983, 3, 282-291.

55. Lawton, S. L.; Rohrbaugh, W. J. ,Science,1990, 247, 1319-1322.

56. Davis, M. E.; Lobo, R. F. ,Chemistry of Materials,1992, 4, 756-768.

57. Barthomeuf, D.; Derouane, E. G.; Hölderich, W. ,1990.

58. Jiang, J.; Yu, J.; Corma, A. ,Angewandte Chemie International Edition,2010, 49, 3120-3145.

59. Wagner, P.; Nakagawa, Y.; Lee, G. S.; Davis, M. E.; Elomari, S.; Medrud, R. C.; Zones, S. I. ,Journal of the American Chemical Society,2000, 122, 263-273.

60. Zones, S. I.; Burton, A. W.; Lee, G. S.; Olmstead, M. M. ,Journal of the American Chemical Society,2007, 129, 9066-9079.

61. Burton, A. W.; Lee, G. S.; Zones, S. I. ,Microporous and Mesoporous Materials,2006, 90, 129-144.

62. Shvets, O. V.; Kasian, N.; Zukal, A.; Pinkas, J.; Čejka, J. ,Chemistry of Materials,2010, 22, 3482-3495.

63. Goretsky, A. V.; Beck, L. W.; Zones, S. I.; Davis, M. E. ,Microporous and Mesoporous Materials,1999, 28, 387-393.

64. Xie, B.; Song, J.; Ren, L.; Ji, Y.; Li, J.; Xiao, F. ,Chemistry of Materials,2008, 20, 4533-4535.

65. Boggs, R. C.; Howard, D. G.; Smith, J. V.; Klein, G. L. ,American Mineralogist,1993, 78, 822.

66. Kamimura, Y.; Chaikittisilp, W.; Itabashi, K.; Shimojima, A.; Okubo, T. ,Chemistry – an Asian Journal,2010, 5, 2182-2191.

67. Zones, S. I. ,Microporous and Mesoporous Materials,2011, 144, 1-8.

68. Liebau, F. ,1985.

69. Lee, H.; Zones, S. I.; Davis, M. E. ,Nature,2003, 425, 385-388.

70. Bibby, D. M.; Dale, M. P. ,Nature,1985, 317, 157-158.

71. Morris, R. E.; Weigel, S. J. ,Chemical Society Reviews,1997, 26, 39-317.

72. Kacirek, H.; Lechert, H. ,The Journal of Physical Chemistry,1976, 80, 1291-1296.

73. Ciric, J. ,Journal of Colloid and Interface Science,1968, 28, 315-324.

74. Goto, K. ,Nippon Kagaku Zassi,1955, 76, 1364-1366.

75. Rees, L. V. C. ,1980.

76. Feoktistova, N. N.; Zhdanov, S. P.; Lutz, W.; Büllow, M. ,Zeolites,1989, 9, 136-139.

77. Cundy, C. S.; Lowe, B. M.; Sinclair, D. M. ,Faraday Discussions,1993, 95, 235-252.

78. Ostwald, W. ,Zeitschrift Fr Physikalische Chemie,1888, 2, 36-37.

79. Serrano, D. P.; van Grieken, R.; Davis, M. E.; Melero, J. A.; Garcia, A.; Morales, G. ,Chemistry – A European Journal,2002, 8, 5153-5160.

80. Bronić, J.; Subotić, B.; Smit, I.; Despotović, L. J. A. ,1988, 37, 107-114.

81. Twomey, T. A. M.; Mackay, M.; Kuipers, H P C E; Thompson, R. W. ,Zeolites,1994, 14, 162-168.

82. Cejka, J.; Bekkum, H. v.; Corma, A.; Schueth, F.; Schueth, F. ,2007.

83. Di Renzo, F.; Remoué, F.; Massiani, P.; Fajula, F.; Figueras, F.; Thierry Des, C. ,Zeolites,1991, 11, 539-548.

84. Zhang, L.; Yao, J.; Zeng, C.; Xu, N. ,Chemical Communications,2003, 0, 2232-2233.

85. Song, Y.; Li, J.; Yu, J.; Wang, K.; Xu, R. ,Topics in Catalysis,2005, 35, 3-8.

86. Qiu, S.; Yu, J.; Zhu, G.; Terasaki, O.; Nozue, Y.; Pang, W.; Xu, R. ,Microporous and Mesoporous Materials,1998, 21, 245-251.

87. Di Renzo, F. ,Catalysis Today,1998, 41, 37-40.

88. Stefano Merlino ,European Journal of Mineralogy,1990, 809-817.

89. Lawton, S. L.; Rohrbaugh, W. J. ,Science,1990, 247, 1319-1322.

90. Estermann, M.; Mccusker, L. B.; Baerlocher, C.; Merrouche, A.; Kessler, H. ,Nature,1991, 352, 320.

91. Bnmner, G. O.; Meier, W. M. ,Nature,1989, 337, 146-147.

92. Stixrude, L.; Bukowinski, M. S. T. ,American Mineralogist,1990, 75.

93. Stixrude, L.; Bukowinski, M. S. T. ,Science,1990, 250, 541-543.

94. Cooper, B. J. ,1978.

95. Hang C, Simonov M A, Belov N V ,Soviet Physics Crystallography,1970, 15, 387-390.

96. Gibbs, G. V.; D'Arco, P.; Boisen, M. B. ,The Journal of Physical Chemistry,1987, 91, 5347-5354.

97. Geisinger, K. L.; Gibbs, G. V.; Navrotsky, A. ,Physics and Chemistry of Minerals,1985, 11, 266-283.

98. Annen, M. J.; Davis, M. E.; Higgins, J. B.; Schlenker, J. L. ,Journal of the Chemical Society, Chemical Communications,1991, 0, 1175-1176.

99. Röhrig, C.; Gies, H. ,Angewandte Chemie International Edition in English,1995, 34, 63-65.

100. Annen, M. J.; Davis, M. E. ,Microporous Materials,1993, 1, 57-65.

101. Camblor, M. A.; Lobo, R. F.; Koller, H.; Davis, M. E. ,Chemistry of Materials,1994, 6, 2193-2199.

102. Takewaki, T.; Beck, L. W.; Davis, M. E. ,Topics in Catalysis,1999, 9, 35-42.

103. Takewaki, T.; Beck, L. W.; Davis, M. E. ,The Journal of Physical Chemistry B,1999, 103, 2674-2679.

104. Dong, M.; Wang, J.; Sun, Y. ,Microporous and Mesoporous Materials,2001, 43, 237-243.

105. Kowalak, S.; Szymkowiak, E.; Gierczyńska, M.; Giordano, G. ,Studies in Surface Science and Catalysis,2002, 142, 351-358.

106. Kowalak, S.; Janiszewska, E.; Gierczyńska, M.; Dolata, V.; Evmiridis, N.; Katranas, T.; Vlessidis, A.; Tsiatouras, V.; Roessner, F.; Schneider, E. ,Studies in Surface Science and Catalysis,2004, 154, 2200-2207.

107. Janiszewska, E.; Kowalak, S.; Gierczyńska, M.; Dolata, V.; Zieliński, M.; Wojciechowska, M. ,Catalysis Letters,2007, 114, 64-70.

108. Wang, L.; Sang, S.; Meng, S.; Zhang, Y.; Qi, Y.; Liu, Z. ,Materials Letters,2007, 61, 1675-1678.

109. Ni, Y.; Sun, A.; Wu, X.; Hai, G.; Hu, J.; Li, T.; Li, G. ,Microporous and Mesoporous Materials,2011, 143, 435-442.

110. de Man, A J M; Ueda, S.; Annen, M. J.; Davis, M. E.; van Santen, R. A. ,Zeolites,1992, 12, 789-800.

111. Suzuki, Y.; Wakihara, T.; Kohara, S.; Itabashi, K.; Ogura, M.; Okubo, T. ,The Journal of Physical Chemistry C,2011, 115, 443-446.

112. Iyoki, K.; Itabashi, K.; Chaikittisilp, W.; Elangovan, S. P.; Wakihara, T.; Kohara, S.; Okubo, T. ,Chemistry of Materials,2014, 26, 1957-1966.

113. Camblor, M. A.; Davis, M. E. ,The Journal of Physical Chemistry,1994, 98, 13151-13156.

114. Yoshikawa, M.; Zones, S. I.; Davis, M. E. ,Microporous Materials,1997, 11, 137-148.

115. Tomlinson, S. R.; McGown, T.; Schlup, J. R.; Anthony, J. L. ,International Journal of Spectroscopy,2013, 2013.

116. McGown, T. ,2007.

117. Mckeen, J. C.; Davis, M. E. ,The Journal of Physical Chemistry C,2009, 113, 9870-9877.

118. Orazov, M.; Davis, M. E. ,Chemical Science; Chem.Sci.,2016, 7, 2264-2274.

119. Davis, M. E.; Saldarriaga, C.; Montes, C.; Garces, J.; Crowder, C. ,Zeolites,1988, 8, 362-366.

120. Freyhardt, C. C.; Khodabandeh, S.; Lewis, J. E. J.; others, a. ,Journal of the American Chemical Society,1996, 118, 7299-7310.

121. Yoshikawa, M.; Davis, S. I.; Yoshikawa, M. E.; Zones, M. E. ,Microporous Materials,1997, 11, 127-136.

122. Serrano, D. P.; Van Grieken, R.; Davis, M. E.; Melero, J. A.; Garcia, A.; Morales, G. ,Chemistry – A European Journal,2002, 8, 5153-5160.

123. Annen, M. J. ,1992.

124. Selbe, T. J. ,2010.

125. Andy, P.; Davis, M. E. ,Industrial & Engineering Chemistry Research,2004, 43, 2922-2928.

126. Deimund, M. A.; Labinger, J.; Davis, M. E. ,ACS Catalysis,2014, 4, 4189-4195.

127. Ro¨hrig, C.; Gies, H.; Marler, B. ,Zeolites,1994, 14, 498-503.

128. Andy, P.; Davis, M. E. ,Industrial & Engineering Chemistry Research,2004, 43, 2922-2928.

129. Deimund, M. A.; Labinger, J.; Davis, M. E. ,ACS Catalysis,2014, 4, 4189-4195.

130. Camblor, M. A.; Zones, S.; Davis, M. E. ,Abstracts of Papers of the American Chemical Society; Abstr.Pap.Am.Chem.Soc.,1995, 209, PETR.

131. Takewaki, T.; Beck, L.; Davis, M. E. ,Topics in Catalysis; Top.Catal.,1999, 9, 35-42.

132. Günter Engelhardt; Hubert Koller ,1994, 31, 1-29.

133. Engelhardt, G. ,1987.

134. te Velde, G.; Bickelhaupt, F. M.; Baerends, E. J.; Fonseca Guerra, C.; van Gisbergen, S. J. A; Snijders, J. G.; Ziegler, T. ,Journal of Computational Chemistry,2001, 22, 931-967.

135. Delley, B. ,The Journal of Chemical Physics,2000, 113, 7756-7764.

136. Anonymous,2017.

137. Perdew, J. P.; Burke, K.; Ernzerhof, M. ,Physical Review Letters,1996, 77, 3865-3868.

138. Anonymous,2016.

139. Dickens, G. R. ,Organic Geochemistry,2001, 32, 1179-1193.

140. Anonymous,Department of Energy (DOE) Documents / FIND,2012.

141. Lunsford, J. H. ,1994, 81, 1-12.

142. Ma, S.; Guo, X.; Zhao, L.; Scott, S.; Bao, X. ,Journal of Energy Chemistry,2013, 22, 1-20.

143. Wang, L.; Tao, L.; Xie, M.; Xu, G.; Huang, J.; Xu, Y. ,Catalysis Letters,1993, 21, 35-41.

144. Liu, B. S.; Zhang, Y.; Liu, J. F.; Tian, M.; Zhang, F. M.; Au, C. T.; Cheung, A. S. -. ,The Journal of Physical Chemistry C,2011, 115, 16954-16962.

145. Luzgin, M. V.; Rogov, V. A.; Arzumanov, S. S.; Toktarev, A. V.; Stepanov, A. G.; Parmon, V. N. ,Angewandte Chemie (International Ed. in English),2008, 47, 4559-4562.

146. Kusmiyati; Amin, N. A. S. ,Catalysis Letters,2005, 102, 69-78.

147. Li-Qiang, H.; Jin-Long, Z.; Guo-Dong, L. I. N.; You-Zhu, Y.; Hong-Bin, Z. ,Acta Chimica Sinica,2004, 62, 1706-1712.

148. Yang, J.; Ma, D.; Deng, F.; Luo, Q.; Zhang, M.; Bao, X.; Ye, C. ,Chemical Communications,2002, 346-347.

149. Xiong, Z.; Chen, L.; Zhang, H.; Zeng, J.; Lin, G. ,Catalysis Letters,2001, 74, 227-232.

150. Zeng, J.; Xiong, Z.; Zhang, H.; Lin, G.; Tsai, K. R. ,Catalysis Letters,1998, 53, 119-124.

151. Ding, W.; Meitzner, G. D.; Marler, D. O.; Iglesia, E. ,The Journal of Physical Chemistry B,2001, 105, 3928-3936.

152. Kozlov, V.; Zaikovskii, V.; Vosmerikov, A.; Korobitsyna, L.; Echevskii, G. ,Kinetics and Catalysis,2008, 49, 110-114.

153. Wang, L.; Ohnishi, R.; Ichikawa, M. ,Catalysis Letters,1999, 62, 29-33.

154. Ohnishi, R.; Ichikawa, M. ,Catalysis Surveys from Japan,2002, 5, 103-110.

155. Wang, L.; Ohnishi, R.; Ichikawa, M. ,Journal of Catalysis,2000, 190, 276-283.

156. Shu, Y.; Ohnishi, R.; Ichikawa, M. ,Applied Catalysis A: General,2003, 252, 315-329.

157. Wang, L.; Murata, K.; Sayari, A.; Grandjean, B.; Inaba, M. ,Chemical Communications,2001, 1952-1953.

158. Li, S.; Zhang, C.; Kan, Q.; Wang, D.; Wu, T.; Lin, L. ,Applied Catalysis A: General,1999, 187, 199-206.

159. Tan, P.; Au, C.; Lai, S. ,Catalysis Letters,2006, 112, 239-245.

160. Ma, D.; Shu, Y.; Zhang, C.; Zhang, W.; Han, X.; Xu, Y.; Bao, X. ,Journal of Molecular Catalysis A: Chemical,2001, 168, 139-146.

161. Anton A. Gabrienko; Vladimir A. Rogov; Alexander V. Toktarev; Valentin N. Parmon; Alexander G. Stepanov ,The Journal of Physical Chemistry C,2010, 114, 21555-21561.

162. Weckhuysen, B. M.; Wang, D.; Rosynek, M. P.; Lunsford, J. H. ,Journal of Catalysis,1998, 175, 338-346.

163. Thomson Reuters Corporation .

164. S H Morejudo; R Zanón; S Escolástico; I Yuste-Tirados; H Malerød-Fjeld; P K Vestre; W G Coors; A Martínez; T Norby; J M Serra; C Kjølseth ,Science,2016, 353, 563-566.

165. Xu, Y.; Bao, X.; Lin, L. ,Journal of Catalysis,2003, 216, 386-395.

Appendix A - Support Documents

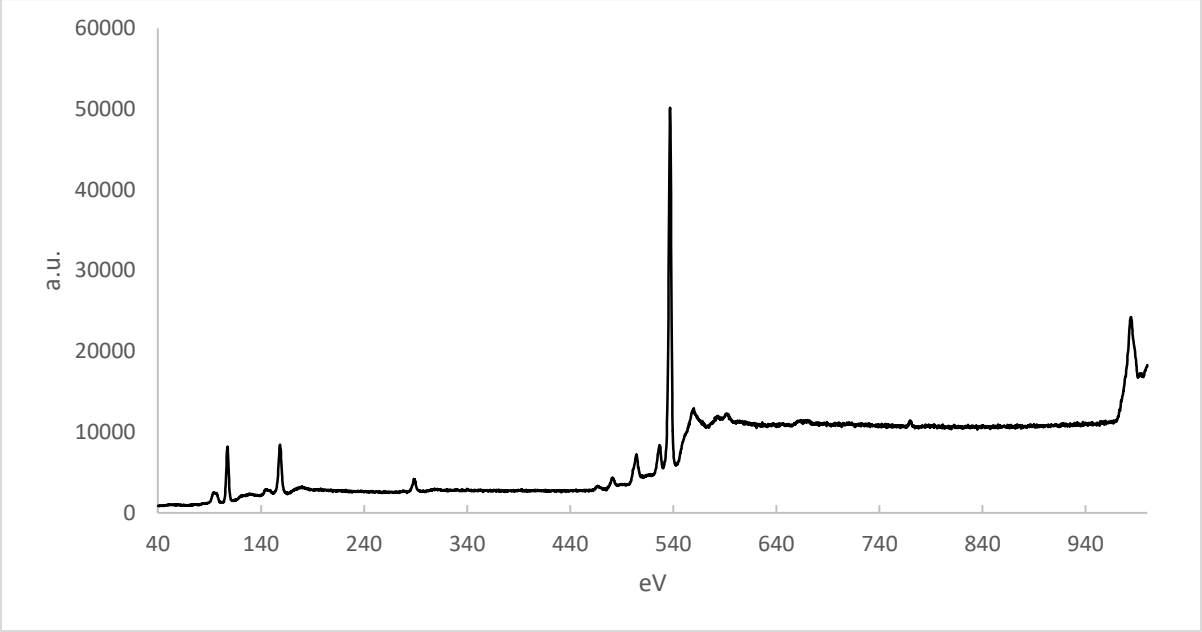

Figure A-1: Survey XPS spectra of Li-VPI-8 (exp. 1)

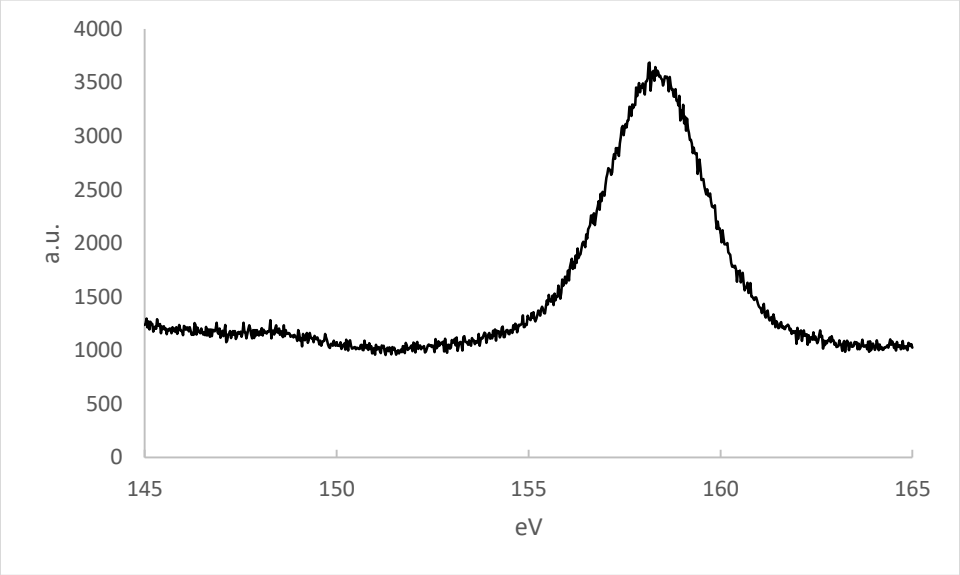

Figure A-2: Multi Si 2s XPS spectra of Li-VPI-8 (exp. 1)

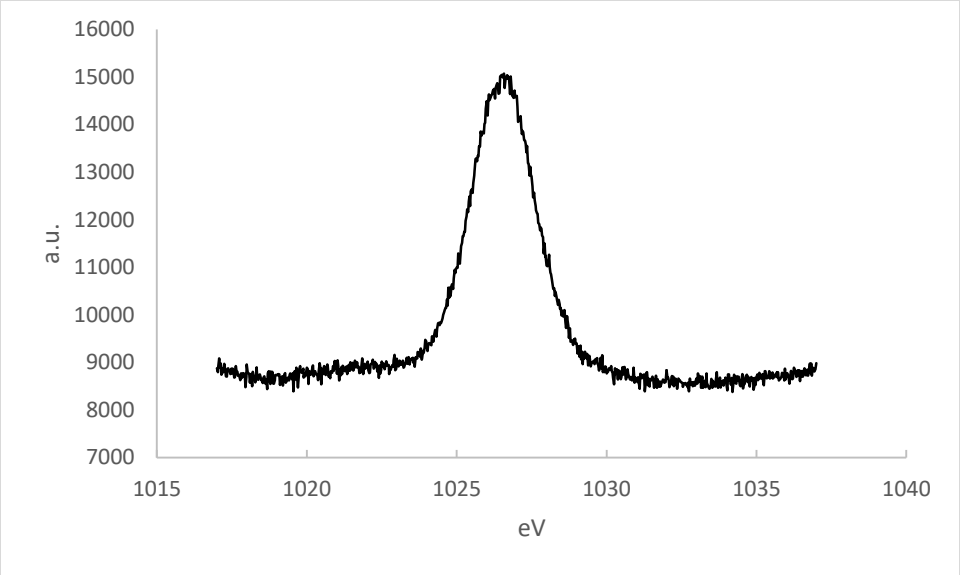

Figure A-3: Multi Zn 2p3 XPS spectra of Li-VPI-8 (exp. 1)

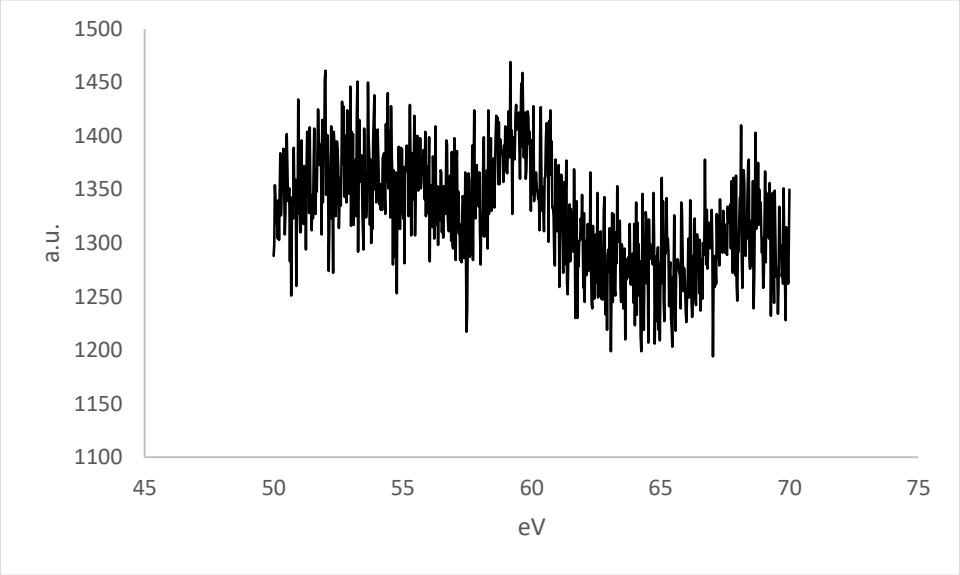

Figure A-4: Multi Li 1s XPS spectra of Li-VPI-8 (exp. 1)

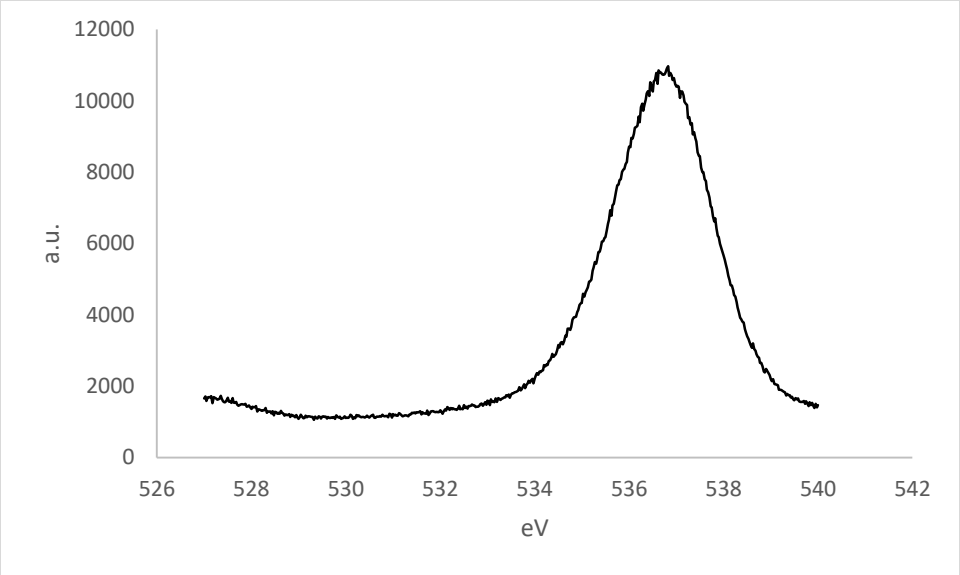

Figure A-5: Multi O 1s XPS spectra of Li-VPI-8 (exp. 1)

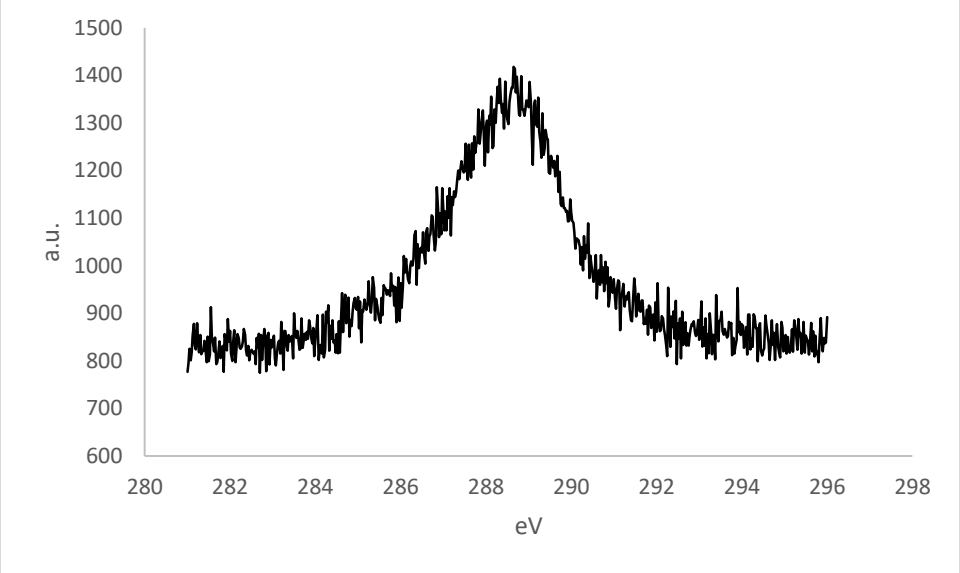

Figure A-6: Multi C 1s XPS spectra of Li-VPI-8 (exp. 1)

Table A-1: Atom coordination of scheme A

Atom Number	Atom	x	y	z
0	O	0	0	0
1	O	11.53517	0	0
2	O	16.09755	45.75245	0
3	O	11.53517	88.4951	18.4103

Atom Number	Atom	x	y	z
4	O	2.625013	29.49196	5.533074
5	O	10.4356	12.47231	332.8873
6	O	13.69141	47.93706	7.846961
7	O	9.340124	81.23282	10.47567
8	O	3.734567	49.89199	75.16747
9	O	11.18461	18.83983	220.9375
10	O	14.81213	48.29084	66.25949
11	O	9.565649	88.65955	343.5143
12	O	12.11262	75.04478	6.413093
13	O	3.595169	90.50445	30.81012
14	O	8.247316	8.551469	226.1082
15	O	14.41047	34.88781	103.4457
16	O	8.676654	20.28485	316.8726
17	O	12.7425	41.50773	52.00775
18	O	9.74588	73.01758	344.8696
19	O	4.537149	55.91351	44.41917
20	O	10.81943	25.83137	296.9686
21	O	12.47666	53.38781	32.90259
22	O	7.313142	79.45543	347.7191
23	O	5.045099	25.526	54.33008
24	O	6.64566	12.66775	304.3186
25	O	11.87516	32.94265	1.391304
26	O	11.13793	63.14035	5.949079
27	O	5.257312	72.41387	8.208231
28	O	7.31298	18.49098	68.08974
29	O	12.72088	34.65797	256.9215
30	O	12.36706	64.19849	39.46529
31	O	5.151399	86.79098	329.4395
32	O	5.515373	10.58177	161.3812
33	O	6.196919	96.87764	221.0705
34	Si	1.611092	35.38229	327.7849

Atom Number	Atom	x	y	z
35	Si	1.611092	133.319	29.81404
36	Si	1.611092	139.4382	241.8299
37	Si	1.611092	110.4538	136.529
38	Si	1.609959	63.52759	336.13
39	Si	1.609959	120.6373	344.4543
40	Si	1.609959	168.4933	123.8614
41	Si	1.609959	31.3387	178.7229
42	Si	2.987964	127.21	356.5185
43	Si	2.987964	127.21	18.32752
44	Si	2.987964	127.21	222.9803
45	Si	2.987964	127.21	132.6645
46	Si	2.955928	124.1749	77.52672
47	Si	2.955928	124.1749	282.4733
48	Si	2.955928	124.1749	77.52672
49	Si	2.955928	124.1749	282.4733
50	Si	1.611122	132.4819	117.8407

Table A-2: Atom coordination of scheme B

Atom Number	Atom	x	y	z
0	O	0	0	0
1	O	11.53517	0	0
2	O	16.09755	45.75245	0
3	O	11.53517	88.4951	18.4103
4	O	2.625013	29.49196	5.533074
5	O	10.4356	12.47231	332.8873
6	O	13.69141	47.93706	7.846961
7	O	9.340124	81.23282	10.47567
8	O	3.734567	49.89199	75.16747
9	O	11.18461	18.83983	220.9375
10	O	14.81213	48.29084	66.25949
11	O	9.565649	88.65955	343.5143

Atom Number	Atom	x	y	z
12	O	12.11262	75.04478	6.413093
13	O	3.595169	90.50445	30.81012
14	O	8.247316	8.551469	226.1082
15	O	14.41047	34.88781	103.4457
16	O	8.676654	20.28485	316.8726
17	O	12.7425	41.50773	52.00775
18	O	9.74588	73.01758	344.8696
19	O	4.537149	55.91351	44.41917
20	O	10.81943	25.83137	296.9686
21	O	12.47666	53.38781	32.90259
22	O	7.313142	79.45543	347.7191
23	O	5.045099	25.526	54.33008
24	O	6.64566	12.66775	304.3186
25	O	11.87516	32.94265	1.391304
26	O	11.13793	63.14035	5.949079
27	O	5.257312	72.41387	8.208231
28	O	7.31298	18.49098	68.08974
29	O	12.72088	34.65797	256.9215
30	O	12.36706	64.19849	39.46529
31	O	5.151399	86.79098	329.4395
32	O	5.515373	10.58177	161.3812
33	O	6.196919	96.87764	221.0705
34	Zn	1.611092	35.38229	327.7849
35	Zn	1.611092	133.319	29.81404
36	Zn	1.611092	139.4382	241.8299
37	Zn	1.611092	110.4538	136.529
38	Si	3.033591	19.64117	227.4536
39	Si	3.033591	19.64117	216.4491
40	Si	3.033591	19.64117	81.79164
41	Si	3.033591	19.64117	77.9696
42	Si	2.987964	101.377	53.40324

Atom Number	Atom	x	y	z
43	Si	2.987964	101.377	306.5968
44	Si	2.987964	101.377	53.40324
45	Si	2.987964	101.377	306.5968
46	Si	2.955928	124.1749	308.1465
47	Si	2.955928	124.1749	51.85347
48	Si	2.955928	124.1749	308.1465
49	Si	2.955928	124.1749	51.85347
50	Si	3.112566	103.7495	14.45818

Table A-3: Atom coordination of scheme C

Atom Number	Atom	x	y	z
0	Li	0	0	0
1	Li	3.04	0	0
2	O	11.45872	76.30549	0
3	O	7.52149	147.6594	355.3361
4	O	4.339535	69.4378	244.403
5	O	8.012418	24.9065	96.63267
6	O	8.873063	78.85813	23.29303
7	O	5.349236	138.8589	338.7604
8	O	4.241528	65.09385	222.8917
9	O	9.7649	34.12589	117.1407
10	O	9.206517	80.92246	57.89633
11	O	7.192394	132.3443	299.0071
12	O	7.833604	121.0555	33.43573
13	O	3.836308	115.0452	238.1498
14	O	7.999174	24.48369	50.1161
15	O	9.754087	60.09651	89.22867
16	O	7.363217	36.75543	300.3345
17	O	7.49963	67.88133	64.78355
18	O	6.255823	115.1698	318.9674
19	O	1.875521	77.21741	252.5855

Atom Number	Atom	x	y	z
20	O	8.13136	43.5368	110.8978
21	O	6.983517	88.25746	35.23975
22	O	4.863814	123.0968	296.1089
23	O	1.961835	89.60318	129.4872
24	O	5.410965	28.14175	280.7919
25	O	7.743019	53.95468	74.34612
26	O	6.29985	104.0793	358.2029
27	O	2.801239	118.0536	282.161
28	O	2.532491	156.5166	158.8822
29	O	9.593286	56.81371	340.3055
30	O	6.606745	108.7528	36.99336
31	O	5.405083	111.8567	257.6387
32	O	6.232644	33.37037	317.3676
33	O	4.964337	140.5049	37.79311
34	Si	1.611092	165.8011	205.9072
35	Si	1.611092	127.6567	41.25736
36	Si	1.611092	154.3222	223.5625
37	Si	1.611092	107.2448	157.7357
38	Si	1.609959	87.39354	328.7555
39	Si	1.609959	125.8568	0.46052
40	Si	1.609959	116.5841	114.5246
41	Si	2.987964	127.21	328.6502
42	Si	2.987964	127.21	355.3746
43	Si	2.987964	127.21	287.6765
44	Si	1.611324	54.83895	257.421
45	Si	2.955928	124.1749	77.52672
46	Si	2.955928	124.1749	282.4733
47	Si	2.955928	124.1749	77.52672
48	Si	2.955928	23.50357	209.1882
49	Si	6.876941	92.04316	218.9282
50	Zn	3.102151	127.0597	243.0225

Atom Number	Atom	x	y	z
51	O	1.611122	64.98687	59.21134
52	O	1.609417	109.193	255.8724

Table A-4: Atom coordination of scheme D

Atom Number	Atom	x	y	z
0	Zn	0	0	0
1	Si	4.659046	0	0
2	Si	10.61902	70.82454	0
3	Si	11.71176	108.199	321.0126
4	Si	5.852273	147.5422	298.4743
5	Si	9.359346	66.66871	84.02009
6	Si	9.749164	113.3996	349.5885
7	Si	5.423382	118.4524	301.3239
8	Si	2.987964	44.9188	12.16886
9	Si	2.987964	87.10787	34.24385
10	Si	2.987964	124.978	97.03274
11	Si	2.955928	124.1749	49.93633
12	Si	2.955928	124.1749	287.9219
13	Si	2.955928	124.1749	36.74678
14	Si	2.955928	96.09626	258.1305
15	Si	5.073039	36.9959	251.026
16	Si	2.987964	39.66698	248.1045
17	Li	2.297743	132.4106	309.7087
18	Li	2.796257	86.96202	30.65274
19	O	2.3	61.18641	6.636818
20	O	1.608878	129.0799	97.44362
21	O	1.608878	129.0799	262.5564
22	O	1.608878	129.0799	127.7653
23	O	2.277984	129.0465	348.1133
24	O	1.611917	23.49441	42.78625
25	O	1.611917	23.49441	54.65737

Atom Number	Atom	x	y	z
26	O	1.611917	23.49441	305.3426
27	O	2.3	41.03084	284.4682
28	O	1.609456	109.7015	40.21336
29	O	1.609456	109.7015	319.7866
30	O	1.609456	109.7015	40.21336
31	O	1.609456	109.7015	350.1083
32	O	1.610224	87.34708	149.5353
33	O	1.610224	87.34708	240.7864
34	O	1.611122	66.47717	16.18645
35	O	1.609417	138.4193	67.07541
36	O	1.609417	170.7095	34.45498
37	O	1.610043	89.38051	344.3326
38	O	1.610043	86.82397	104.4791
39	O	1.610043	108.2061	305.8491
40	O	1.610043	76.45156	176.5368
41	O	1.609698	108.5894	94.37664
42	O	1.609698	150.2887	339.9972
43	O	1.609698	139.366	149.7919
44	O	1.609417	106.1682	24.74481
45	O	1.609698	126.358	280.537
46	O	1.61031	89.89103	127.1225
47	O	1.61031	59.94263	171.241
48	O	1.61031	89.89103	140.312
49	O	1.61031	89.89103	197.5462
50	O	1.610039	21.9028	293.2959
51	O	1.610039	21.9028	44.56225
52	O	1.610039	21.9028	280.1064

Table A-5: Atom coordination of scheme E

Atom Number	Atom	x	y	z
0	Zn	1.496606	6.281307	3.549695

Atom Number	Atom	x	y	z
1	Si	0	0	2.474
2	Si	2.80793	0.656314	3.645686
3	Si	12.39169	2.80793	1.302314
4	Si	10.24007	12.39169	3.645686
5	Si	0.656314	10.24007	1.302314
6	Si	10.88334	3.744776	3.761964
7	Si	9.303224	10.88334	1.186036
8	Si	2.164663	9.303224	3.761964
9	Si	3.744776	2.164663	1.186036
10	Si	8.522954	1.912837	3.739204
11	Si	11.13516	8.522954	1.208796
12	Si	4.525046	11.13516	3.739204
13	Si	1.912837	4.525046	1.208796
14	Si	6.766693	1.496606	1.398305
15	Si	11.55139	6.766693	3.549695
16	Si	6.281307	11.55139	1.398305
17	O	9.882555	9.437618	0.776836
18	O	3.610382	9.882555	4.171164
19	O	3.165445	3.610382	0.776836
20	O	10.86898	5.34968	3.888633
21	O	7.69832	10.86898	1.059367
22	O	2.179016	7.69832	3.888633
23	O	5.34968	2.179016	1.059367
24	O	7.543049	2.338202	2.532881
25	O	10.7098	7.543049	2.415119
26	O	5.504951	10.7098	2.532881
27	O	2.338202	5.504951	2.415119
28	O	7.655262	1.43267	0.057892
29	O	11.61533	7.655262	4.890108
30	O	5.392738	11.61533	0.057892
31	O	1.43267	5.392738	4.890108

Atom Number	Atom	x	y	z
32	O	6.524	0	1.940606
33	O	0	6.524	3.007394
34	O	1.227817	0.463204	3.408677
35	O	12.5848	1.227817	1.539323
36	O	11.82018	12.5848	3.408677
37	O	0.463204	11.82018	1.539323
38	O	3.340288	1.858035	2.713978
39	O	11.18997	3.340288	2.234022
40	O	9.707712	11.18997	2.713978
41	O	1.858035	9.707712	2.234022
42	O	3.110643	1.032097	0.23404
43	O	12.0159	3.110643	4.71396
44	O	9.937357	12.0159	0.23404
45	O	1.032097	9.937357	4.71396
46	O	3.577762	12.34471	3.256774
47	O	0.703287	3.577762	1.691226
48	O	9.470238	0.703287	3.256774
49	O	12.34471	9.470238	1.691226
50	O	9.437618	3.165445	4.171164
51	Li	3.148062	7.836034	1.930026
52	Li	4.079128	5.868442	1.154384

Table A-6: Atom coordination of scheme F

Atom Number	Atom	x	y	z
0	Li	0	0	0
1	Li	3.04	0	0
2	Zn	10.34863	81.67209	0
3	Zn	3.114144	64.38193	134.1581
4	O	1.610043	130.5276	255.1415
5	O	8.012418	24.9065	339.4
6	O	1.611092	21.80974	43.10694

Atom Number	Atom	x	y	z
7	O	5.349236	138.8589	341.4534
8	O	1.609698	114.031	106.4834
9	O	9.7649	34.12589	321.4858
10	O	9.206517	80.92246	57.89633
11	O	7.192394	132.3443	299.0071
12	O	7.833604	121.0555	33.43573
13	O	3.836308	115.0452	238.1498
14	O	7.999174	24.48369	50.1161
15	O	9.754087	60.09651	89.22867
16	O	7.363217	36.75543	300.3345
17	O	7.49963	67.88133	64.78355
18	O	6.255823	115.1698	318.9674
19	O	1.610333	78.17757	359.8277
20	O	8.13136	43.5368	110.8978
21	O	6.983517	88.25746	35.23975
22	O	4.863814	123.0968	296.1089
23	O	1.609959	32.66835	197.6038
24	O	5.410965	28.14175	283.8201
25	O	7.743019	53.95468	74.34612
26	O	6.29985	104.0793	358.2029
27	O	2.801239	118.0536	282.161
28	O	2.532491	156.5166	155.854
29	O	9.593286	56.81371	343.3337
30	O	6.606745	108.7528	36.99336
31	O	5.405083	111.8567	257.6387
32	O	6.232644	33.37037	317.3676
33	O	4.964337	140.5049	37.79311
34	O	1.609417	130.4648	28.70603
35	O	7.52149	147.6594	358.3643
36	O	6.365419	85.26023	234.9955
37	O	9.836095	12.75035	102.337

Atom Number	Atom	x	y	z
38	Si	1.609417	66.63431	30.65193
39	Si	1.609417	58.0123	131.1484
40	Si	1.609417	19.34643	207.4081
41	Si	1.609959	87.39354	328.7555
42	Si	1.609959	125.8568	0.46052
43	Si	1.609959	116.5841	114.5246
44	Si	2.987964	127.21	328.6502
45	Si	2.987964	127.21	355.3746
46	Si	2.987964	127.21	287.6765
47	Si	1.611324	54.83895	257.421
48	Si	2.955928	124.1749	77.52672
49	Si	2.955928	124.1749	282.4733
50	Si	2.955928	124.1749	77.52672
51	Si	2.955928	23.50357	209.1882
52	Si	1.611122	101.7533	239.481

Table A-7: Atom coordination of scheme G

Atom Number	Atom	x	y	z
0	Zn	0	0	0
1	Zn	5.776619	0	0
2	Si	3.112566	89.67236	0
3	Si	11.65409	60.05075	215.5355
4	Si	10.66743	111.8118	345.6388
5	Si	4.629105	151.8866	88.82328
6	Si	9.725727	61.74371	271.2051
7	Si	9.3653	107.0654	15.91552
8	Si	3.102151	153.9672	334.0424
9	Si	3.033591	64.68889	95.11971
10	Si	2.987964	52.93696	0.011373
11	Si	2.987964	96.94762	354.1633
12	Si	2.987964	140.0717	15.65967

Atom Number	Atom	x	y	z
13	Si	2.987964	101.377	338.3898
14	Si	2.955928	124.1749	70.95241
15	Si	2.955928	124.1749	302.5947
16	Si	2.955928	124.1749	65.54509
17	O	1.610039	21.9028	59.23505
18	O	1.610039	21.9028	308.9047
19	O	1.610039	21.9028	168.4939
20	O	1.608878	129.0799	97.44362
21	O	1.608878	129.0799	262.5564
22	O	1.609959	15.46923	337.352
23	O	1.608878	129.0799	262.5564
24	O	1.611917	23.49441	42.78625
25	O	1.611917	23.49441	54.65737
26	O	1.611917	23.49441	305.3426
27	O	1.611324	108.9206	71.96753
28	O	1.609456	109.7015	40.21336
29	O	1.609456	109.7015	319.7866
30	O	1.609456	109.7015	40.21336
31	O	1.609456	57.15129	100.8514
32	O	1.610224	87.34708	149.5353
33	O	1.610224	111.306	1.313696
34	O	1.611122	14.87016	293.6259
35	O	1.609417	112.1101	353.6353
36	O	1.609417	150.7061	19.71525
37	O	1.609417	142.1766	190.5244
38	O	1.610043	19.6545	31.79299
39	O	1.610043	103.2157	78.98338
40	O	1.610043	93.63987	264.3445
41	O	1.610043	97.97725	114.3111
42	O	1.609698	90.4598	229.3151
43	O	1.609698	142.6285	289.3238

Atom Number	Atom	x	y	z
44	O	1.609698	145.4248	132.1259
45	O	1.609698	105.8253	226.9099
46	O	1.61031	89.89103	155.9208
47	O	1.61031	89.89103	321.4778
48	O	1.61031	89.89103	161.3281
49	O	1.61031	89.89103	212.219
50	O	1.610039	21.9028	314.312
51	Li	2.293417	79.25946	312.4794
52	Li	2.310827	165.0202	144.9598